CYCLIC BEHAVIOR OF LIGHTLY REINFORCED CONCRETE BEAMS

by

Charles K. Nmai

David Darwin

A Report on Research Sponsored by

THE NATIONAL SCIENCE FOUNDATION

Research Grant

PFR 79-24696

UNIVERSITY OF KANSAS

LAWRENCE, KANSAS

June 1984

50272-101

REPORT DOCUMENTATION PAGE	1. REPORT NO.	2.	3. Recipient's Accession No.

4. Title and Subtitle
Cyclic Behavior of Lightly Reinforced Concrete Beams

5. Report Date
June 1984

6.

7. Author(s)
Charles K. Nmai and David Darwin

8. Performing Organization Rept. No.
SM Report No. 12

9. Performing Organization Name and Address
University of Kansas Center for Research, Inc.
2291 Irving Hill Drive, West Campus
Lawrence, KS 66045

10. Project/Task/Work Unit No.

11. Contract(C) or Grant(G) No.
(C)
(G) NSF PFR 79-24696

12. Sponsoring Organization Name and Address
National Science Foundation
Washington, D.C. 20550

13. Type of Report & Period Covered

14.

15. Supplementary Notes

16. Abstract (Limit: 200 words)

The cyclic behavior or seven lightly reinforced concrete cantilever beams is studied as a function of reinforcement ratio, nominal stirrup capacity, stirrup spacing, and ratio of positive to negative reinforcement. An energy dissipation index, D_i, is developed to serve as a measure of the performance of reinforced concrete beams subjected to cyclic loading. D_i is used to compare the test results of this study with those of four other studies. Recommendations for design are made.

Based on the experimental work, the use of a low reinforcement ratio reduces the maximum shear and compressive stresses in beams subjected to cyclic loading, and thus, reduces the rate of degradation. A reduced stirrup spacing and an increased positive to negative steel ratio, A_s'/A_s, increases the number of inelastic cycles endured and the total energy dissipated. However, an increased A_s'/A_s ratio also increases the induced shear and the energy demand, thus reducing the effectiveness of the increased positive reinforcement. D_i appears to provide a consistent measure of beam performance. The analyses based on D_i indicate that a decrease in maximum shear stress, and an increase in concrete strength and nominal stirrup capacity will improve the performance of reinforced concrete beams subjected to cyclic loading.

17. Document Analysis a. Descriptors
beams (supports), concrete (reinforced), design, earthquakes, hinges, loads (forces), reinforcement, shear, shear strength, stirrups, strains, stresses, structural engineering

b. Identifiers/Open-Ended Terms

c. COSATI Field/Group

18. Availability Statement	19. Security Class (This Report)	21. No. of Pages
Release unlimited	Unclassified	
	20. Security Class (This Page) Unclassified	22. Price

(See ANSI-Z39.18) *See Instructions on Reverse*

OPTIONAL FORM 272 (4-77)
(Formerly NTIS-35)
Department of Commerce

ACKNOWLEDGEMENTS

This report is based on a thesis submitted by Charles K. Nmai to the Civil Engineering Department of the University of Kansas in partial fulfillment of the requirements for the MSCE degree.

The research was supported by the National Science Foundation under NSF Grant No. PFR 79-24696. Sheffield Steel Corporation and ARMCO, Inc., respectively, donated the deformed bars and wire reinforcing steel.

Numerical calculations were performed on the Honeywell 66/60 computer system of the Academic Computer System of the University of Kansas.

TABLE OF CONTENTS

TABLE OF CONTENTS (continued)

LIST OF TABLES

LIST OF FIGURES

LIST OF FIGURES (continued)

LIST OF FIGURES (continued)

LIST OF FIGURES (continued)

LIST OF FIGURES (continued)

Chapter 1

INTRODUCTION

1.1 General

Earthquakes can cause severe deformations in structures. In extreme cases, these deformations cause collapse, resulting in loss of life and major property damage. To minimize the hazards to life and property, structural design for seismic loading is based on the dual requirements that structures withstand moderate earthquakes without damage and major earthquakes without collapse.

Designing a structure to respond elastically during an earthquake is costly and may not be feasible. Hence, inelastic deformations must be accommodated in the design of most structures for seismic loading. Ductile behavior and the ability of the structure to dissipate energy in the inelastic range are, thus, very important. Failures of structural members subjected to earthquake loading have been due to a number of factors, including loss of anchorage of the main reinforcement, compressive failure of the concrete, and shear failure of the concrete (25,27,28). Structural members with adequate shear capacity under static loading have failed in shear when subjected to cyclic loading during major earthquakes. This reduces the ductility and energy dissipation capabilities of the structure.

Cyclic shear failure may be prevented or delayed in several ways. Designing structural members for low shear stress has been considered to be one of the best ways to achieve this goal and also improve the energy dissipation capacity of the member (4,5,12,18). Research indicates that reducing the shear stress improves the ability of a member to withstand inelastic cyclic loading (4,5,18). In spite of this recommendation and the fact that present building codes (3,30) permit the use of reinforcement ratios as low as 0.33 percent for both negative and positive reinforcement, previous experimental research has been limited to reinforcement ratios in excess of one percent and close to the maximum allowable values. Increased shear reinforcement, including increases in total steel and reduced stirrup spacing, has been advocated based on the results of these tests.

These recommendations, which are sometimes complicated and expensive to execute, may not be necessary for structures with the low amounts of flexural reinforcement permitted by present building codes (3,30). Although reducing the flexural reinforcement ratio, ρ, has been recommended to improve the behavior of flexural members under cyclic loading, very little is known about the cyclic behavior of reinforced concrete beams with low amounts of flexural reinforcement. A better understanding of the cyclic shear behavior of reinforced concrete beams with low amounts of flexural reinforcement is needed. This knowledge will contribute to improved procedures in the design and construction of reinforced concrete structures subject to seismic loading.

1.2 Previous Work

Early experimental work on the behavior of reinforced concrete beams subjected to repeated, unidirectional loading showed that reinforced concrete flexural members do not suffer stiffness degradation as a result of repeated loading (9,18,22). However, reinforced concrete members under complete load reversals, or cyclic loading, have been found to undergo marked degradation in stiffness and strength (4,5,7,8,12,13,14,16,18,20,21,23,24,29,31,32). Previous experimental work on the behavior of reinforced concrete members subject to cyclic loading has been limited to flexural reinforcement ratios in excess of one percent.

Brown and Jirsa (7,8) used reinforcement ratios of 1.5 and 2.6 percent, with equal amounts of top and bottom steel, to investigate the behavior of doubly-reinforced concrete beams subjected to load reversals. Large displacement excursions of five and ten times the yield displacement were imposed on the beams. From the results of these tests, they concluded that performance increased with decreased flexural reinforcement ratio, decreased stirrup spacing, and increased shear-span. A reduction in the reinforcement ratio and an increase in the shear-span both result in a lower shear stress.

Wight and Sozen (31,32) tested twelve reinforced concrete column specimens under cyclic loading. The specimens represented a column between the points of contraflexure below and above a story level and had a flexural reinforcement ratio of 2.4 percent. They observed that for specimens without axial loads, the shear-carrying

mechanism changed when deflections were imposed that were larger than the deflection at which longitudinal splitting cracks first occurred in the compressed concrete. As the applied deflection was increased beyond the deflection at first splitting, the formation of spalling cracks and the degradation of the core reduced the shear capacity of the concrete until virtually all of the applied shear was carried by the stirrups. This led Wight and Sozen to recommend that the maximum displacement ductility factor, μ, a member might experience, defined as the ratio of maximum displacement to displacement at first yield, be considered in the design of shear reinforcement for reinforced concrete members proportioned for cyclic loading. They also recommended that the shear capacity of a member be based on the shear capacity of the confined core only and that for members with no axial load, the contribution of the concrete to shear strength should be ignored.

Bertero, Popov et al. (4,5,18,21) tested a series of beams with reinforcement ratios of 1.4 and 1.58 percent. To avoid excessive damage and severe degradation, the researchers recommended a limitation on the shear stress that may be developed within the critical region of a member subjected to severe cyclic loading. They also recommended that the ratio of positive to negative reinforcement be increased above the 50% allowed by the then current ACI Building Code, ACI 318-71 (1). This change has yet to be adopted (3).

Scribner and Wight (23,24) studied the effect of intermediate longitudinal reinforcement in preventing shear strength and stiffness deterioration in reinforced concrete flexural members subjected to cyclic loading. A total of twelve beams were tested, with reinforcement ratios varying from 1.27 percent to 2.62 percent. Maximum shear stresses ranged from $2\sqrt{f'_c}$ to about $6.2\sqrt{f'_c}$. Scribner and Wight observed that the response of the beams depended on the maximum shear stress. Beams with high shear stresses responded primarily in shear, while beams with maximum shear stresses below $3\sqrt{f'_c}$ responded in flexure, with little tendency to develop significant planes of shear slippage. The inclusion of intermediate longitudinal reinforcement was most beneficial in beams with maximum shear stresses between $3\sqrt{f'_c}$ and $6\sqrt{f'_c}$.

A more recent study by Hwang and Scribner (13,14) of the effect of beam tip displacement history variations on the cyclic response of flexural members, involved tests of eleven beams, with reinforcement ratios of 1.65 and 2.34 percent. Maximum shear stresses ranged from $3\sqrt{f'_c}$ to $7.4\sqrt{f'_c}$, and the imposed tip displacements corresponded to two and four percent of the shear span. The performance of the beams depended strongly on the maximum imposed displacements. Strength and stiffness degradation were found to be functions of applied shear stress and maximum displacement.

The behavior of reinforced concrete members subjected to cyclic loading strongly depends on the load history used during the tests (5,12,13,14,18,29,31,32). However, there has been a lack of agreement as to what load history to use to evaluate and compare

member response. Since each investigator has used a different load history, it is difficult to compare the test results obtained by various researchers or to use these results to determine transverse reinforcement requirements for reinforced concrete members subjected to cyclic loading. In an attempt to make comparisons between members subjected to widely varying load histories, Gosain, Brown, and Jirsa (12) proposed the "work index" as a measure of the energy absorption capability within the hinging zone, defined as:

$$I_w = \sum P_n \Delta_n / P_y \Delta_y \qquad (1.1)$$

in which P_n = peak load in the nth cycle

P_y = yield load

Δ_n = displacement corresponding to P_n

Δ_y = yield displacement

The summation is carried over cycles in which $P_n \geq 0.75 P_y$.

Only beams in which flexural yield occurred were considered. Thus, the ratio of P_n/P_y during the first cycle was greater than or equal to one. Also, since only cycles in which P_n/P_y was greater than or equal to 0.75 were used in the study, the ratio P_n/P_y was most likely to be in the range of about 0.75-1.25 and was approximated as being equal to one. The ratio Δ_n/Δ_y in each cycle was determined from the load-deflection curves and the "work indices" were calculated on the assumption that the shape of the load-deflection curve remained about the same for each cycle. However, examination of the load-deflection curves for most of the specimens showed that the shear-span and the magnitude of the axial

load applied to a specimen had a significant effect on member response. Hence, modifications were made to account for the influence of axial compression, N, and shear-span, a, on member response. These modifications were also introduced in an attempt to reduce the scatter of the data used in the investigation. The resulting expression for the "modified work index" was

$$I'_w = I_w(1 - d_c/a)(1 + 0.0005N/A_{core}) \qquad (1.2)$$

in which d_c = overall stirrup depth

A_{core} = area of the core

From studies of the measured ultimate shear stresses and modified work indices of sixty-five reinforced concrete members subjected to cyclic loading, Gosain et al. recommended that to achieve adequate performance and energy dissipation in reinforced concrete members under inelastic deformation, the ultimate shear stress on the core should not exceed 6 to $7\sqrt{f'_c}$, provided that the axial compressive stress does not exceed 1500 psi, and the transverse reinforcement should be designed to carry the maximum shear imposed on the section. To prevent the buckling of the longitudinal reinforcement, the researchers also recommended that stirrup spacing should not exceed six longitudinal bar diameters.

In addition to Gosain et al. (12), other researchers (5,18,19,20,21,31,32) have also recommended that stirrups in reinforced concrete members subjected to cyclic loading be designed to carry the maximum shear expected, and that the contribution of the concrete be neglected. These researchers have also advocated a

decrease in stirrup spacing within the hinging zone to improve confinement of the core and to prevent buckling of the flexural reinforcement. The use of closely spaced stirrups, however, can make concrete placement and consolidation more difficult and may prevent a design from being properly executed.

1.3 Object and Scope

The primary objective of this investigation is to study the behavior of hinging regions in reinforced concrete beams with low amounts of flexural reinforcement subjected to cyclic loading. Seven beam-column subassemblages were tested. The primary variables were the reinforcement ratio, ρ, the ratio of negative to positive reinforcement, A_s'/A_s, the amount of transverse reinforcement, v_s, and the stirrup spacing, s. The results are compared with the results obtained for more heavily reinforced sections. An improved energy index is proposed to evaluate the performance of reinforced concrete beams subjected to cyclic loading and recommendations are made for the seismic design of reinforced concrete beams.

Chapter 2

EXPERIMENTAL INVESTIGATION

2.1 General

The main objective of this investigation is to study the cyclic behavior of reinforced concrete beams with low amounts of flexural reinforcement.

The specimens, all cantilevers, represent a beam as it frames into a column (Fig. 2.1). Positive anchorage of the beam flexural steel within the column was used in the tests to isolate beam behavior, independent of anchorage failure. The specimens were cast and tested in the vertical position, as in an actual structure. Large displacements, on the order of five times the yield displacement, were imposed on the beams to simulate the forces and displacements that a beam-column connection might experience in a severe earthquake.

Downward shears and displacements were considered positive (Fig. 2.1).

2.2 Test Specimens

Seven cantilever beams with 7.5 x 18 in. cross-sections were tested. Top reinforcement for the beams consisted of either four or six #4 deformed bars. Bottom reinforcement equaled one-half the top reinforcement, except for beam F-6 in which the bottom steel was three-fourths of the top steel. The flexural reinforcement

ratio, ρ, was either 0.69 or 1.03 percent, and represented the lower range of reinforcement ratios permitted by the ACI Building Code (1,2,3) and the Uniform Building Code (30). The positive to negative steel ratio of 0.5 in six of the beams tested, also represented the minimum ratio permitted by the codes (1,2,3,30). Each beam had a shear-span of 60 inches and a shear-span to depth ratio, a/d, of about 3.9. A summary of beam and reinforcement properties is presented in Table 2.1.

Shear reinforcement for the beams consisted of annealed wire stirrups. The nominal shear stress provided by the stirrups, v_s ($=A_v f_{vy}/bs$), varied between 121 and 161 psi. The total shear capacity of each beam, V_n, was satisfactory to insure a flexural failure under monotonic loading. The value of shear resisted by the stirrups alone, V_s, however, varied both above and below the maximum shear imposed on the beam. Calculated and measured shear forces and stresses are tabulated in Table 2.2. The nominal shear stresses were computed in accordance with the provisions of ACI 318 (1,2,3). The maximum stirrup spacing was d/4, and the first stirrup was placed one inch from the column face.

2.3 Materials and Fabrication

Concrete, with 3/4 in. nominal maximum size aggregate, was obtained from a local ready-mix plant. The mix proportions by weight for cement, fine and coarse aggregate, were 1.0:2.88:2.88 for all beams. Type I cement was used. For each beam, ten 6 x 12 in. cylinders and two 6 x 6 x 22 in. flexural specimens were prepared.

Cylinders were tested on the third and seventh days after casting to monitor the concrete strength. The remaining cylinders and the flexural specimens were tested after beam failure. A summary of concrete properties is presented in Table 2.3.

The flexural reinforcement for the beams consisted of #4 ASTM A 615 Grade 60 deformed bars. A typical stress-strain curve is shown in Fig. 2.2. The longitudinal reinforcement for the column-stub consisted of four #6 and four #8 deformed bars (Fig. 2.1). Column ties were made from #3 deformed bars. The beam longitudinal reinforcement was welded to a 3/4 x 8 x 18 in. plate which was firmly wired to the column reinforcement. This procedure was taken to limit slip and prevent anchorage failure.

The annealed wires for the shear reinforcement were preyielded, bent and welded into closed stirrups. The wires, 0.179 and 0.3 in. in diameter, were delivered in coils. 50 in. long pieces were cut from the coils, straightened in a roller, and preyielded to eliminate residual stresses and to obtain a well defined yield point. Due to strain aging, specimens of the wire were tested after failure of the beam to obtain the actual yield load of the stirrups. Typical stress-strain curves for the wires are shown in Fig. 2.3. The yield stresses of the #4 bars and the wires are presented in Table 2.1.

The formwork was built from 3/4 in. BB-plyform and assembled using all-thread rods. The forms were used for all seven beams and were maintained by cleaning and coating with polyurethane after each casting. Prior to casting, form release was applied to

the surface of the forms to facilitate stripping. The beams were stripped at a concrete strength of about 3000 psi. At a concrete strength of 3500 psi, the test specimens were prestressed to a "permanent" column-stub (Fig. 2.1) with a force of 160 kips and moved into position under the testing frame (Fig. 2.4(a) and 2.4(b)). The "permanent" column-stub, had the same dimensions and reinforcement as the column-stub that was cast monolithically with each beam. The two column-stubs were then prestressed to the structural floor using a system of four I-sections and four 1.5 in. load rods. A total prestress force of 200 kips was applied to the column-stubs to minimize the rigid body rotation of the test specimen (Fig. 2.5).

2.4 Instrumentation

Micromeasurements EA-06-031DE-120 electrical resistance strain gages were bonded to the longitudinal reinforcement and to stirrups placed within a distance equal to the beam depth from the column face. At the points where strain gages were bonded to the longitudinal reinforcement, a small area of about 1/4 x 1 in. was filed off to remove the deformations and surface scale, and to provide a flat surface for the gage. This procedure was not required for the stirrups which were made from annealed wire. The surface of the steel was cleaned with Micromeasurements M-Prep Conditioner A and M-Prep Neutralizer 5, and the gages bonded with M-Bond 200 adhesive after application of M-Bond 200 catalyst. The gages were then coated with M-Coat D, for insulation, and waterproofed with a coating of M-Coat G. The M-Coat G coating also

protected the gages from abrasion during casting of the specimen. The location of strain gages was similar in all specimens, as shown in Fig. 2.6.

A total of ten linear variable displacement transducers, or LVDTs, were used. Load point deflection was measured with a Schaevitz 5000 DC-D LVDT, with a total range of ten inches. The core rod of this LVDT was extended and pivoted to a frame independent of the beam to minimize rotation of the core rod when the beam grew longitudinally. Two pairs of diagonally crossing LVDTs were used to measure shear deformations over two regions, each approximately equal to the beam effective depth, adjacent to the column face (Fig. 2.7(a)). Other LVDTs were used to measure flexural deformation of the beam relative to the column-stub (Fig. 2.7(b)), rigid body movement of the column-stub relative to the floor, and beam deflection at a distance of 18 inches from the column face.

A micrometer dial gage was used to measure the longitudinal growth of the beam. The locations of the LVDTs and the dial gage are shown in Fig. 2.7(c). The applied load was measured by a load cell fixed to the loading ram of the actuator.

2.5 Test Procedure

Prior to testing, the specimen was white-washed and the stirrup and flexural reinforcement positions were shown on the side of the beam where the cracks were to be marked.

Load was applied by a 110 kip MTS servo-hydraulic actuator under displacement control. The actuator was fixed to a steel frame prestressed to the structural floor of the laboratory (Fig. 2.4(a)).

After a mini-cycle in which a preload of 1 kip was applied to check the instrumentation, the beam was loaded continuously until the longitudinal reinforcement yielded. In the first test, the beam was unloaded immediately after the longitudinal reinforcement reached the calculated yield strain, but due to the use of an incorrect value of yield strain, the beam was unloaded before the longitudinal reinforcement actually yielded, and this resulted in the use of an incorrect yield deflection in calculating the deflection amplitude for the cyclic stage. To eliminate this error from occurring in other tests, loading was continued slightly beyond the yield point to insure complete yielding before the beam was unloaded. The yield deflection was then obtained from a continuous plot of load versus load-point deflection on an X-Y recorder. Loading was resumed with the beam being cycled at four to five times the yield deflection. This type of loading has been shown to be a more severe condition than gradually increasing deflection amplitudes (18). A typical loading schedule is shown in Fig. 2.8.

The deflection amplitude used for beam F-1 was 3.9 times the true yield deflection. The corresponding values for beams F-2 and F-3 were 5.1 and 4.4 times their respective yield deflections.

The criteria for selecting the deflection amplitude used for beams F-4 through F-7 were either the yield deflection times the displacement ductility factor, μ, of beam F-3, which was 4.4, or the deflection amplitude used for beam F-3, whichever was greater. This was to insure that beams F-4 to F-7 had a displacement ductility factor of at least 4.4. Each of these beams, however, had a lower yield deflection than beam F-3, and as such, the deflection amplitude used in beam F-3 governed and was selected as the deflection amplitude used for beams F-4 through F-7. The actual displacement ductility factors and other principal results are given in Table 2.4.

Instrumentation readings were taken at points which were selected to best describe the continuous load-deflection plot on the X-Y recorder. At each data point, loading was temporarily halted. Typically, twenty readings were taken during each complete cycle. Each cycle took about twenty minutes. After six cycles, the loading rate was increased and the time taken to complete a cycle decreased to about ten minutes.

Cracks were marked continuously up to the end of the first inelastic cycle. Thereafter, cracks were marked at the end of each cycle and photographed.

Two criteria were used to independently define failure of a beam: (i) when the peak load in a cycle dropped below 50% of the initial yield load, P_y, or (ii) upon fracture of the bottom reinforcing bars. In all but one of the beams, the second criterion controlled.

2.6 Test Results

Several pieces of data were recorded in each test. However, only the principal experimental results are given in Table 2.4. These include the yield load, maximum load, yield deflection, maximum deflection, displacement ductility factor, and growth of each beam.

The load-deflection curves for all seven beams are presented in Fig. 2.9(a) through 2.9(g). These curves represent the most important data recorded in each test and are an indication of the rate of stiffness and strength decay in each beam. For example, the difference in behavior between beams F-2 and F-4 can be seen by comparing the load-deflection curves for the two beams (Fig. 2.9(b) and 2.9(d), respectively). Beam F-2 suffered severe degradation, indicated by the rapid drop in load with each cycle (Fig. 2.9(b)). By contrast, the degradation of beam F-4 was gradual, as shown by the closeness of the load-deflection curves for this beam (Fig. 2.9(d)). The area enclosed by the curves represents the energy dissipated, a measure by which the performance of each beam can be evaluated.

The relationships between applied load and hinging zone shear deformation are presented in Fig. 2.10(a) through 2.10(n). Plots of applied load versus flexural rotation are presented in Fig. 2.11(a) through 2.11(g).

As a result of their relatively low yield strengths, the yield strains of the wire stirrups were exceeded in most cases. A typical load versus stirrup strain plot is shown in Fig. 2.12. Anchorage behavior was very stable due to the precautions taken to prevent anchorage failure. The strains in the beam longitudinal reinforcement within the anchorage zone were low and in no instance was the yield strain of the #4 deformed bars exceeded. The strains in the longitudinal reinforcement within the anchorage zone were obtained from strain gages #5 and #6 (Fig. 2.5), and typical plots from these gages are shown in Fig. 2.13(a) and 2.13(b), respectively.

2.7 Specimen Behavior

2.7.1 General

All of the beams developed intersecting vertical and inclined cracks, as well as cracks at the column face. The cracking patterns varied, but all major cracks usually formed by the end of the first inelastic cycle.

Cracking started with the formation of short vertical cracks. As the applied load increased, inclined cracks extended out from these vertical cracks and penetrated deeper into the section. The formation of cracks when the direction of loading was reversed was similar.

Short longitudinal cracks, or splitting cracks, formed along the level of the flexural reinforcement, the extent of cracking being greater within a distance d/2 from the column face. The splitting cracks developed into spalling cracks and led to spalling of concrete in compression within this region and the eventual loss of cover. Since the ratio of bottom to top steel areas was 0.5 in six beams and 0.75 in one, spalling and crushing of the concrete occurred only at the bottom of the beams. However, minor crushing of the top concrete occurred in all the beams at the column face. By the end of the first inelastic cycle, each beam had developed a vertical crack through the entire section at the column face.

Deterioration in the form of grinding and crushing of the concrete adjacent to the cracks was limited to major cracks that formed within the hinging zone. Cracks formed between the hinging zone and the load point, usually by the end of the second inelastic cycle, and remained stable throughout the tests. Cracking within the column-stub varied from beam to beam, but was relatively light and virtually no damage occurred.

Buckling of the bottom bars occurred in all of the beams, and eventually resulted in the fracture of the bars, except in beam F-5. Buckling of the bottom bars was dependent on the extent of spalling of the bottom cover and occurred during different cycles in different beams. The extent and rate of deterioration of the hinging zone also varied, and was dependent upon the reinforcement ratio, the stirrup spacing, and the amount of shear reinforcement. A summary of the individual member behavior is presented below.

2.7.2 Beam F-1 (ρ=1.03%, A'_s/A_s=0.5, s=3.8 in., v_s/v_m=0.80, $v_m/\sqrt{f'_c}$=3.01, μ=3.9)

This beam was inadvertently loaded in the upward direction prior to testing and developed four vertical cracks within the hinging zone. These cracks extended about two-thirds the depth of the beam into the section. As a result, the beam developed only 92% of its expected yield load and had a higher than expected yield displacement. Cracks were evenly distributed; cracks that formed during upward loading had a larger spacing than those that formed during downward loading (Fig. 2.14(a)). Spalling of the compressed concrete started during the first cycle, and by the third cycle, the cover had spalled off, completely exposing the bottom bars.

The bottom bars buckled in the fourth cycle between the second and third stirrups, and in the fifth cycle, one of the three bars fractured. Though the test was over, the beam was subjected to an additional cycle, and as expected, the two remaining bars also fractured (Fig.2.14(b)). The concrete crushed within a distance of d/2 from the column face, extending about 0.4d into the cross-section. The beam survived five and a half cycles of inelastic loading (Fig. 2.9(a)).

2.7.3 Beam F-2 (ρ=1.02%, A'_s/A_s=0.5, s=3.8 in., v_s/v_m=0.78, $v_m/\sqrt{f'_c}$=3.31, μ=5.1)

This beam was similar to beam F-1, except that it had less cover and thus, a larger core, and was subjected to a higher displacement ductility factor. Deterioration was rapid and the beam survived only four cycles of inelastic loading, the least of all of the beams tested (Fig. 2.9(b)). Extensive spalling of the bottom concrete occurred during the first quarter cycle of inelastic loading. The concrete cover came off early in the second cycle and led to buckling of the bottom bars in the same cycle.

As in beam F-1, buckling occurred between the second and third stirrups (Fig. 2.15(a)). However, buckling of the middle bar was so severe that the second and third stirrups were severely distorted, as shown in Fig. 2.15(b). Also, the outside bars buckled inward moving laterally along the second and third stirrups. Some of the tie wires used in building the reinforcement cage were broken in the third cycle. The middle bar fractured in the fourth cycle. Continued loading fractured another bar and the test was stopped. Crushing of the bottom concrete was again limited to a distance of d/2 from the column face. Extensive deterioration was observed along a flexure-shear crack that formed within the hinging zone. The maximum crack width was about 1/4 inch.

In addition to the cracks at the column face, a vertical crack also developed about three inches into the column-stub parallel to the column longitudinal reinforcement. However, no spalling of the column concrete occurred.

As a result of the extensive spalling that occurred, an all-thread rod within the hinging zone, to which one of the diagonal LVDTs was attached, loosened and further measurement of shear distortion was not possible. The appearance of the beam at the end of the test is shown in Fig. 2.15(c).

2.7.4 Beam F-3 (ρ=0.69%, A'_s/A_s=0.5, s=3.8 in., v_s/v_m=1.15, $v_m/\sqrt{f'_c}$=2.22, μ=4.4)

This beam was similar to beam F-2, except that the reinforcement ratio was reduced from 1.02% to 0.69%. Cracks were uniformly distributed and deterioration was observed along two major cracks within the hinging zone. Moderate spalling occurred in the first cycle through the second cycle. Partial loss of cover occurred in the third and fourth cycles, leading to buckling of the bottom bars in the fourth cycle. However, fracture did not occur until the sixth cycle. Deterioration within the hinging zone was not uniform. Crushing of the concrete extended to a distance of about d/2 from the column face on one side of the beam, but only to a distance of about d/3 on the other side (Fig. 2.16(a) and 2.16(b)). Also, crushing of the concrete was not as extensive as in the first two beams and did not penetrate as deep into the section, as can be seen from the photograph of the beam at the end of the test (Fig. 2.16(c)).

2.7.5 Beam F-4 (ρ=0.69%, A'_s/A_s=0.5, s=1.6 in., v_s/v_m=1.16, $v_m/\sqrt{f'_c}$=2.14, μ=5.1)

Beam F-4 had the smallest stirrup spacing of all the beams tested. Extensive cracking occurred within the hinging zone and most of the cracks that formed were concentrated at the level of the longitudinal reinforcement. Outside the hinging zone, the crack spacing was larger and portions of the core were left uncracked (Fig. 2.17).

Prior to the fourth cycle, only minor spalling had occurred. As in beam F-3, spalling was not uniform on both sides of the beam and by the fifth cycle, partial spalling of the cover had occurred on only one side. Ultimately, spalling on that side of the beam was greater than on the other. Major spalling started in the eighth cycle, and in the ninth cycle, the cover at the bottom of the beam close to the column face spalled off completely, exposing the bottom bars. However, buckling did not occur until the eleventh cycle, leading to fracture in the twelveth cycle. The bottom bars buckled between the first and second stirrups. Some deterioration was observed along three of the cracks in the hinging zone.

2.7.6 Beam F-5 (ρ=0.69%, A'_s/A_s=0.5, s=2.1 in., v_s/v_m=0.87, $v_m/\sqrt{f'_c}$=2.16, μ=4.6)

Though this beam had a slightly wider stirrup spacing than beam F-4 and only 74% of the shear steel in beam F-3, it survived twelve cycles of inelastic loading (Fig. 2.9(e)) without fracture of the bottom bars. The distribution of cracks was uniform and similar

to that of beam F-4, but the cracks were spaced wider within the hinging zone (Fig. 2.18(a)). Two major cracks formed within a distance d/2 from the column face, spaced about 5.5 in. from each other. The concrete core between these two cracks was uncracked. Major deterioration due to sliding was observed along these two cracks within the hinging zone, starting as early as the fifth cycle (Fig. 2.18(b)). One bottom bar was partially exposed in the sixth cycle, and in the ninth cycle, the cover came off completely. The bottom bars buckled in the tenth cycle, the buckled shape extending over the first three stirrups. Buckling was not as severe as in the other beams.

2.7.7 Beam F-6 (ρ=0.69%, A'_s/A_s=0.75, s=3.8 in., v_s/v_m=1.15, $v_m/\sqrt{f'_c}$=2.20, μ=5.3)

This beam was similar to beam F-3, except that it had an extra #4 bar at the bottom, which increased A'_s/A_s to 0.75. As in beam F-3, spalling started in the first cycle of inelastic loading, and a partial loss of cover occurred in the fifth cycle. Buckling of the bottom bars occurred during the sixth cycle, although the concrete cover was not lost completely until the seventh cycle. One bottom bar fractured in the eighth cycle and another in the ninth cycle. Extensive deterioration occurred along two cracks within the hinging zone (Fig. 2.19(a)). The appearance of the beam at the end of the test is shown in Fig. 2.19(b).

2.7.8 Beam F-7 (ρ=0.69%, A'_s/A_s=0.5, s=3.8 in., v_s/v_m=0.95, $v_m/\sqrt{f'_c}$=2.22, μ=5.1)

This beam differed from beam F-3 only in the amount and type of shear reinforcement provided (v_s=133 psi versus 160 psi for beam F-3). Shear reinforcement for this beam consisted of double-stirrups made from 0.179 in. wire, while that of beam F-3 consisted of single 0.3 in. wire stirrups. Though the area of shear reinforcement provided was less, the 0.179 in. wire had a higher yield stress, 38.2 ksi versus 32.5 ksi, than the 0.3 in. wire used in beam F-3. The cracking pattern was basically the same, except that more cracks were observed within the hinging zone of this beam, especially at the location of the third and fourth stirrups. The behavior of this beam was also very similar to beam F-3. Loss of the concrete cover occurred in the fourth cycle, and the beam survived six cycles of inelastic loading, the same number as beam F-3. The extent of deterioration along the major cracks in the hinging zone was, however, greater than in beam F-3. A photograph of the beam at the end of the test is shown in Fig. 2.20.

Chapter 3

DISCUSSION AND EVALUATION OF TEST RESULTS

3.1 General

This chapter presents a discussion of the differences in beam behavior based on energy dissipation for the beams tested in this study. Beam behavior was mainly influenced by reinforcement ratio, stirrup spacing, and ratio of positive to negative reinforcement.

An energy dissipation index, D_i, is also developed to give a relative measure of beam performance under cyclic loading. The test results of this study and those by four other researchers (4,13,14,18,23,24,31,32) are compared based on the energy dissipation index.

Finally, recommendations are made for the design of reinforced concrete beams subjected to cyclic loading.

3.2 Energy Dissipation

One of the most important aspects of structural performance under seismic loading is the ability of the structure to adequately dissipate energy. The energy dissipated by the beams in this study was taken as the area enclosed by the load-deflection curves. Though there are several criteria for evaluating beam performance, such as total number of cycles and rate of degradation, energy dissipation has been used most often

(4,5,7,12,13,14,18,23,24). Hence, an evaluation of beam performance is first made based on the measured energy dissipation.

As described in Section 2.5, two criteria were used to independently define beam failure: (i) when the peak load in a cycle dropped below 50% of the initial yield load, P_y, and (ii) upon fracture of the bottom reinforcement bars. Due to the fracture of the bottom bars in six of the tests, failure occurred in different cycles in different beams, and a computation of the dissipated energy based on the complete load-deflection curves up to failure would introduce inconsistencies into the results. To eliminate these inconsistencies, only cycles for which the peak load, P_n, was greater than or equal to 75% of the initial yield load, P_y, are considered in the computation of dissipated energy. Though somewhat arbitrary, the value of $0.75P_y$ may be considered to represent the lower limit of the "usable" capacity of the beam. This criterion has been used by other researchers (12,13,14,23,24). Energy dissipation values based on this criterion are presented in Table 3.1 for the current study.

3.3 Factors Influencing Member Behavior and Energy Dissipation

3.3.1 Reinforcement Ratio, ρ

The shear imposed on a section is a function of the moment capacity of the beam, which is in turn, a function of the amount of tensile reinforcement. Hence, the larger the reinforcement ratio, the higher the moment capacity and the applied shear. In addition,

as the tensile reinforcement ratio is increased, the compressive stresses in the concrete are also increased, inducing earlier spalling of the compressed concrete and thereby accelerating the rate of degradation. This is seen by comparing beams F-2 and F-3. These two beams differed only in the amount of flexural reinforcement used, 1.02% in beam F-2 and 0.69% in beam F-3. Beam F-2 had a maximum shear stress of $3.31\sqrt{f'_c}$ and survived only four cycles of inelastic loading (Fig. 2.9(b)), while beam F-3, with a maximum shear stress of $2.22\sqrt{f'_c}$, survived six cycles of inelastic loading (Fig. 2.9(c)). The energy dissipated by beam F-3 was higher than by beam F-2, 201 kip-in. versus 169 kip-in. However, beam F-2 did have a higher displacement ductility factor than beam F-3, 5.1 versus 4.4, which may have contributed to its rapid degradation.

3.3.2 Stirrup Spacing, s

The effect of stirrup spacing can be studied by comparing beams F-3, F-4, F-5 and F-7. Beams F-4 and F-5 had stirrup spacings of 1.6 in. and 2.1 in., respectively, compared to 3.8 in. for beams F-3 and F-7, and both dissipated more energy, 297 kip-in. and 262 kip-in., respectively, than either beam F-3 or F-7, both of which dissipated 201 kip-in.

The nominal shear contributions of the stirrups, v_s, for beams F-3, F-4, F-5 and F-7 were, 160, 158, 121 and 133 psi, respectively. Hence, the 48% increase in energy dissipation for beam F-4 compared to beam F-3 can be attributed to the smaller stirrup spacing. The effect of stirrup spacing is further highlighted by

the observations that although beam F-7 had a lower value of v_s than beam F-3, both beams had the same stirrup spacing and dissipated the same amount of energy, while beam F-5, which had only 75% of the v_s of beam F-3, dissipated 30% more energy.

The main effect of smaller stirrup spacing is to provide greater concrete confinement. Smaller stirrup spacing also improves energy dissipation by delaying buckling of the bottom reinforcement.

3.3.3 Ratio of Positive to Negative Steel Area, A_s'/A_s

One suggested method of improving the performance of a beam subjected to cyclic loading is to increase the ratio of positive to negative steel (18). An increase in the A_s'/A_s ratio has the effect of increasing the moment capacity in positive bending, and thus, the area enclosed by the load-deflection curves is increased. In addition, an increase in A_s' reduces the concrete compressive stresses under negative bending, thus delaying compressive spalling. Hence, an increase in the A_s'/A_s ratio will increase the dissipated energy. This is illustrated by beam F-6, which had an A_s'/A_s ratio of 0.75. Beam F-6 survived three more cycles of inelastic loading than beam F-3 (A_s'/A_s=0.5) and dissipated 328 kip-in., compared to 201 kip-in. for beam F-3. Beam F-6 also dissipated more energy than beam F-4 which had an A_s'/A_s ratio of 0.5, but a stirrup spacing of 1.62 in. compared to 3.8 in. in beam F-6. Both beams had the same amount of shear reinforcement, v_s.

The extra energy dissipation capacity obtained with the addition of positive steel, however, may not improve building performance under seismic loading. For a structure subjected to earthquake loading, part of this extra energy dissipation capacity will be needed, because the induced shear will increase as the result of an increase in the A'_s/A_s ratio.

3.3.4 Displacement Ductility Factor, μ

Though displacement ductility factor was not a major variable in this investigation, its effect on the performance of two of the beams, F-1 and F-2, was obvious. Beam F-2 was subjected to a displacement ductility factor of 5.1 compared to 3.9 in beam F-1, and even though beam F-2 had a larger core, it dissipated far less energy than beam F-1, 169 kip-in. versus 287 kip-in., respectively. The larger displacement factor used in beam F-2 resulted in higher compressive stresses and shear in the concrete and a much more rapid degradation than beam F-1, and hence, a lower amount of dissipated energy. The influence of other factors as discussed above somewhat overshadowed the effect of displacement ductility factor in the other beams.

3.4 Energy Dissipation Index, D_i

Specimens of various sizes, reinforcement details and shear-span to depth ratios have been subjected to different load histories by different researchers. A comparison of the performance of these specimens should be based on a measure of performance which accounts for these differences. The most important differences are specimen geometry, strength, and load history.

Gosain, Brown and Jirsa's (12) modified work index, I'_w, was developed to compare beam performance by taking into account the geometry and strength, but not the actual load history. Rather than compute the dissipated energy from the area under the load-deflection curves, the product of the number of cycles times the deflection ductility factor, coupled with modifications for the shear-span to depth ratio and axial load, was used to calculate I'_w (Eq. (1.2)). I'_w was intended to be used only as an indication of the severity of loading (12). In the current study, a similar approach is followed. However, a new index is selected which gives a more realistic measure of beam performance in an actual structure.

In order to help normalize the results with respect to specimen geometry and strength, the energy dissipated by a beam can be normalized with respect to the elastic energy stored in the beam at yield, approximated as $0.5P_y\Delta_y$ (Fig. 3.1). The elastic energy is characteristic of the design capacity of the beam and is dependent on the beam geometry and the amount of flexural reinforcement.

As a frame deforms inelastically under lateral load, the shear imposed on a beam is a function of the span length, L, and the sum of the negative and the positive moment capacities at opposite ends of the span, $M_1^+ + M_2^-$ and $M_1^- + M_2^+$. As shown in Fig. 3.2, $V = (M_1^+ + M_2^-)/L$. If either the positive or negative moment capacity is increased, the shear due to lateral deformation will also be increased. Hence, if additional positive reinforcement is added at the supports, some of the additional energy dissipation capacity obtained (see Section 3.3.3) will be required by the beam. This additional requirement should be considered when evaluating the performance of a beam under cyclic loading.

In this analysis, it is assumed that the beam being modeled is symmetric about midspan, and that the test beam approximates the portion of the beam between the inflection point and the column. It should be noted that although this type of model has been widely used (4,5,7,8,12,13,14,16,18,21,23,24), it is, in fact, only an approximation. In the test beams, the inflection point remains constant for both positive and negative bending, while in a structure subjected to seismic loading, the inflection point will generally be different for positive and negative bending. For example, considering lateral loading only, the shear-spans for positive and negative bending will be $M^+L/(M^+ + M^-)$ and $M^-L/(M^+ + M^-)$, respectively. It is assumed that correlations of beam performance are not sensitive to this approximation.

For beams with $A_s' < A_s$, the yield load and yield deflection in negative and positive bending will be different due to the difference in moment capacities. Since most test procedures involve loading in the strong direction (usually negative bending) before loading in the weak direction (positive bending), the yield load and yield deflection can be obtained in the strong direction only. Due to the Bauschinger effect, it is not possible to measure the corresponding values during the reverse cycle. Since both the yield load and yield deflection are approximately proportional to the area of reinforcing steel, A_s, and effective depth, d, the yield load and yield deflection in positive bending, P_y' and Δ_y', can be approximated in terms of the corresponding values for negative bending.

$$P_y' = (A_s' d_1 / A_s d) \times P_y \tag{3.1a}$$

$$\Delta_y' = (A_s' d_1 / A_s d) \times \Delta_y \tag{3.2a}$$

in which A_s' = area of reinforcing steel, and d_1 = effective depth in positive bending. Since d_1 and d are approximately equal, the following can be used without significant error and is used in this study.

$$P_y' = (A_s' / A_s) \times P_y \tag{3.1b}$$

$$\Delta_y' = (A_s' / A_s) \times \Delta_y \tag{3.2b}$$

The total elastic energy up to yield for both ends of a span is thus approximated by

$$0.5P_y\Delta_y[1 + (A_s'/A_s)^2] \tag{3.3}$$

The energy dissipated by a test specimen can be normalized with respect to Eq. (3.3) to give a relative measure of beam performance under cyclic loading, referred to as the "Energy Dissipation Index":

$$D_i = \frac{\text{Energy Dissipated}}{0.5P_y\Delta_y[1 + (A_s'/A_s)^2]} \tag{3.4}$$

The energy dissipation index compares the usable energy dissipation capacity with a measure of the energy dissipation required by the prototype beam. For example as discussed earlier, an increase in positive flexural steel increases the energy dissipation capacity of a beam (Section 3.3.3 and (18)), but also increases the shear induced by the lateral loading, and thus increases the energy demand. This additional energy demand is accounted for in D_i. D_i also accounts for any "pinching" in the load-deflection plot for a beam, and thus the effects of high shear (low a/d) are automatically accounted for, without modification, as required with I_w' (12).

The values of D_i obtained using Eq. (3.1b) and (3.2b) typically differ from those obtained using Eq. (3.1a) and (3.2a) by less than 1%, with extreme values under 3% in the current study.

The influence of beam strength and loading on the energy dissipation index, D_i, was investigated by plotting D_i versus dimensionless parameters representing strength and applied load. Since the plots showed a linear trend, they were fitted with straight lines and the correlation coefficients, r, obtained from linear regression analyses of the data were used as the basis for determining which variables most strongly influenced D_i.

The results from the tests performed in this investigation and the results for more heavily reinforced sections from four other studies (4,13,14,18,23,24,31,32) were used in the analyses (Table 3.2). Beams which had special reinforcement schemes as well as those with severe anchorage deterioration are included in Table 3.2, but excluded from the linear regression analyses. The regression analyses are also limited to beams subjected to displacement ductility factors of at least 3.9. The need for this limitation will be explained below (Section 3.7.4).

The results of these analyses, which are discussed in detail in the following sections, indicate that D_i is controlled by a combination of factors and not by any single factor. Plots of various combinations of three principal factors, the maximum applied shear stress, v_m, the concrete strength, f'_c, and the stirrup capacity, v_s, were made, and good correlation was obtained by combining the ratio of stirrup strength to the maximum shear stress, v_s/v_m, and the ratio of the square root of the concrete strength to the maximum shear stress, $\sqrt{f'_c}/v_m$, in the form $(v_s f'_c)^{0.5}/v_m^{1.5}$. v_s and v_m are based on the web width and effective

depth of the members, rather than the concrete core area, because a better correlation was obtained in the current analyses when using the larger section dimensions.

Another combined form, $(\alpha v_s + \beta\sqrt{f'_c})/v_m$, was investigated. The results of the linear regression analyses between D_i and this combined form was controlled by the value of β and indicated that the ratio $\sqrt{f'_c}/v_m$ was far more dominant than v_s/v_m. As the value of β was increased, the correlation coefficient also increased, but was less than that obtained by using the combined form, $(v_s f'_c)^{0.5}/v_m^{1.5}$.

The particular form of the expression representing the controlling variables, $(v_s f'_c)^{0.5}/v_m^{1.5}$, is in itself of some interest. It suggests that not only do concrete strength and stirrup capacity relative to the applied shear affect beam performance under cyclic load, but that they do so independently of each other, contributing to different aspects of the performance. Additional shear reinforcement increases shear strength and improves confinement. A higher strength concrete withstands higher stresses imposed in both shear and compression, dilates less, and thus requires less confinement.

3.5 D_i versus v_s/v_m

Due to the progressive decrease in the amount of shear carried by concrete in reinforced concrete beams subjected to cyclic loading, researchers (5,12,18,19,20,21,31,32) have recommended that the transverse reinforcement be designed to carry the maximum shear that a beam might experience. To study its effect, D_i is plotted

against the ratio of v_s to v_m in Fig. 3.3(a) for the beams in Table 3.2 (beams considered: $\mu \geq 3.9$, without special reinforcing schemes and without anchorage deterioration). Although there is considerable scatter, the general trend is for D_i to increase with an increase in v_s/v_m. Due to the scatter, there is poor correlation between D_i and v_s/v_m (r=0.343).

A plot of D_i versus v_s/v_m (Fig. 3.3(b)) for the beams tested in this investigation alone shows a positive trend between D_i and v_s/v_m. The correlation coefficient, r, between the two parameters is 0.711.

3.6 D_i versus $\sqrt{f'_c}/v_m$

As a result of the severe degradation of concrete in beams subjected to cyclic loading, the shear strength of the concrete is normally neglected in seismic design. Under current practice (3,30), the concrete contribution is not considered in the design of shear reinforcement if the factored axial compressive force in a member is less than $A_g f'_c/10$, in which A_g is the gross cross-sectional area. This, however, does not imply that concrete strength and confinement of the concrete core do not affect beam performance.

A plot of D_i versus $\sqrt{f'_c}/v_m$ is presented in Fig. 3.4(a). This plot shows a strong tendency for D_i to increase with $\sqrt{f'_c}/v_m$ and this is reflected in the correlation coefficient, r, of 0.793.

The effect of the maximum imposed shear on reinforced concrete beams subjected to cyclic loading was investigated by Scribner and Wight (23,24) and is generally accepted as a major factor in beam performance (5,12,18,20,23,24). However, because of the narrow range of concrete strengths used in tests, very little is known specifically about the effects of concrete strength on the performance of reinforced concrete beams subjected to cyclic loading. For the tests used in the analyses presented here, the concrete strengths, f'_c, varied within the range 3750 psi to 5900 psi. This narrow range in f'_c means that the test results illustrated in Fig. 3.4 are dominated by v_m.

To help evaluate the impact of concrete strength on the trend shown in Fig. 3.4(a), a separate regression analysis between D_i and $\sqrt{f'_c}/v_m$ was performed with the true values of f'_c replaced by a constant value of 4000 psi. The correlation coefficient was reduced slightly to 0.758, indicating that the concrete strength has at least some impact on beam performance. A wider range in the value of f'_c than used in the tests to date will be required to accurately measure the influence of concrete strength.

The plot of D_i versus $\sqrt{f'_c}/v_m$ for the beams tested in this investigation is shown in Fig. 3.4(b). The five points lying at about the same value of $\sqrt{f'_c}/v_m$, representing beams F-3 to F-7, show that for specimens with the same value of $\sqrt{f'_c}/v_m$, D_i can be increased by a closer stirrup spacing and increased positive reinforcement.

3.7 D_i versus $(v_s f'_c)^{0.5}/v_m^{1.5}$

As mentioned previously, the energy dissipation index, D_i, is influenced by more than one combination of factors. The regression analyses indicate that the combination $(v_s f'_c)^{0.5}/v_m^{1.5}$ provides a good correlation with D_i.

Plots of D_i versus $(v_s f'_c)^{0.5}/v_m^{1.5}$ for this investigation and the four other investigations (4,13,14,18,23,24,31,32) are presented in Fig. 3.5(a) through 3.5(h).

3.7.1 Current Study:

The plot of D_i versus $(v_s f'_c)^{0.5}/v_m^{1.5}$ (Fig. 3.5(a)) shows the relative performance of the beams tested in this investigation. The values of D_i ranged from 25 to 89. The equation of the best fit line obtained from a linear regression analysis is given by

$$D_i = 205(v_s f'_c)^{0.5}/v_m^{1.5} - 26 \qquad (3.5)$$

with correlation coefficient r = 0.861.

Beams which had a reinforcement ratio of 0.69% had values of D_i greater than or equal to 50, while those with a reinforcement ratio of about 1.0% had values of D_i less than 50. This indicates that the performance of a reinforced concrete beam subjected to cyclic loading can be improved by reducing the flexural reinforcement ratio, and thereby, reducing the maximum shear stress imposed on the beam.

It is worth noting that this improvement is not as clear, if beam performance is compared solely on the basis of dissipated energy, since beams with higher reinforcing ratios may have an increased energy dissipation capacity because of their greater moment capacity. D_i, however, takes into account both energy dissipation capacity and energy dissipation demand.

The effects of small stirrup spacing and increased positive to negative steel ratio, A_s'/A_s, are seen by observing that beams F-4, F-5 and F-6, which had values of D_i of 89, 79 and 70, respectively, performed relatively better than beam F-3 which had a D_i value of 50. Beams F-4 (v_s/v_m=1.16) and F-5 (v_s/v_m=0.87) had the same or lower values of shear steel than beam F-3 (v_s/v_m=1.15), but had smaller stirrup spacings, while beam F-6 (v_s/v_m=1.15) was similar to beam F-3, but had an A_s'/A_s ratio of 0.75, versus 0.5 for beam F-3 (Table 2.1).

Beam F-6 appears to have performed slightly better than the overall trend shown by all of the beams, and about as well as beams F-4 and F-5, based on the value of $(v_s f_c')^{0.5}/v_m^{1.5}$. This suggests that most of the extra energy dissipation capacity obtained through the use of the extra positive steel would be required to satisfy the higher energy demand caused by the higher shear resulting from the increased positive moment capacity (Fig. 3.2).

These results also suggest a possible trade-off to obtain improved seismic performance: (1) Stirrup spacing can be reduced (as in beams F-4 and F-5) below d/4 (beams F-3, F-6 and F-7) or (2) additional positive steel can be added while maintaining the same

value of v_s and stirrup spacing. Although the second option requires more total steel, this may be preferred to the use of a reduced stirrup spacing, due to the greater difficulty in concrete placement with a smaller stirrup spacing.

The use of double stirrups and/or an increased stirrup yield strength also appear to have improved performance, as can be seen by comparing the values of Di for beams F-3 and F-7. Beam F-7, which had double stirrups with a higher yield stress (38.2 ksi vs 32.5 ksi for beam F-3), showed an increase in D_i from 50 to 59, although the value of v_s dropped from 160 to 133 ksi and v_s/v_m dropped from 1.15 to 0.95.

3.7.2 Scribner and Wight:

Fig. 3.5(b) shows a plot of D_i versus $(v_s f'_c)^{0.5}/v_m^{1.5}$ for the beams tested by Scribner and Wight (23,24). The best fit line obtained from a linear regression analysis is given by

$$D_i = 223(v_s f'_c)^{0.5}/v_m^{1.5} - 4 \qquad (3.6)$$

with correlation coefficient r = 0.999.

This test series shows the best correlation between D_i and $(v_s f'_c)^{0.5}/v_m^{1.5}$, and this may be due to the fact that all the beams were subjected to the same load history.

A plot of D_i versus $(v_s f'_c)^{0.5}/v_m^{1.5}$ for all of the beams tested by Scribner and Wight (23,24) is presented in Fig. 3.5(c). In this figure, the circles represent beams that had intermediate longitudinal reinforcement; the inverted triangle represents a beam

that had intermediate longitudinal reinforcement, but suffered severe anchorage deterioration, and the square represents a beam that had a large amount of shear reinforcement, but suffered severe anchorage deterioration and failed as a result of sliding along a vertical plane of weakness. The triangle represents a beam that performed particularly poorly and may not have been totally representative of all specimens having similar section properties (24). That the last three points lie below the statistical mean is significant and is discussed later.

With the exception of the data point at a value of D_1 of about 100 and the beam represented by the square, most of the data points closely match the best fit line. The data points at values of D_1 of 75 and 100, represent two nearly identical beams which were subjected to maximum shear stresses between $3\sqrt{f'_c}$ and $4\sqrt{f'_c}$. The beams differed in that the beam with $D_1 = 100$ had intermediate longitudinal reinforcement; the other beam did not. The 34% increase in D_1 shows the possible beneficial effect of intermediate longitudinal reinforcement on reinforced concrete beams subjected to moderate shear stresses (23,24). However, the other beams with intermediate longitudinal reinforcement lie very close to the best fit line, indicating that the inclusion of intermediate longitudinal reinforcement may not be of benefit in all cases.

3.7.3 Wight and Sozen:

A similar plot for the investigation by Wight and Sozen (31,32) is presented in Fig. 3.5(d). The equation of the best fit line is given by

$$D_i = 248(v_s f'_c)^{0.5}/v_m^{1.5} - 23 \qquad (3.7)$$

with correlation coefficient r = 0.808.

The test specimens were reinforced concrete columns with no axial load and were subjected to maximum shear stresses greater than $4\sqrt{f'_c}$. The load-deflection curves for these specimens exhibited severe pinching, as is characteristic of specimens subjected to high shear stress. This reduced the energy dissipation capacity, resulting in values of D_i less than 40 for all test specimens.

3.7.4 Hwang and Scribner:

A plot of D_i versus $(v_s f'_c)^{0.5}/v_m^{1.5}$ for the beams with $\mu = 4$ tested by Hwang and Scribner (13,14) is presented in Fig. 3.5(e). The equation of the best fit line is given by

$$D_i = 223(v_s f'_c)^{0.5}/v_m^{1.5} - 12 \qquad (3.8)$$

with correlation coefficient r = 0.923, which illustrates further the very good correlation between D_i and $(v_s f'_c)^{0.5}/v_m^{1.5}$ for beams subjected to the same load history (see Section 3.7.2).

The data points lying between values of D_i of 20 and 30 represent beams which were subjected to maximum shear stresses greater than $5\sqrt{f'_c}$. The data points with D_i near 50 represent beams with maximum shear stresses less than $4\sqrt{f'_c}$.

The effect of the displacement ductility factor, μ, on the performance of reinforced concrete beams is seen in Fig. 3.5(f) by comparing the performance of these beams to beams in the same study subjected to a ductility factor of 2. The reduced value of results in a 60 to 110% increase in D_i. This observation points out the fact that comparisons of beam performance under cyclic loading will be valid only for limited ranges in μ, for example 4 to 6. Additional work is necessary before the factors which control beam performance can be adequately compared when displacement ductility factors differ by 100% or more.

3.7.5 Ma, Bertero and Popov:

The test series by Ma, Bertero and Popov (18) is presented to illustrate the effects of both slippage within the anchorage zone and special reinforcement schemes. The plot of D_i versus $(v_s f'_c)^{0.5}/v_m^{1.5}$ for this test series is presented in Fig. 3.5(g). This figure shows the most scatter, as reflected in the correlation coefficient, $r = 0.758$, obtained from the linear regression analysis. The equation of the best fit line is given by

$$D_i = 120(v_s f'_c)^{0.5}/v_m^{1.5} - 6 \qquad (3.9)$$

The coefficient of $(v_s f'_c)^{0.5}/v_m^{1.5}$ and the correlation coefficient for this group of tests are the lowest of the five test series used in this analysis. The significant slippage of the longitudinal reinforcement that occurred in most of the beams may have contributed to both low coefficients, and the fact that the beams were subjected to different load histories may have also contributed to the scatter.

The effect of special reinforcement schemes on beam performance is shown in Fig. 3.5(h). This figure is similar to Fig. 3.5(g) except that data points representing two beams with special web reinforcement, tested in an earlier series by Bertero, Popov and Wang (4), are also shown. Of these two beams, the beam with inclined bar shear reinforcement (represented by the triangle) has a higher value of D_i than the beam with heavy conventional shear reinforcement (circle), 90 versus 62. In both cases, D_i greatly exceeds the values obtained with conventional reinforcement ($D_i \leq 47$). These reinforcement schemes are, however, complicated or make concrete placement difficult, and may not be economical to implement (4,5).

3.8 Additional Observations

3.8.1 Combined Results

The test results of this study and those of Hwang and Scribner (13,14), Scribner and Wight (23,24), and Wight and Sozen (31,32) are presented in Fig. 3.6(a), along with the statistical mean and the 95% confidence limits. The equation of the best fit line is given by

$$D_i = 188(v_s f'_c)^{0.5}/v_m^{1.5} - 9 \qquad (3.10)$$

with correlation coefficient r = 0.910.

A comparison of Eq. (3.10) with Eq. (3.5), (3.6), (3.7), and (3.8), which represent the individual studies included in Eq. (3.10), shows that the coefficient of $(v_s f'_c)^{0.5}/v_m^{1.5}$ for the combined data, 188, is well below the coefficients for all four of these test series which range from 208 to 248 (see Fig. 3.6(b)). This is the result of a bias in the data.

Values of D_i from the current study, which tend to be below the statistical mean for all of the tests, predominate at high values of $(v_s f'_c)^{0.5}/v_m^{1.5}$; most of the other tests, which tend to be above the overall statistical mean, have low values of $(v_s f'_c)^{0.5}/v_m^{1.5}$. The result is a flatter slope than obtained for the individual studies.

The bias in Eq. (3.10) means that it does not represent the trend line that would be expected if additional data were available. A better estimate of an overall trend line can be obtained by introducing "dummy" variables in the regression analysis (10) and averaging the intercepts of the resulting straight line equations. This procedure yields the following expression,

$$D_i = 222(v_s f'_c)^{0.5}/v_m^{1.5} - 17 \qquad (3.11)$$

which compares favorably with all four equations. Eq. (3.11) is compared to the test results in Fig. 3.7.

3.8.2 Other Controlling Factors

The positive correlation between D_i and $(v_s f'_c)^{0.5}/v_m^{1.5}$ is evident. However, the scatter in the test results about the statistical mean, the effects of special reinforcing schemes and anchorage deterioration, and the differences between the individual test results clearly indicate that the combined parameter, $(v_s f'_c)^{0.5}/v_m^{1.5}$, does not fully control the energy dissipation index and that there are other variables that need to be considered as well.

As mentioned earlier, the location of a data point with respect to the statistical mean does have some significance. In Fig. 3.8, three points with the same value of $(v_s f'_c)^{0.5}/v_m^{1.5}$ but different values of D_i are shown, as well as a line representing the statistical mean. One of the points lies on the line, another point lies below the line, and a third point lies above the line. The point lying on the mean line represents an "ideal" beam, whose performance is consistent with the trend of the data as controlled by v_m, f'_c, and v_s.

Since the points all have the same value of $(v_s f'_c)^{0.5}/v_m^{1.5}$, the beams represented by the other two points differ from the ideal beam in ways that are not reflected by the value of $(v_s f'_c)^{0.5}/v_m^{1.5}$.

Points that lie above the mean represent beams that perform better than expected. These beams have values of D_i greater than the mean value and may be termed "efficient". Points that lie below the mean represent beams that have values of D_i less than the

mean value. They do not perform as well as expected and are thus, "less efficient".

An example of an "efficient" beam is given in Fig. 3.5(h), where the improvement in beam performance due to the special reinforcement schemes is illustrated by the large margin that the two points (circle and triangle) lie above the mean. "Less efficient" beams are illustrated by the two beams, that suffered severe anchorage deterioration in the tests by Scribner and Wight (23,24) (square and inverted triangle in Fig. 3.5(c)) that lie below the mean.

3.8.3 Differences between Test Series

Fig. 3.6(b) and 3.7 show the statistical mean of each data group. These figures reveal a banding effect, with beams tested by different investigators lying along different means. A closer examination of beam properties shows that beams with deeper cross-sections and lower width to depth ratios, b/d, lie below the overall statistical mean (i.e. they are relatively less efficient), while those with shallower sections and higher b/d ratios lie on or above the mean (more efficient). For example, the statistical mean of the beams tested in this study lies below the overall statistical mean. These beams had b/d and d values of approximately 0.49 and 15.3 in. The beams tested by Hwang and Scribner (13,14) and Scribner and Wight (23,24) lie above the statistical mean. These beams had b/d and d values of 0.8 and 10 in. and 0.93 and 8.6 in.

The specimens tested by Wight and Sozen (31,32) had an effective depth, d, of 10 in., but a b/d value of only 0.6. The statistical mean for these specimens lies just below the overall statistical mean.

These observations strongly suggest that both size and shape affect the performance of reinforced concrete beams subject to cyclic loading. Some effects of section geometry on beam behavior are recognized in current seismic provisions (3,30): The minimum width to depth ratio is 0.3 for flexural members, and the minimum width is 10 in.

The effects of beam depth and b/d ratio on the concrete contribution to the shear strength of rectangular beams have been observed for statically loaded beams (15,17,26). The current analyses indicate similar size and shape effects and suggest that adequate confinement may depend not only on stirrup spacing as a function of beam depth (i.e. d/4), but also beam width, and possibly as a multiple of some critical material dimension such as the maximum aggregate size.

3.9 Practical Application of Findings

As developed in the current research, the energy dissipation index, D_i, is a research tool, used to compare the performance of beams with differing geometries, reinforcing ratios, and load histories. However, D_i also has potential as a design tool.

The analyses presented above indicate that in addition to the maximum applied shear stress, v_m, the concrete strength, f'_c, and the stirrup capacity, v_s, D_i is sensitive to the positive effects of special reinforcing schemes and the negative effects of bond deterioration. This sensitivity to several aspects of member performance may eventually offer the greatest potential for design applications. However, more study is required.

Two questions deserve particular attention: Is D_i a true measure of a member's performance? And if so, what values of D_i are desirable in practice?

While definitive answers to these questions await additional research, some guidelines can be set. These guidelines can be selected based on a minimum performance criterion. It is suggested that for beams serving in a lateral load resisting frame designed for a severe earthquake, the minimum criterion should be the ability to endure five full cycles of inelastic loading ($P_n \geq 0.75P_y$) when subjected to maximum displacement ductility factors between approximately 4 and 6. Gosain et. al. (12) used a similar criterion with $\mu = 5$. Beams satisfying this requirement would exhibit good toughness under severe cyclic loading.

The beams in the five studies considered in this report were evaluated using this criterion. Of the thirty five beams without special reinforcing subjected to values of μ between 3.9 and 6, sixteen were able to withstand five full cycles (Table 3.3). Of these sixteen beams, 50% had energy dissipation indices greater than or equal to 50, 81% had values of D_i in excess of 40, and 100% had

values of D_f greater than 35. Assuming that $v_s/v_m = 1.0$, these three values of D_f imply maximum shear stresses of $3.3\sqrt{f'_c}$, $3.9\sqrt{f'_c}$, and $4.3\sqrt{f'_c}$, respectively, based on Eq. (3.11)(used here as a guide). Twelve of the sixteen beams had $v_s > v_m$ (fourteen had $v_s \geq 0.95v_m$), and thirteen of the sixteen had a $v_m < 4.3\sqrt{f'_c}$.

Of the nineteen beams with $\mu \geq 3.9$ that did not sustain five complete cycles of an inelastic loading, fifteen had either a nominal stirrup strength, v_s, less than v_m or a maximum shear stress, v_m, in excess of $4.3\sqrt{f'_c}$. Of these fifteen beams, six had both $v_s < v_m$ and $v_m > 4.3\sqrt{f'_c}$.

Four beams that did not sustain four cycles had $v_s > v_m$ and $v_m < 4.3\sqrt{f'_c}$. However, these beams, from the study by Ma, Bertero and Popov (18), exhibited severe bond deterioration within the joint, and are not completely applicable to establishing design criteria for flexural members alone.

Based on this analysis, it is recommended that the current procedure (3,30) of disregarding the concrete contribution to shear capacity, V_c, should be continued for flexural members subjected to severe seismic loading. The result of this requirement is to require the design stirrup capacity, ϕv_s, to be greater than the factored shear, v_u ($=V_u/b_w d$). In addition, design values of $D_f \geq 35$ are desirable in terms of member behavior. This value of D_f represents a maximum shear stress of approximately $4.6\sqrt{f'_c}$, for $\phi v_s/v_m = 1$ ($v_s/v_m = 1.18$), the minimum required for flexural members subjected to severe seismic loading (3,30). Higher values of applied shear could be sustained with added shear steel. However, Eq. (3.10) and (3.11)

suggest that v_s would have to be increased more rapidly than v_m (or v_u) to maintain a desired value of D_i.

For example using Eq. (3.11) to maintain a value of D_i = 35 for an 30% increase in v_m from $4.6\sqrt{f'_c}$ to $6.0\sqrt{f'_c}$, requires an 68% in v_s from $1.18v_m$ to $1.98v_m$. The required increases in shear reinforcement to maintain D_i become unrealistic very rapidly, and it may be more efficient to increase the beam width, with no increase in reinforcing steel. The moment capacity would be maintained, while the induced shear stress would be reduced. An increase in concrete strength would be another option to consider, to be used alone or in conjunction with an increase in v_s and a decrease in v_m.

Chapter 4

SUMMARY AND CONCLUSIONS

4.1 Summary

The primary objective of this research is to study the cyclic behavior of lightly reinforced concrete beams subjected to large displacement excursions, on the order of four to five times the yield displacement.

Seven cantilever beams with enlarged end blocks were tested. The beams had reinforcement ratios of 0.69 or 1.0 percent, stirrup capacities ranging from 78 to 116% of the applied shear, stirrup spacings ranging from 0.11d to 0.25d, and ratios of positive to negative longitudinal reinforcement of 0.5 and 0.75. The longitudinal reinforcement was firmly anchored to prevent slip within the joint.

The dissipated energy is used to compare beam behavior under cyclic load, and an energy dissipation index, D_1, is developed to serve as a measure of the performance of reinforced concrete beams subjected to cyclic loading. The test results from this study and those of four other test series are compared, and recommendations for design are made.

4.2 Conclusions

The following conclusions are based on the tests and analyses presented in this report.

1. For a beam subjected to cyclic loading, the use of a low reinforcement ratio reduces the maximum shear and compressive stresses to which the beam is subjected and thus reduces the rate of degradation.

2. The number of inelastic cycles endured and the total energy dissipated can be increased by:

   a) The use of a reduced stirrup spacing to improve concrete confinement and delay buckling of the longitudinal steel. This improvement can be obtained even with some reduction in total stirrup capacity.

   b) An increase in the ratio of positive to negative steel to delay spalling of the compressed bottom concrete and buckling of the bottom (positive) steel.

   c) A decrease in the maximum displacement ductility factor, μ.

3. The energy dissipation index, D_1, developed in this study appears to provide a consistent measure of beam performance under cyclic loading and should prove useful in applications to structural design. D_1 appears to be primarily controlled by the maximum shear stress imposed

on the beam, the concrete strength, and the nominal capacity of the shear reinforcing. It is also sensitive to modifications in detailing, anchorage slip, and beam geometry.

4. The energy dissipation index analyses of test results indicate that:

a) The performance of reinforced concrete beams subjected to cyclic loading will improve with a decrease in maximum shear stress, and an increase in concrete strength and nominal stirrup capacity.

b) Performance also appears to improve with an increase in the ratio of positive to negative reinforcement at the face of the support, but a sizeable portion of the increased energy dissipation capacity is required by the structure to satisfy the added energy dissipation demand. However, the net effect of the increase in the ratio of positive to negative reinforcement is to improve performance.

c) Special reinforcement schemes can improve beam performance significantly.

d) Bond slip within a joint will sizeably reduce the performance of a beam.

e) The shape and size of a beam may affect its performance under cyclic loading. Beams with low width to effective depth ratios, b/d, and large effective depths appear to be less efficient when compared to beams with higher b/d values and smaller effective depths.

f) A value of 35 for the energy dissipation index, D_1, appears to provide adequate performance under cyclic loading. This corresponds to a maximum shear stress of approximately $4.3\sqrt{f'_c}$ for a nominal value of shear reinforcing, V_s, equal to the maximum applied shear, V_u, and $4.6\sqrt{f'_c}$ for $\phi V_s = V_u$.

4.3 Recommendations for Future Work

1. The maximum shear stress is considered to be one of the most important factors in the design of reinforced concrete beams subjected to cyclic loading, and recommendations have been made to limit its value to $6\sqrt{f'_c}$ (5,12). To effect this, one of the recommendations that has been made is to reduce the flexural reinforcement ratio. Another option to improve performance, however, is to increase the concrete strength. A higher strength concrete will withstand higher compressive and shear stresses, dilate less under load, allow for the use of less congested reinforcement, and thus, make concrete placement and consolidation less difficult. Tests run to date have

used only a very limited range of concrete strength. This narrow range limits how much confidence can be placed in a relationship based on the square root of the concrete strength. Therefore, to help more fully evaluate the effect of concrete strength on beam performance, tests with concrete strengths considerably above 5000 psi are needed. With current technology, concrete strengths up to 15,000 psi appear to be worth investigation for special applications in seismic resistant structures.

2. The energy dissipation index, D_f, is a measure of beam performance under cyclic load. It was developed to represent performance within a structure. How well it measures that performance, however, needs additional study: Are the approximations used realistic? Will structures perform well if the individual members have high energy dissipation indices? If so, what values of D_f are desirable in practice and what are the best ways to achieve a high value of D_f? Can the concept be extended to members under axial load? The answers to these questions may offer important opportunities for improvements in the design and construction of lateral load resisting frames subject to severe earthquakes.

REFERENCES

1. ACI Committee 318, "Building Code Requirements for Reinforced Concrete (ACI 318-71)," American Concrete Institute, Detroit, Michigan, 1971, 78 pp.

2. ACI Committee 318, "Building Code Requirements for Reinforced Concrete (ACI 318-77)," American Concrete Institute, Detroit, Michigan, 1977, 102 pp.

3. ACI Committee 318, "Building Code Requirements for Reinforced Concrete (ACI 318-83)," American Concrete Institute, Detroit, Michigan, 1983, 111 pp.

4. Bertero, V. V., Popov, E. P., and Wang, T. Y., "Hysteretic Behavior of Reinforced Concrete Flexural Members with High Shear," Earthquake Engr. Research Center, University of California, Berkeley, Report No. EERC 74-9, Aug. 1972, 126 pp.

5. Bertero, V. V., and Popov, E. P., "Seismic Behavior of Ductile Moment- Resisting Reinforced Concrete Frames," Reinforced Concrete Structures in Seismic Zones, Publ. SP-53, American Concrete Institute, Detroit, 1977, pp. 247-291.

6. Bresler, B., and Scordelis, A. C., "Shear Strength of Reinforced Concrete Beams," Journal of the American Concrete Institute, Vol. 60, No. 1, Jan. 1963, pp. 51-74.

7. Brown, R. H., and Jirsa, J. O., "Reinforced Concrete Beams Under Load Reversals," Journal of the American Concrete Institute, Vol. 68, No. 5, May 1971, pp. 380-390.

8. Brown, R. H., and Jirsa, J. O., "Shear Transfer of Reinforced Concrete Beams Under Load Reversals," Shear in Reinforced Concrete, Publ. SP-42, American Concrete Institute, 1974, pp. 347-357.

9. Burns, N. H., and Siess, C. P., "Repeated and Reversed Loading in Reinforced Concrete," Journal of the Structural Division, ASCE, Vol. 92, No. ST5, Oct. 1966, pp. 65-78.

10. Draper, N. R., and Smith, H., Applied Regression Analysis, Second Edition, John Wiley & Sons, Inc., 1981, pp. 241-249.

REFERENCES (continued)

11. Ehsani, R. M., and Wight, J. K., "Behavior of External Reinforced Concrete Beam to Column Connections Subjected to Earthquake Type Loading," Report No. UMEE 82R5, Department of Civil Engineering, University of Michigan, Ann Arbor, MI., 243 pp.

12. Gosain, N. K., Brown, R. H., and Jirsa, J. O., "Shear Requirements for Load Reversals on RC Members," Journal of the Structural Division, ASCE, Vol. 103, No. ST7, July 1977, pp. 1461-1476.

13. Hwang, T. H., "Effects of Variation in Load History on Cyclic Response of Concrete Flexural Members," Thesis submitted to the University of Illinois, at Urbana-Champaign, Ill., in July 1982, in partial fulfillment of the requirements for the degree of Doctor of Philosophy, 232 pp.

14. Hwang, T. H., and Scribner, C. F., "R/C Member Cyclic Response during Various Loadings," Journal of Structural Engineering, ASCE, Vol. 110, No. 3, March 1984, pp. 477-489.

15. Kani, G. N. J., "How Safe Our Large Reinforced Concrete Beams?," Journal of the American Concrete Institute, Vol. 64, No. 3, March 1967, pp. 128-141.

16. Lee, D. L. N., Wight, J. K., and Hanson, R. D., "RC Beam-Column Joints under Large Load Reversals," Journal of the Structural Division, ASCE, Vol. 103, No. ST12, Dec. 1977, pp. 2337-2350.

17. Leonhardt, F., and Walther, R., "The Stuttgart Shear Tests, 1961," Translation No. 111, Cement and Concrete Association, London, England, 1964.

18. Ma, S. M., Bertero, V. V., and Popov, E. P., "Experimental and Analytical Studies on the Hysteretic Behavior of Reinforced Concrete Rectangular and T-Beams," Earthquake Engr. Research Center, University of California, Berkeley, Report No. EERC 76-2, May 1976, 254 pp.

19. Park, R., Kent, D. C., and Sampson, R. A., "Reinforced Concrete Members with Cyclic Loading," Journal of the Structural Division, ASCE, Vol. 98, No. ST7, July 1972, pp. 1341-1360.

REFERENCES (continued)

20. Paulay, T., "Simulated Seismic Loading of Spandrel Beams," Journal of the Structural Division, ASCE, Vol. 97, No. ST9, Sept. 1971, pp. 2407-2419.

21. Popov, E. P., Bertero, V. V., and Krawinkler, H., "Cyclic Behavior of Three Reinforced Concrete Flexural Members with High Shear," Earthquake Engr. Research Center, University of California, Berkeley, Report No. EERC 72-5, Oct. 1972, 78 pp.

22. Ruiz, W. M., and Winter, G., "Reinforced Concrete Beams under Repeated Loads," Journal of the Structural Division, ASCE, Vol. 95, No. ST6, June 1969, pp. 1189-1211.

23. Scribner, C. F., and Wight, J. K., "Strength Decay in Reinforced Concrete Beams under Load Reversals," Journal of the Structural Division, ASCE, Vol. 106, No. ST4, April 1980, pp. 861-875.

24. Scribner, C. F., and Wight, J. K., "Delaying Shear Strength Decay in Reinforced Concrete Flexural Members under Large Load Reversals," Report No. UMEE 78R2, Department of Civil Engineering, University of Michigan, Ann Arbor, MI., 221 pp.

25. Sozen, M. A., "The Caracas Earthquake of July 29, 1967," Journal of the American Concrete Institute, Vol. 65, No. 5, May 1968, pp. 394-401.

26. Swarmi, R. M., and Qureshi, S. A., "Strength, Cracking and Deformation Similitude in Reinforced T-Beams under Bending and Shear," Journal of the American Concrete Institute, Vol. 68, No. 3, March 1971, pp. 187-195.

27. "The San Fernando, California Earthquake of February 9, 1971," Geological Survey Professional Paper 733, U. S. Department of Interior - U. S. Department of Commerce, Washington, D. C., 1971, pp. 188-200.

28. "The Imperial Valley, California Earthquake of October 15, 1979," Geological Survey Professional Paper 1254, U. S. Department of Interior - Geological Survey Department, Washington, D. C., 1982, pp. 273-280.

29. Townsend, W. H., and Hanson, R. D., "Reinforced Concrete Connection Hysteresis Loops," Reinforced Concrete Structures in Seismic Zones, Publ. SP-53, American Concrete Institute, Detroit, 1977, pp. 351-370.

REFERENCES (continued)

30. Uniform Building Code, 1982 Edition, International Conference of Building Officials, Whittier, California, 780 pp.

31. Wight, J. K., and Sozen, M. A., "Shear Strength Decay in Reinforced Concrete Columns Subjected to Large Deflection Reversals," Civil Engineering Studies, SRS No. 403, University of Illinois at Urbana-Champaign, Aug. 1973, 290 pp.

32. Wight, J. K., and Sozen, M. A., "Strength Decay of RC Columns under Shear Reversals," Journal of the Structural Division, ASCE, Vol. 101, No. ST5, May 1975, pp. 1053-1065.

TABLE 2.1 BEAM AND REINFORCEMENT PROPERTIES

PROPERTY	BEAM						
	F-1	F-2	F-3	F-4	F-5	F-6	F-7
Length, l(in.)	68	68	68	68	68	68	68
Height, h(in.)	18	18	18	18	18	18	18
Width, b(in.)	7.5	7.5	7.5	7.5	7.5	7.5	7.5
Effective Depth, d(in.)	15.25	15.38	15.38	15.25	15.25	15.38	15.38
Effective Depth, d_1(in.)	15.75	16.25	16.25	16.38	16.38	16.25	16.38
Core Width, b_c(in.)	4.5	5.5	5.5	5.25	5.25	5.5	5.5
Core Depth, d_c(in.)	15.0	16.0	16.0	15.75	15.75	16.0	15.75
Shear Span, a(in.)	60	60	60	60	60	60	60
a/d	3.9	3.9	3.9	3.9	3.9	3.9	3.9
Reinf. Ratio, (%)	1.03	1.02	0.69	0.69	0.69	0.69	0.69
Top Reinf., A_s($in.^2$)	6#4	6#4	4#4	4#4	4#4	4#4	4#4
Bot Reinf., A'_s($in.^2$)	3#4	3#4	2#4	2#4	2#4	3#4	2#4
A'_s/A_s	0.5	0.5	0.5	0.5	0.5	0.75	0.5
f_y (ksi)	73.8	73.8	73.8	73.8	73.8	73.8	73.8
Stirrup dia. (in.)	.300	.300	.300	.179	.179	.300	.179(1)
Stirrup Spacing, s(in.)	3.8	3.8	3.8	1.6	2.1	3.8	3.8
f_{vy} (ksi)	32.5	32.5	32.5	38.2	38.2	32.5	38.2

(1) Double Stirrups

COLUMN-STUB (ALL SPECIMENS) : Height, H = 60 in.
Length, L_1 = 28 in.
Width, W = 15 in.

TABLE 2.2 COMPUTED AND MEASURED SHEARS

BEAM	NOMINAL STIRRUP CAPACITY		CALCULATED SHEARS		TEST SHEARS		MAXIMUM SHEAR STRESS	
	V_s (1) (kips)	v_s (2) (psi)	V_y (3) (kips)	V_m (4) (kips)	V_y (kips)	V_m (kips)	v_m (psi)	$v_m/\sqrt{f'_c}$
F-1	18.0	161	19.8	24.0	18.2	22.5	197	3.01
F-2	19.3	161	19.9	24.2	19.7	24.8	215	3.31
F-3	19.2	160	13.8	16.9	13.5	16.7	145	2.22
F-4	18.7	158	13.7	16.8	13.0	16.1	141	2.14
F-5	14.3	121	13.7	16.8	13.0	16.3	143	2.16
F-6	19.2	160	13.8	16.9	13.3	16.7	145	2.20
F-7	15.7	133	13.8	16.9	13.3	16.6	144	2.22

(1) $V_s = A_v f_{vy}$

(2) $v_s = A_v f_{vy}/bs$

(3) V_y = shear force at yielding of main longitudinal reinforcement

(4) V_m = maximum shear force

TABLE 2.3 CONCRETE PROPERTIES

Beam	Mix Proportions by weight	Slump (in.)	Air Content (%)	f'_c (1) (psi)	f_r (2) (psi)	Age at Testing (days)
F-1	1.0:2.88:2.88	2.50	2.5	4260	420	10
F-2	1.0:2.88:2.88	2.75	5.5	4220	535	7
F-3	1.0:2.88:2.88	2.00	4.5	4260	390	13
F-4	1.0:2.88:2.88	4.00	3.5	4330	530	14
F-5	1.0:2.88:2.88	2.00	2.5	4370	440	9
F-6	1.0:2.88:2.88	1.50	2.5	4320	480	11
F-7	1.0:2.88:2.88	1.75	2.0	4220	475	13

(1) f'_c - compressive strength from 6 x 12 in. cylinders.

(2) f_r - modulus of rupture from 6 x 6 x 22 in. flexural specimens, third point loading on an 18 in. span.

TABLE 2.4 PRINCIPAL EXPERIMENTAL RESULTS

Beam	Yield Load (kips)	Max. Load (kips)	Yield Defl. (in.)	Max. Defl. (in.)	μ*	Growth (in.)	# of Cycles $P_n \geq 0.75P_y$	# of Cycles Total
F-1	18.2	22.5	0.656	2.54	3.9	0.404	5	$5\frac{1}{2}$
F-2	19.7	24.8	0.533	2.73	5.1	0.442	2	4
F-3	13.5	16.7	0.467	2.04	4.4	0.371	6	6
F-4	13.0	16.1	0.400	2.04	5.1	0.406	9	11
F-5	13.0	16.3	0.447	2.04	4.6	0.423	8	12
F-6	13.3	16.7	0.383	2.04	5.3	0.383	9	9
F-7	13.3	16.6	0.400	2.04	5.1	0.357	6	6

* Displacement ductility factor

TABLE 3.1 ENERGY DISSIPATION FOR BEAMS IN CURRENT STUDY

Beam	Energy Dissipated[1] (kip-in.)
F-1	287
F-2	169
F-3	201
F-4	297
F-5	262
F-6	328
F-7	201

(1) Cycles with $P_n \geq 0.75P_y$

Table 3.2 Test Results used in D_1 Analyses

Beam	ρ (%)	A'_s/A_s	b (in.)	d (in.)	f'_c (psi)	v_s/v_m	$v_m/\sqrt{f'_c}$	P_y (kips)	Δ_y (in.)	E (kip-in.)	μ_{max}	# of Cycles* $\mu\geq 2$	# of Cycles* $\mu\geq 4$	$(v_s f'_c)^{0.5}/v_m^{1.5}$	D_1
Current Study:															
F-1	1.03	0.5	7.5	15.25	4260	0.80	3.01	18.2	0.66	287	3.9	5	5	0.30	38
F-2	1.02	0.5	7.5	15.38	4220	0.78	3.31	19.7	0.53	169	5.1	2	2	0.27	25
F-3	0.69	0.5	7.5	15.38	4260	1.15	2.22	13.5	0.47	201	4.4	6	6	0.48	50
F-4	0.69	0.5	7.5	15.25	4330	1.16	2.14	13.0	0.40	297	5.1	9	9	0.50	87
F-5	0.69	0.5	7.5	15.25	4370	0.87	2.16	13.0	0.45	262	4.6	8	8	0.43	70
F-6	0.69	0.75	7.5	15.38	4320	1.15	2.20	13.3	0.38	328	5.3	9	9	0.49	79
F-7	0.69	0.5	7.5	15.38	4220	0.95	2.22	13.3	0.40	201	5.1	6	6	0.44	59
Scribner & Wight (22,23):															
1	1.27	0.69	8.0	8.6	4970	1.85	2.06	8.9	0.39	366	6.0	12	12	0.66	142
2(1)	1.27	0.69	8.0	8.6	4970	1.68	2.24	8.9	0.47	394	6.0	12	12	0.58	127
3(2)	1.63	0.69	8.0	10.1	4970	1.01	3.06	14.4	0.54	274	6.0	7	7	0.33	47
4(1)	1.63	0.69	8.0	10.1	4970	0.89	3.45	16.4	0.66	407	6.0	8	8	0.27	51
5	1.27	0.69	8.0	8.6	3980	1.29	3.35	11.6	0.43	275	6.0	10	10	0.34	74
6(1)	1.27	0.69	8.0	8.6	3980	1.23	3.44	12.0	0.37	327	6.0	12	12	0.32	99
7(3)	1.63	0.69	8.0	10.1	3980	3.72	3.60	15.0	0.70	365	6.0	10	10	0.54	47
8(1)	1.63	0.69	8.0	10.1	3980	0.89	3.84	17.0	0.80	418	6.0	10	10	0.25	41
9	2.62	0.77	10.0	12.1	4940	1.14	4.92	34.2	1.10	1267	6.0	7	7	0.22	42
10(1)	2.62	0.77	10.0	12.1	4940	1.12	5.09	35.8	1.07	1358	6.0	7	7	0.21	45
11	2.62	0.77	10.0	12.1	4940	0.92	6.16	41.0	0.72	723	6.0	4	4	0.16	31
12(1)	2.62	0.77	10.0	12.1	4940	0.91	6.23	46.0	0.90	792	6.0	5	5	0.15	24
Wight & Sozen (30,31):															
00.033W	1.47	1.0	5.9	10.1	4640	0.57	4.34	17.3	0.44	131	4.0	7	1	0.17	17
00.048W	1.47	1.0	6.0	10.1	3750	0.74	5.20	16.3	0.50	182	4.0	7	1	0.17	22
00.067W	1.47	1.0	6.2	10.0	4610	0.98	4.85	15.2	0.44	240	4.0	9	3	0.20	36
00.105E	1.47	1.0	6.1	10.1	4850	1.22	5.50	18.4	0.50	189	4.0	3	3	0.20	21
00.105W	1.47	1.0	6.2	10.0	4850	1.26	5.33	18.4	0.53	220	4.0	3	3	0.21	22
00.147E	1.47	1.0	6.0	10.1	4900	1.77	5.45	17.0	0.44	293	4.0	6	6	0.24	39
00.147W	1.47	1.0	5.9	10.0	4900	1.77	5.45	18.1	0.47	327	4.0	6	6	0.24	38
Hwang & Scribner (12,13):															
1-1(4)	1.65	0.69	8.0	9.9	5900	1.07	3.3	18.9	0.41	590	2.0	110	-	0.31	103
1-2	1.65	0.69	8.0	10.1	5880	0.97	3.6	18.6	0.41	343	4.0	13	13	0.27	61
1-4	1.65	0.69	8.0	9.9	4980	1.20	3.5	17.2	0.40	248	4.0	13	7	0.31	49
2-1(4)	2.34	0.73	8.0	9.6	5100	0.73	5.1	25.9	0.38	360	2.0	60	-	0.17	48
2-2	2.34	0.73	8.0	9.6	5300	0.70	5.2	24.6	0.37	160	4.0	4	4	0.16	23
2-3	2.34	0.73	8.0	9.7	4710	0.71	6.0	25.9	0.44	171	4.0	7	3	0.14	20
2-4	2.34	0.73	8.0	9.6	4780	0.68	5.6	25.9	0.37	151	4.0	5	3	0.15	21
3-1(4)	2.34	0.73	8.0	9.7	4910	1.68	7.1	35.8	0.25	320	2.0	50	-	0.18	47
3-2	2.34	0.73	8.0	9.8	4970	1.64	7.3	34.4	0.25	155	4.0	4	4	0.18	23
3-3	2.34	0.73	8.0	9.6	4980	1.68	7.0	35.5	0.25	196	4.0	8	4	0.19	29
3-4	2.34	0.73	8.0	9.7	5060	1.57	7.4	36.1	0.25	178	4.0	6	4	0.17	26
Ma, Bertero & Popov (16):															
R-2(3)	1.4	0.53	9.0	14.0	4190	1.03	2.94	22.5	0.56	267	4.9	7	1	0.35	32
R-4(3)	1.4	0.53	9.0	14.0	4380	1.76	3.38	22.8	0.60	336	7.2	1	1	0.39	38
R-5(3)	1.4	1.0	9.0	14.0	4580	1.13	5.16	39.3	0.36	349	4.4	10	3	0.21	24
R-6(3)	1.4	1.0	9.0	14.0	4340	1.68	3.55	24.0	0.62	738	4.4	13	5	0.37	47
T-1(3)	1.4	0.53	9.0	14.0	4790	1.48	3.84	32.9	0.72	519	4.1	7	1	0.32	33
T-2(3)	1.4	0.53	9.0	14.0	4610	1.32	4.38	32.0	0.75	234	5.5	-	-	0.26	15
T-3(3)	1.4	1.0	9.0	14.0	4470	1.41	4.18	31.2	0.75	803	4.2	10	4	0.28	33
Bertero, Popov & Wang (4):															
33(5)	1.58	1.0	15.0	25.5	5400	1.64	5.80	130.0	0.80	6470	5.25	13	6	0.22	62
351(5)	1.58	1.0	15.0	25.5	5500	1.91	6.2	132.0	0.80	9510	6.4	14	7	0.23	90

(1) Intermediate Reinforcement
(2) Performed Poorly
(3) Severe Anchorage Deterioration
(4) Displacement Ductility Factor = 2
(5) Special Web Reinforcement
* Number of Complete Cycles in which $P_n \geq 0.75 P_y$

TABLE 3.3 BEAMS THAT SURVIVED AT LEAST FIVE CYCLES OF INELASTIC LOADING, $3.9 \leq \mu \leq 6$

Investigation	$D_i \leq 50$	$D_i \geq 50$	$D_i \leq 40$	$D_i \geq 40$	$D_i \leq 35$	$D_i \geq 35$
Current Study	1	5	1	5	0	6
Scribner & Wight (23,24)	3	2	0	5	0	5
Wight & Sozen (31,32)	2	0	2	0	0	2
Hwang & Scribner (13,14)	1	1	0	2	0	2
Ma, Bertero & Popov (18)	1	0	0	1	0	1
TOTAL	8	8	3	13	0	16
%	50	50	19	81	0	100

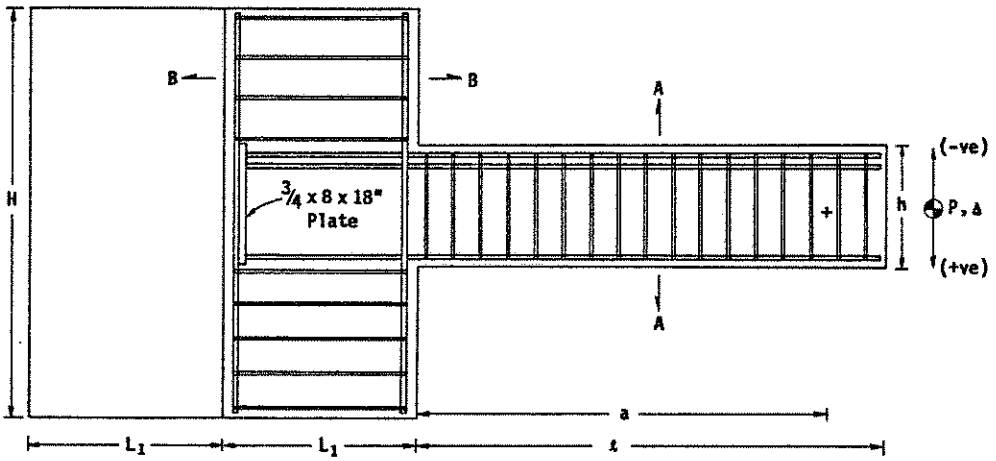

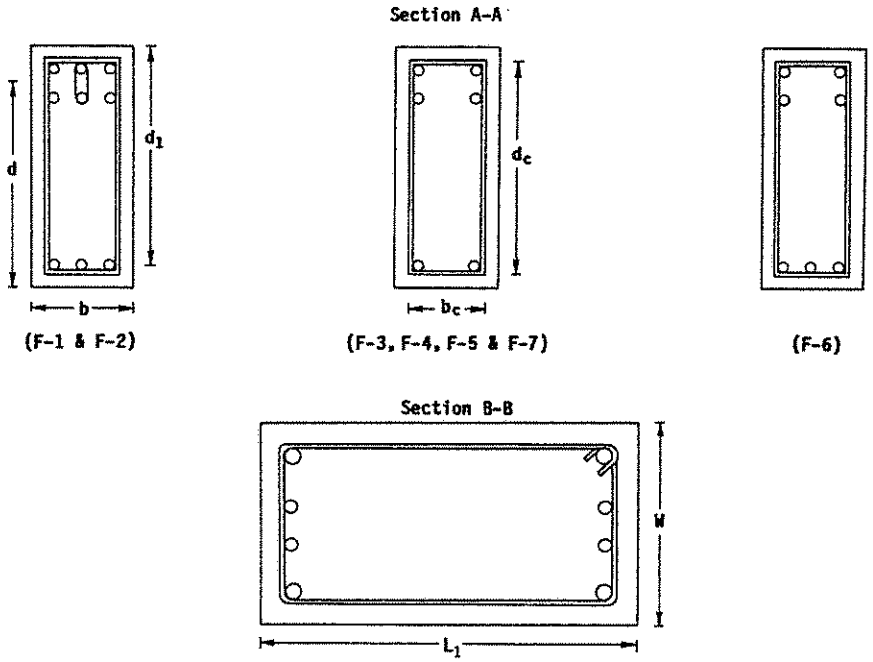

Fig. 2.1 Schematic Diagram of Test Beam showing Details of Reinforcement

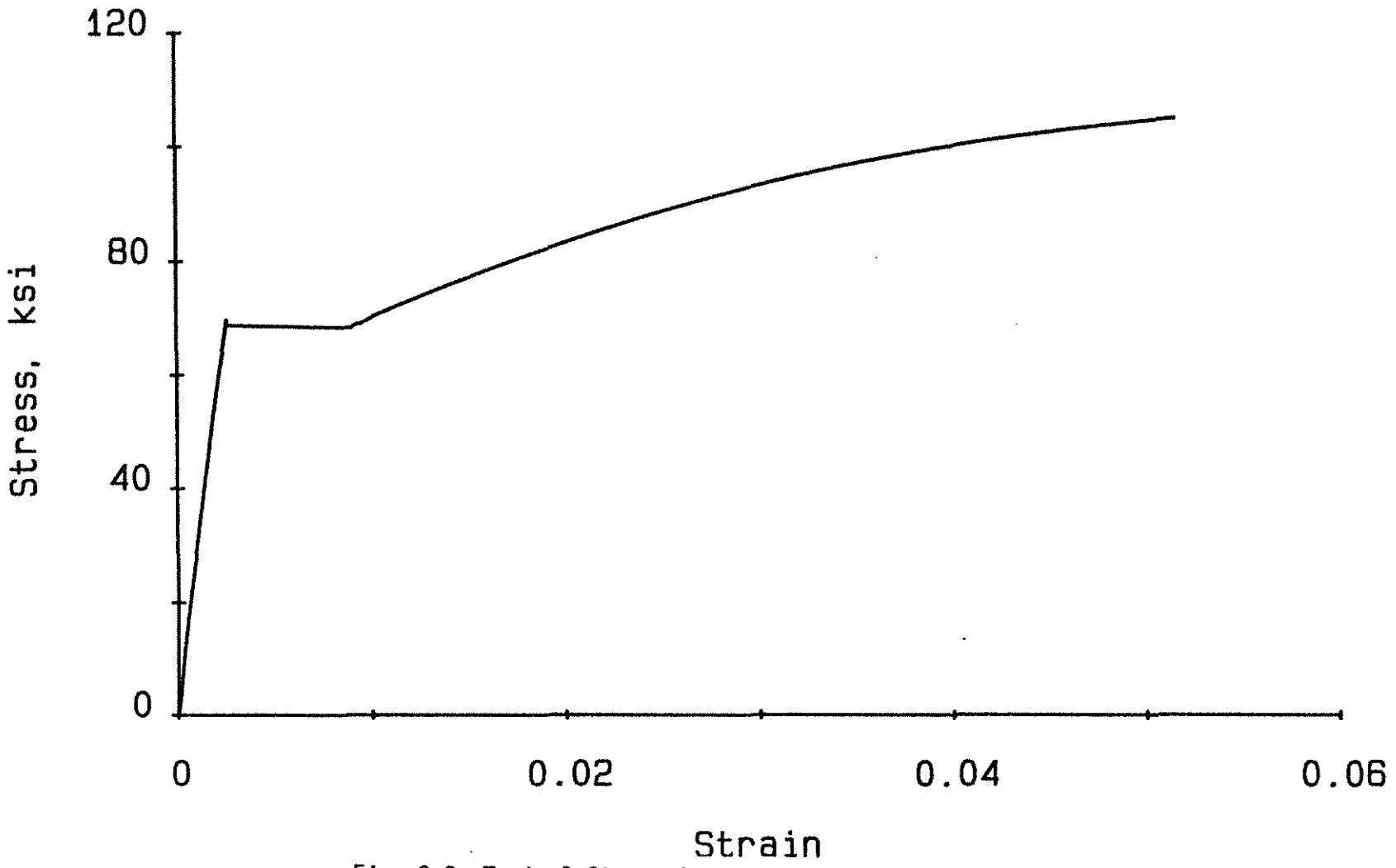

Fig. 2.2 Typical Stress-Strain Curve for #4 Deformed Bar

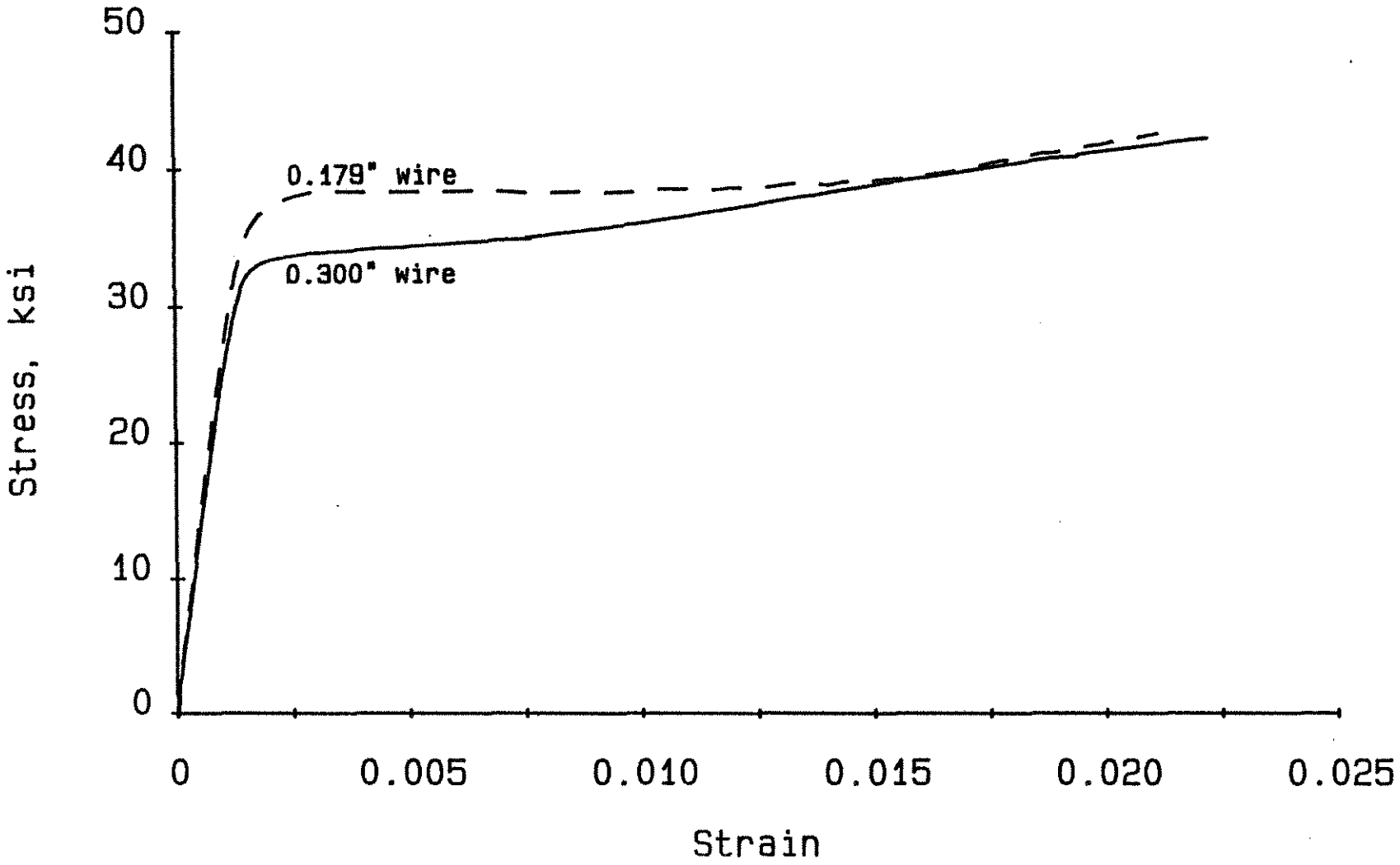

Fig. 2.3 Typical Stress-Strain Curves for 0.179 in. and 0.3 in. Wire Stirrups

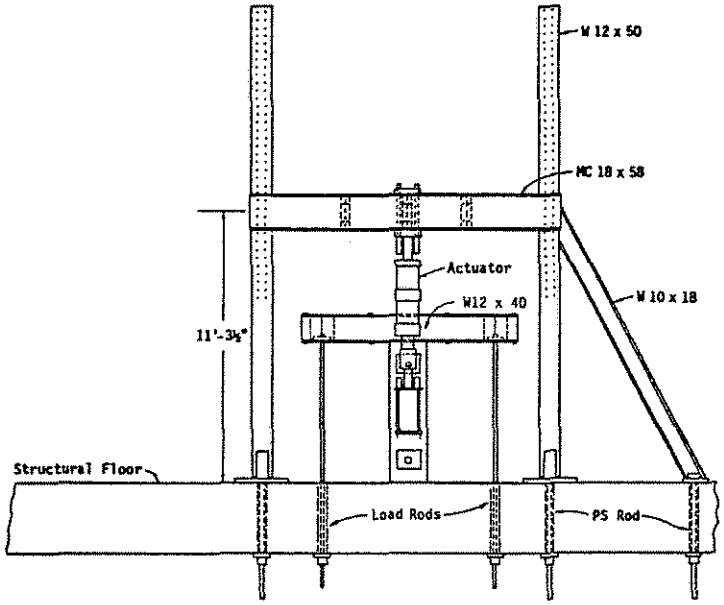

Fig. 2.4(a) Specimen in Test Position, End View

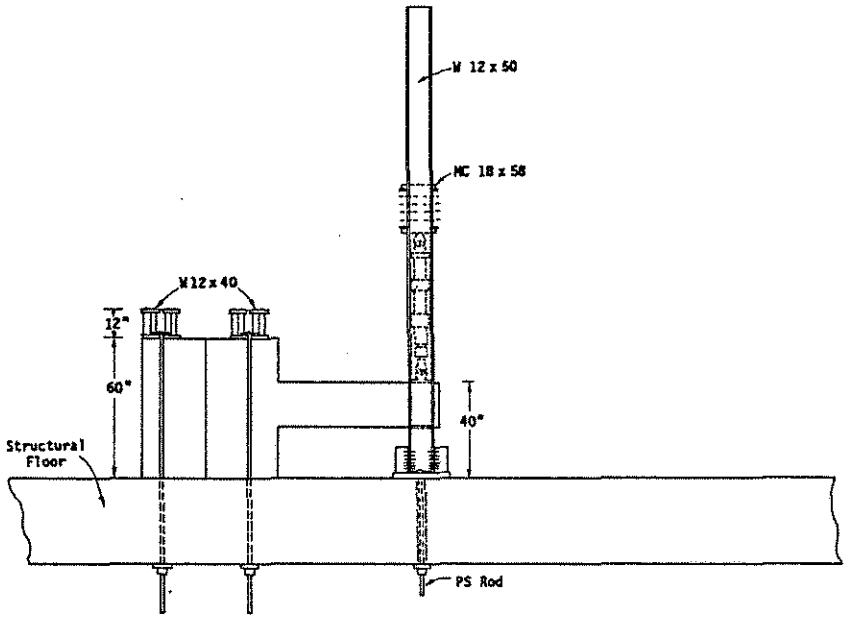

Fig. 2.4(b) Specimen in Test Position, Side View

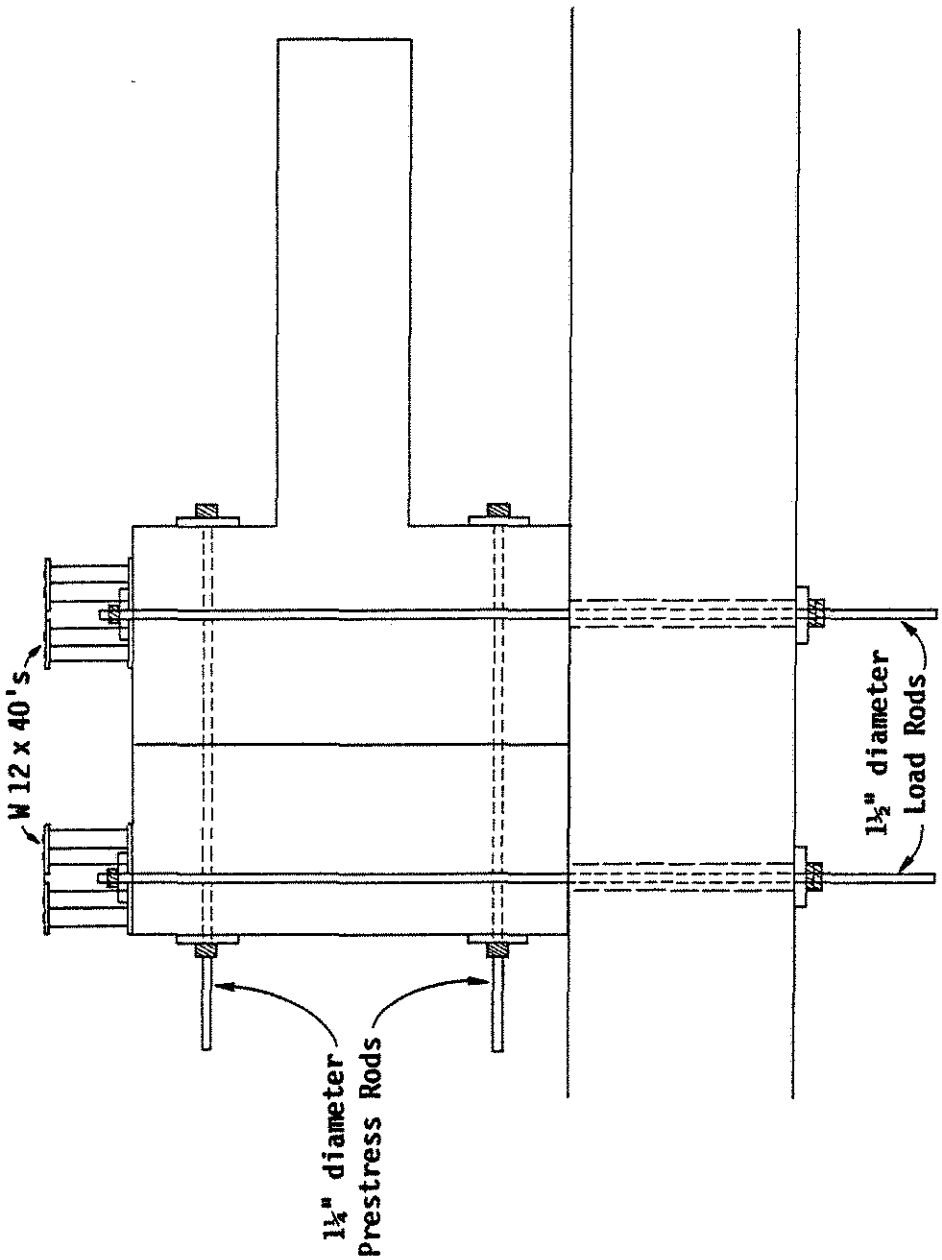

Fig. 2.5 Prestress Arrangement for Column-Stubs

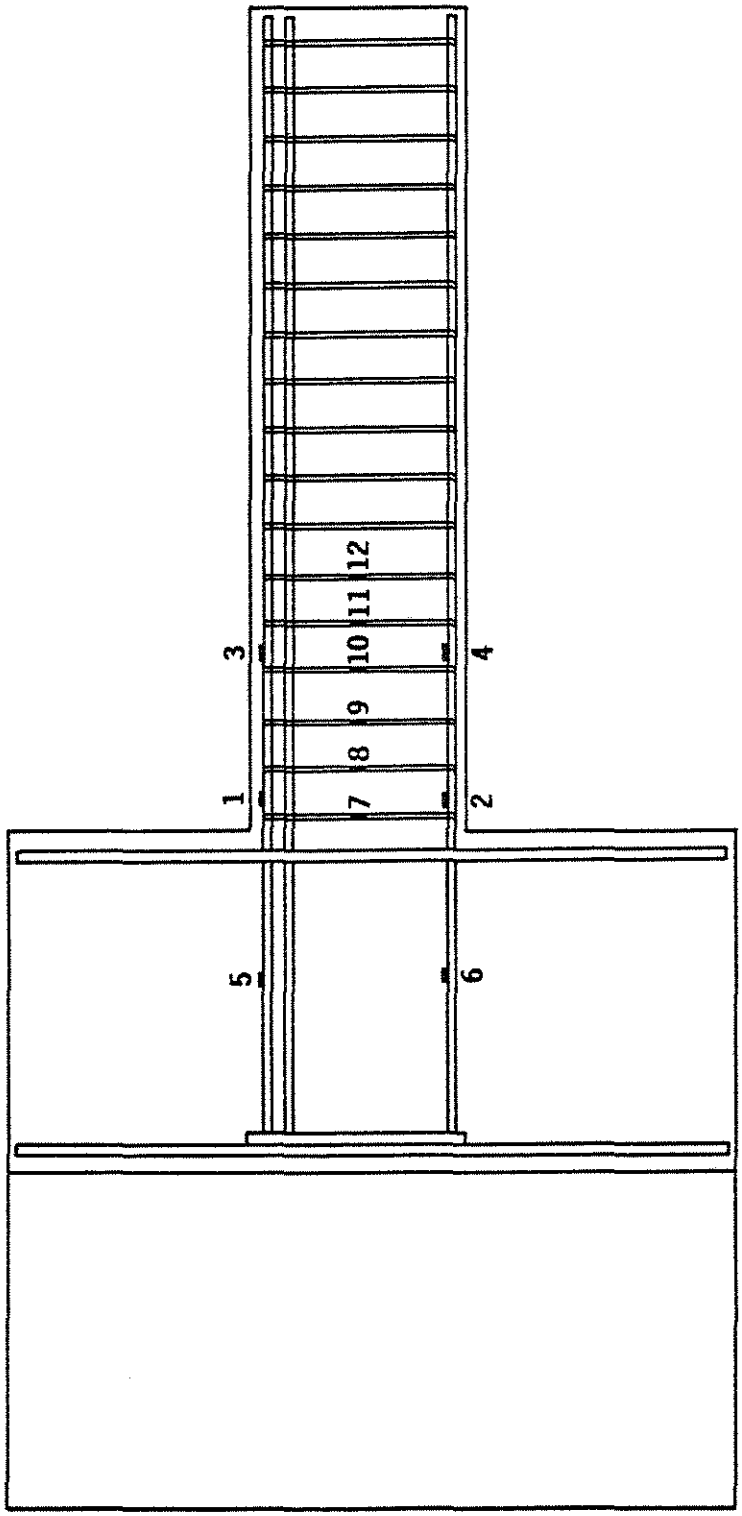

Fig. 2.6 Location of Strain Gages

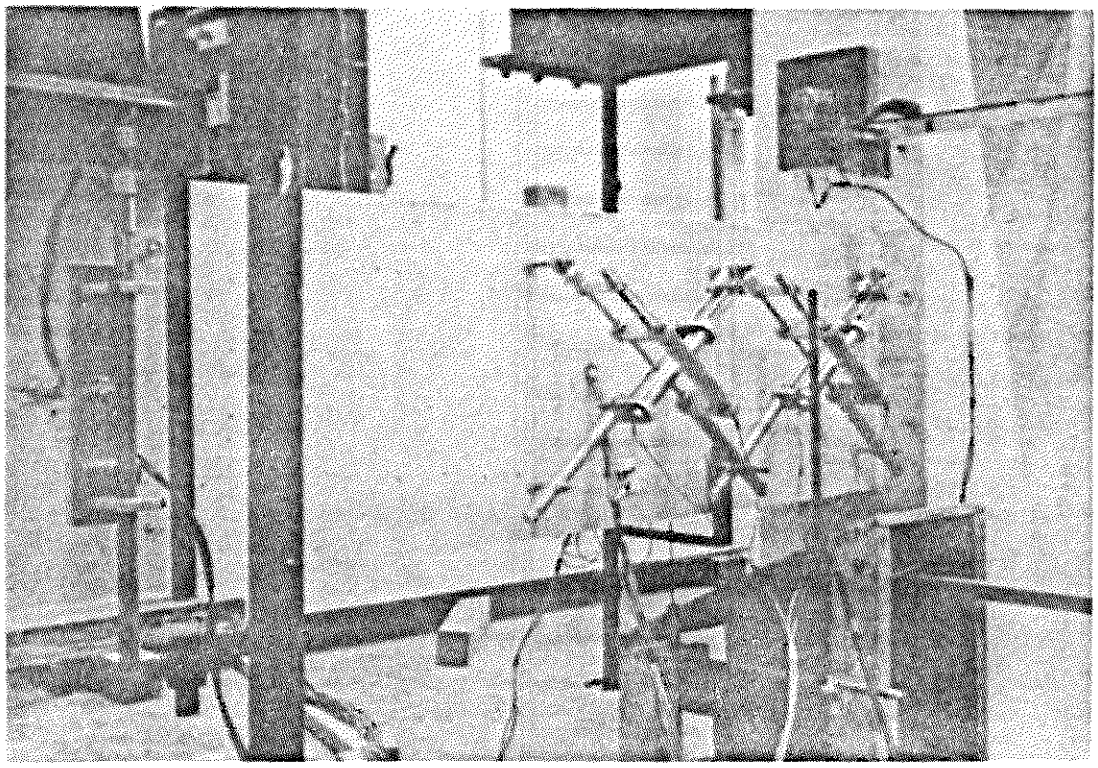

Fig. 2.7(a) LVDT Arrangement for Measurement of Shear Deformation

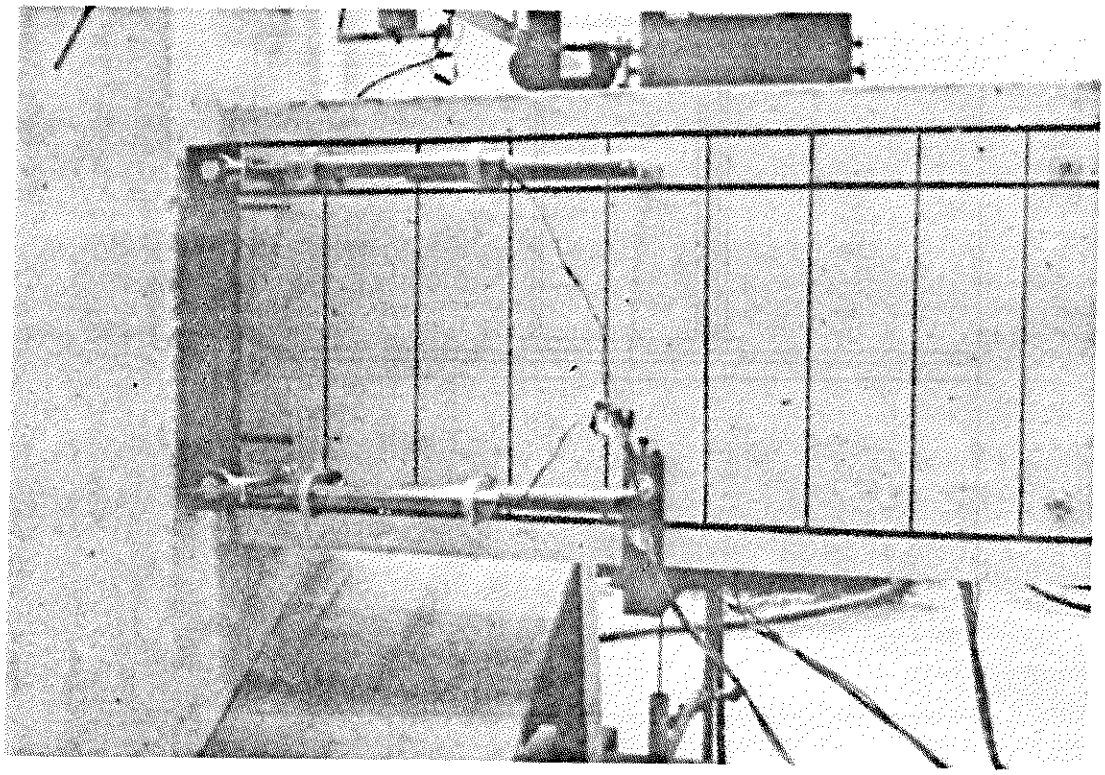

Fig. 2.7(b) LVDT Arrangement for Measurement of Flexural Rotation of Beam Relative to Column-Stub

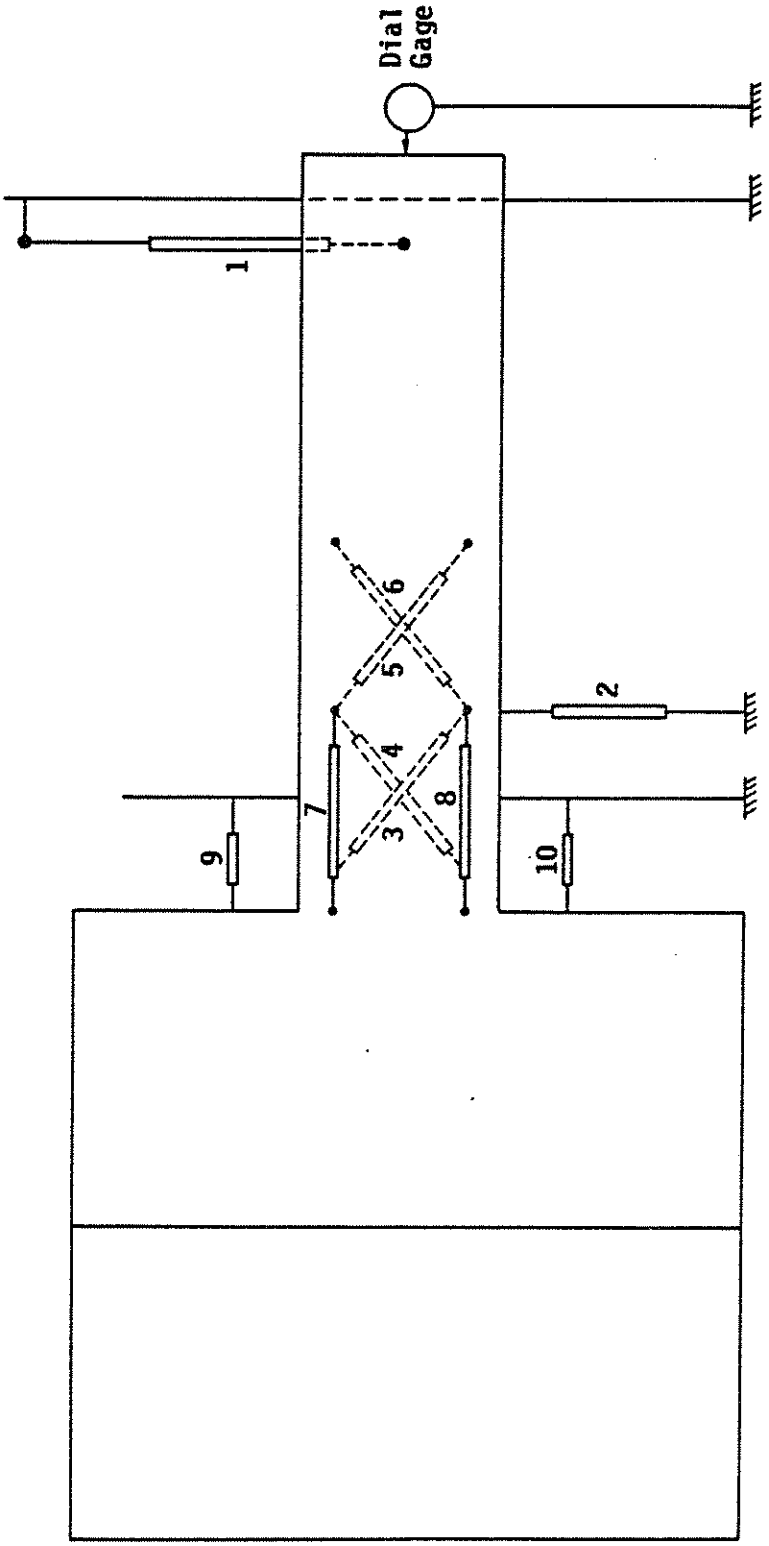

Fig. 2.7(c) Location of Dial Gage and LVDTs

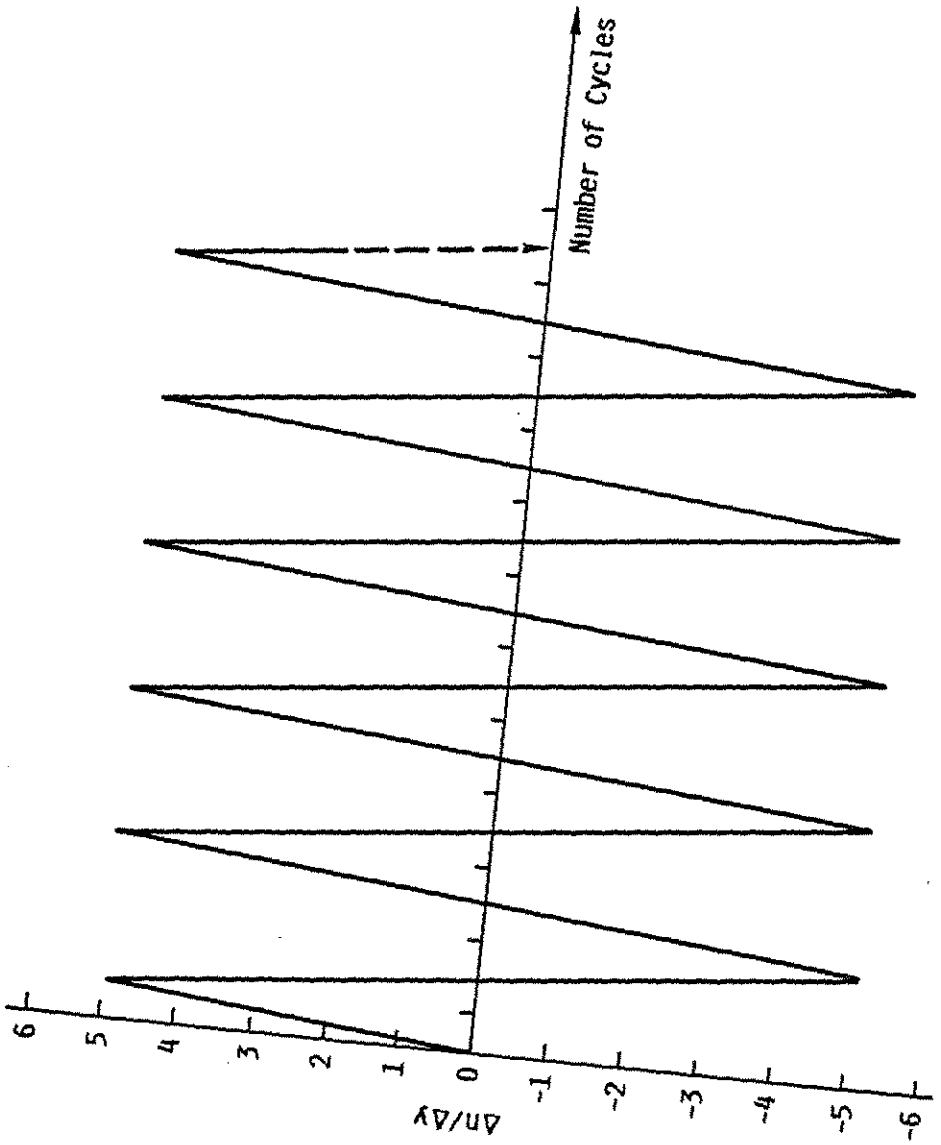

Fig. 2.8 Typical Loading Schedule

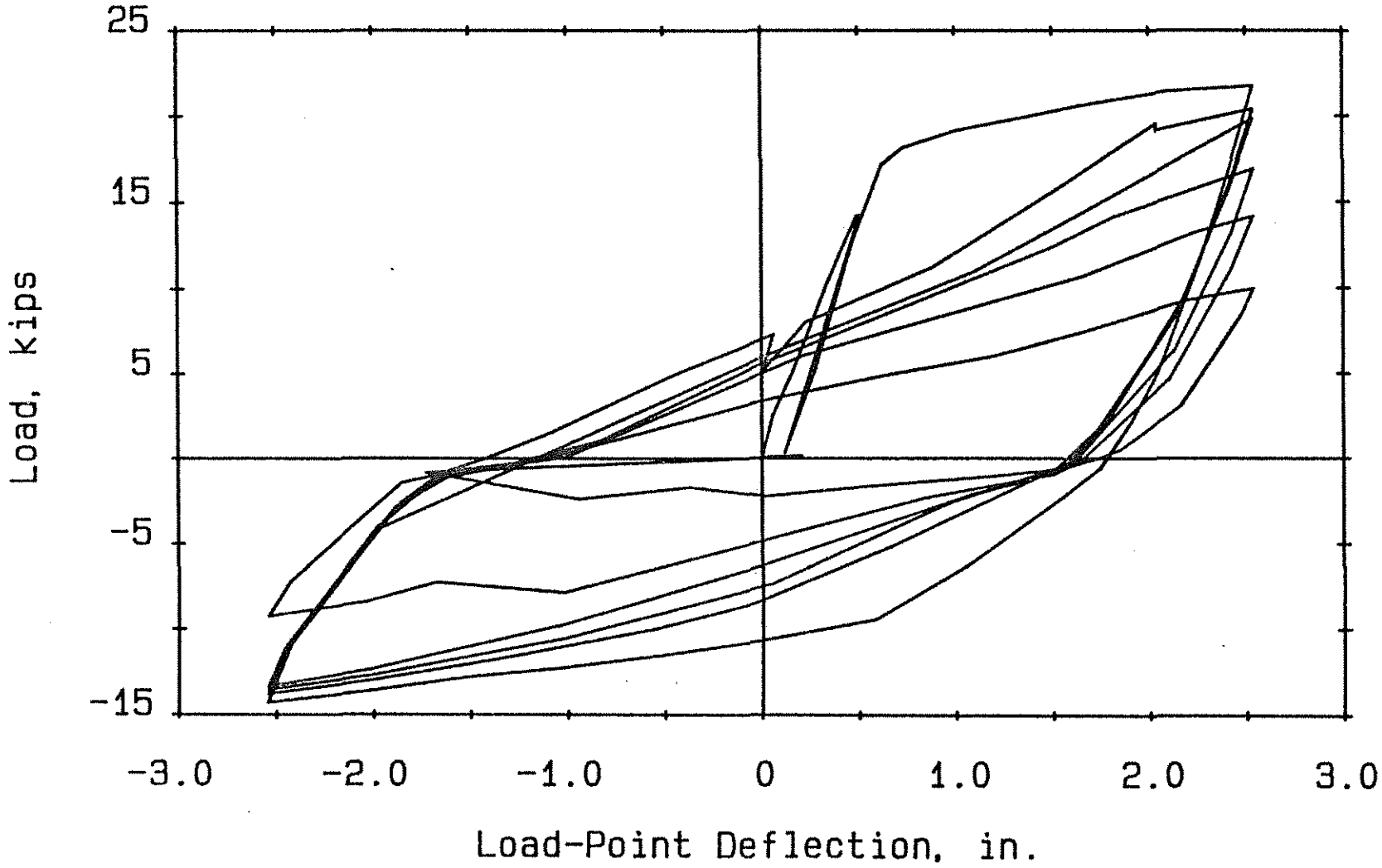

Fig. 2.9(a) Load-Deflection Curve, Beam F-1

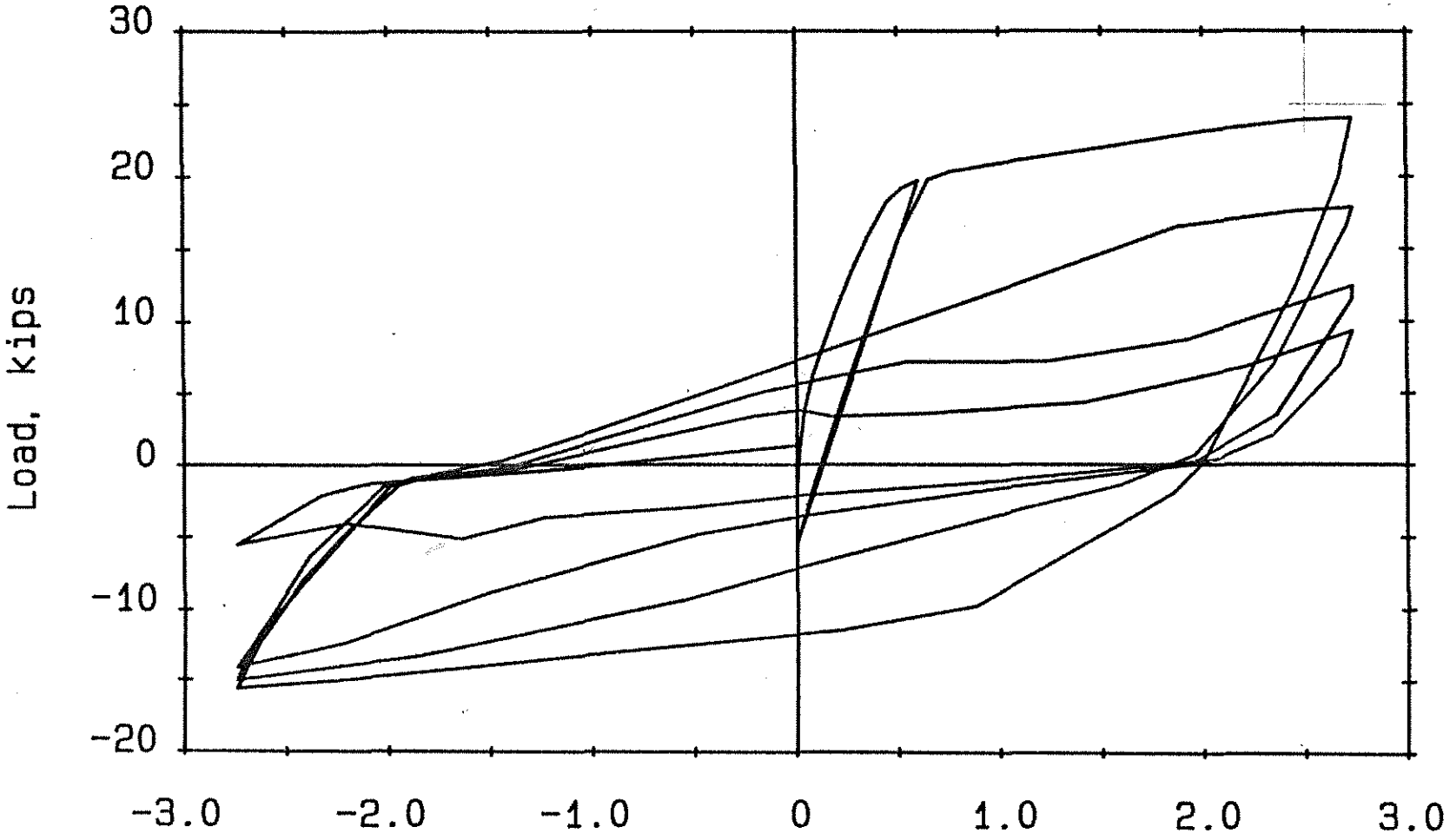

Fig. 2.9(b) Load-Deflection Curve, Beam F-2

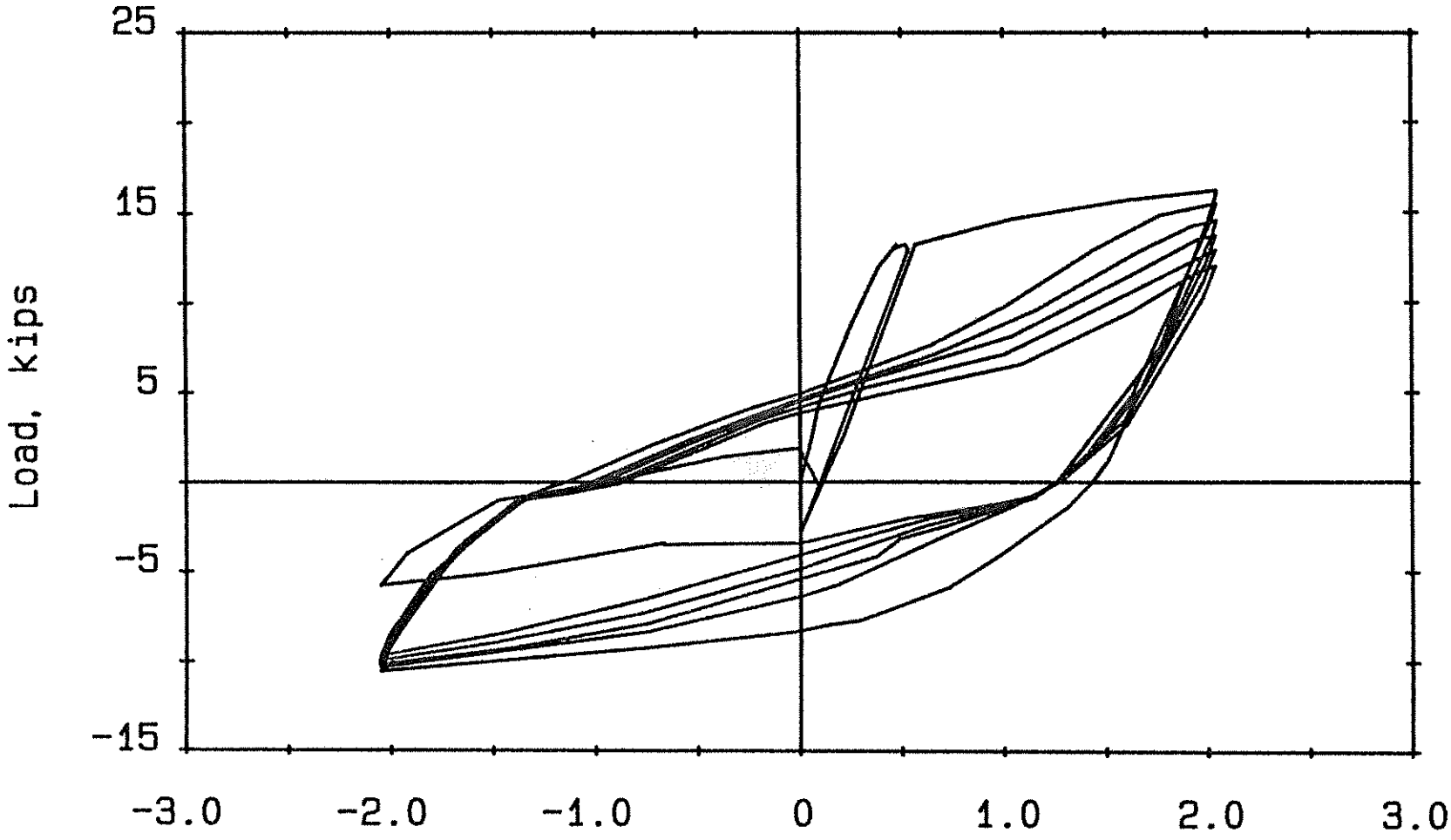

Fig. 2.9(c) Load-Deflection Curve, Beam F-3

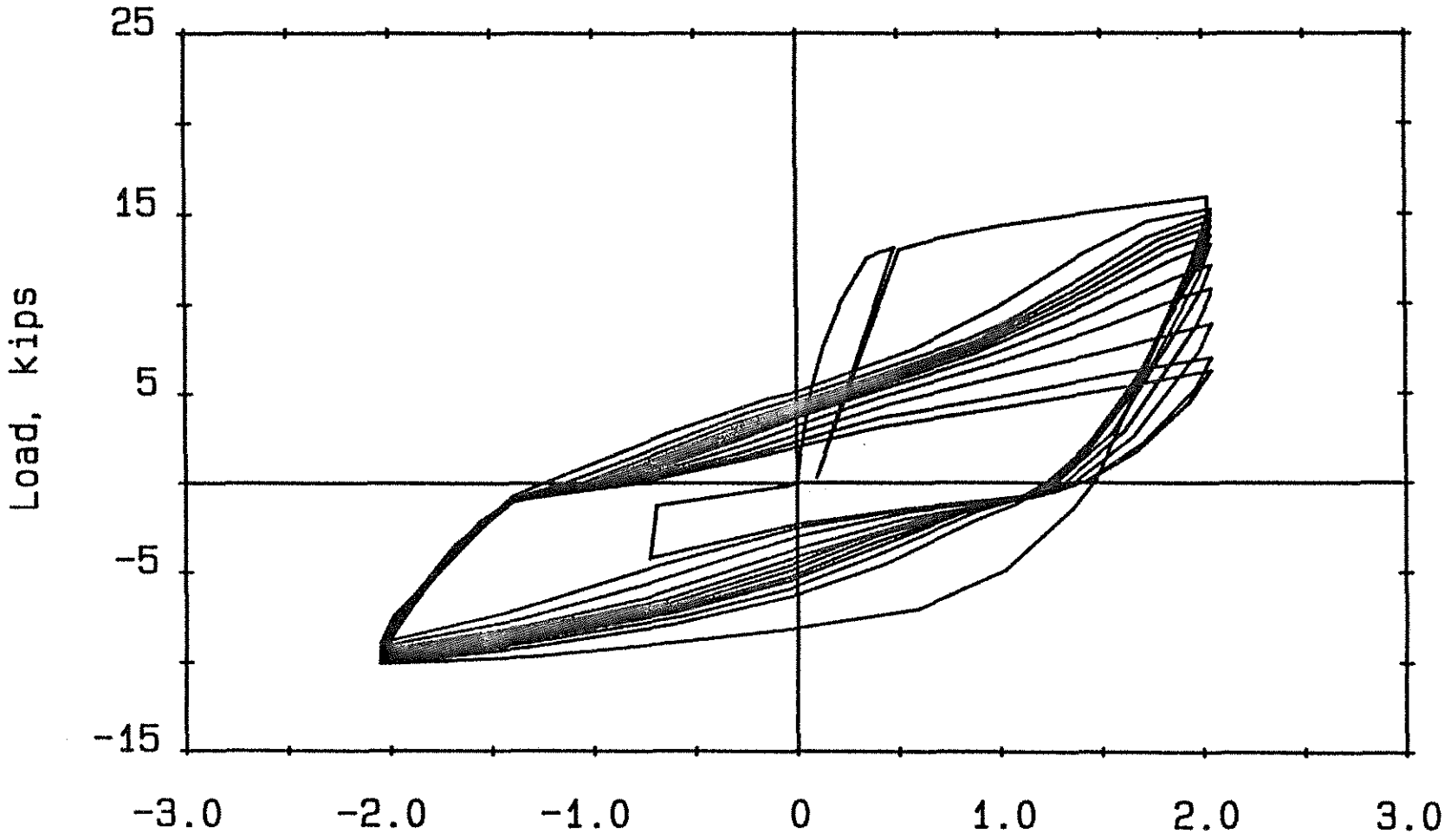

Fig. 2.9(d) Load-Deflection Curve, Beam F-4

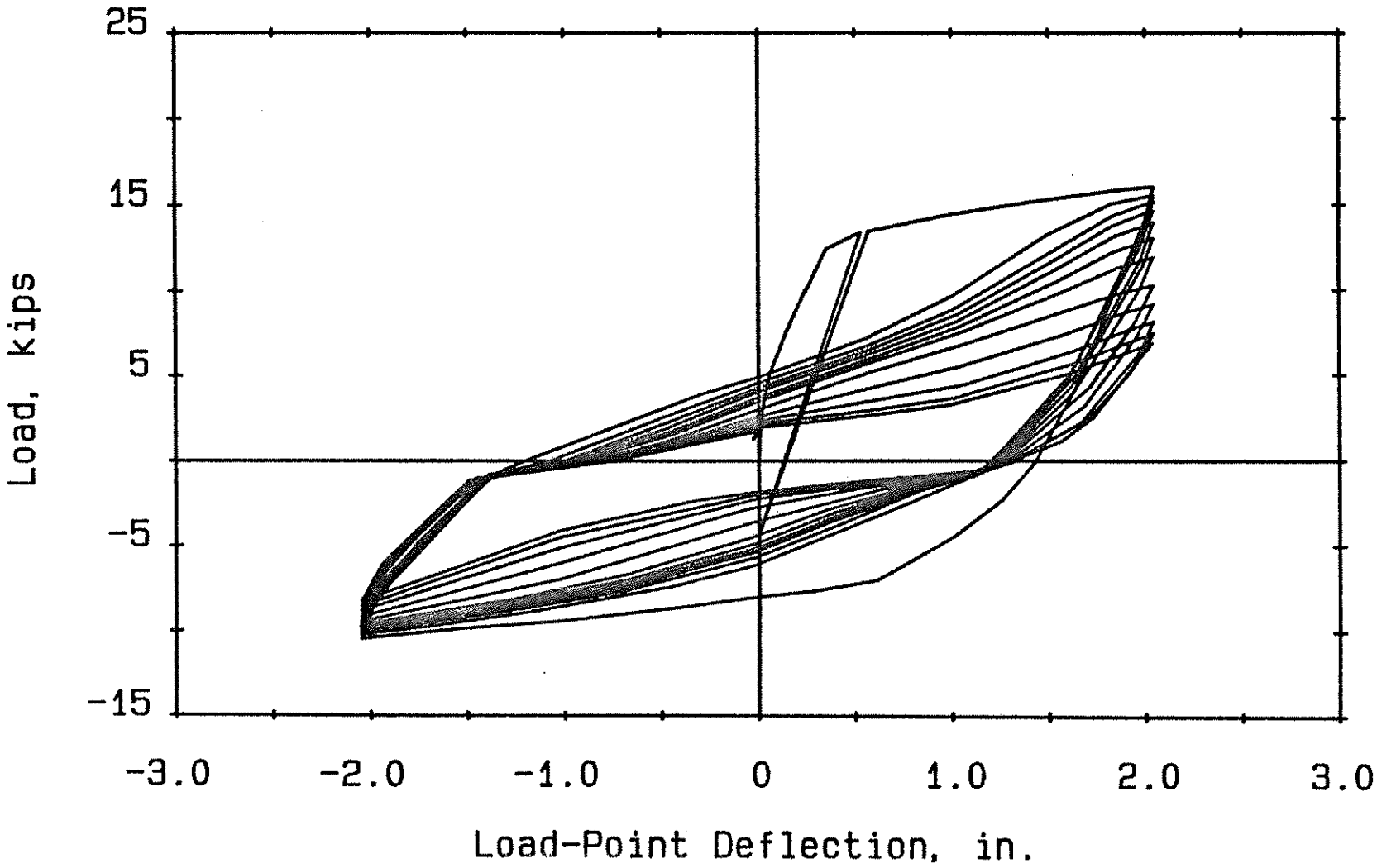

Fig. 2.9(e) Load-Deflection Curve, Beam F-5

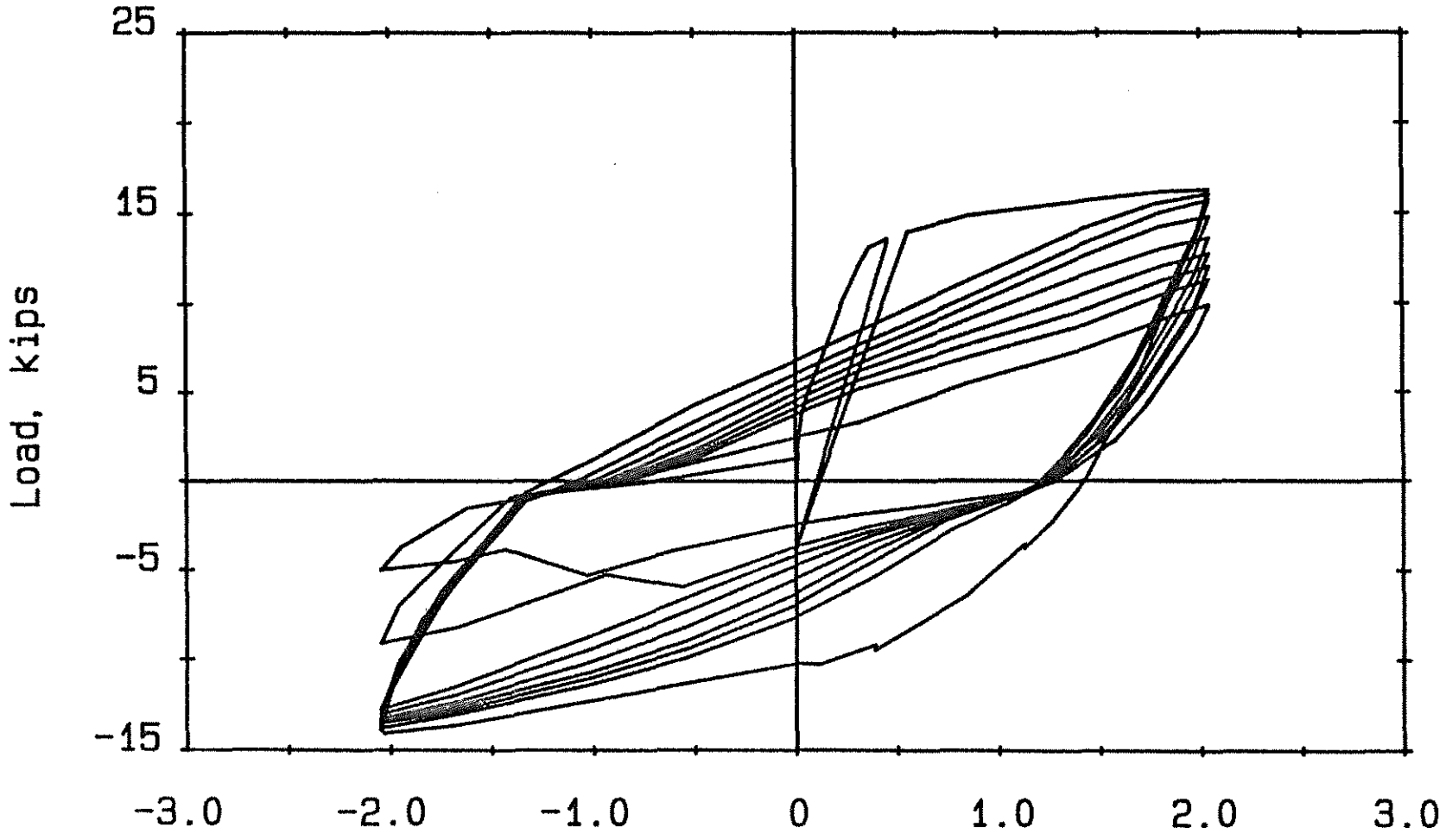

Fig. 2.9(f) Load-Deflection Curve, Beam F-6

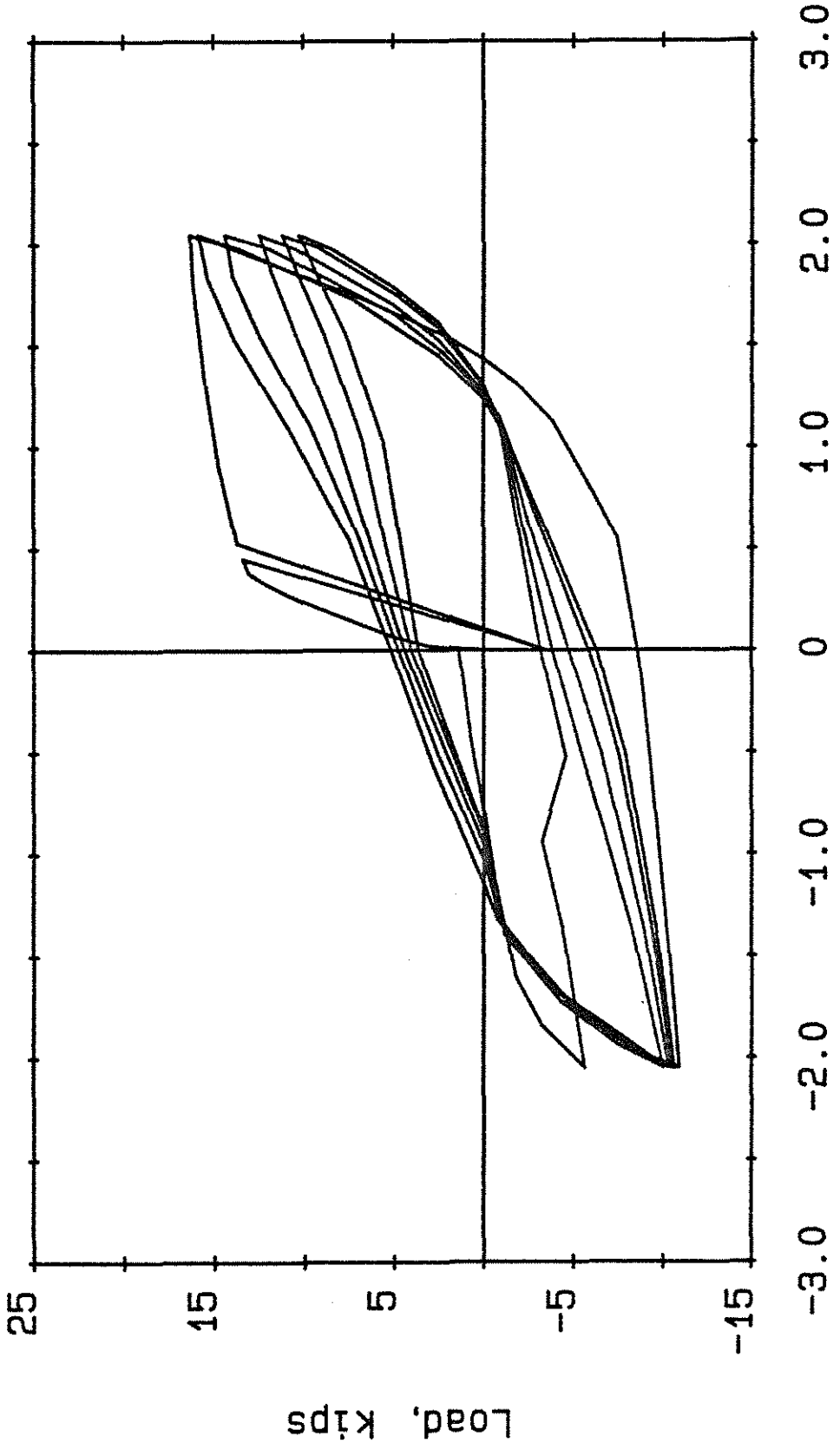

Fig. 2.9(g) Load-Deflection Curve, Beam F-7

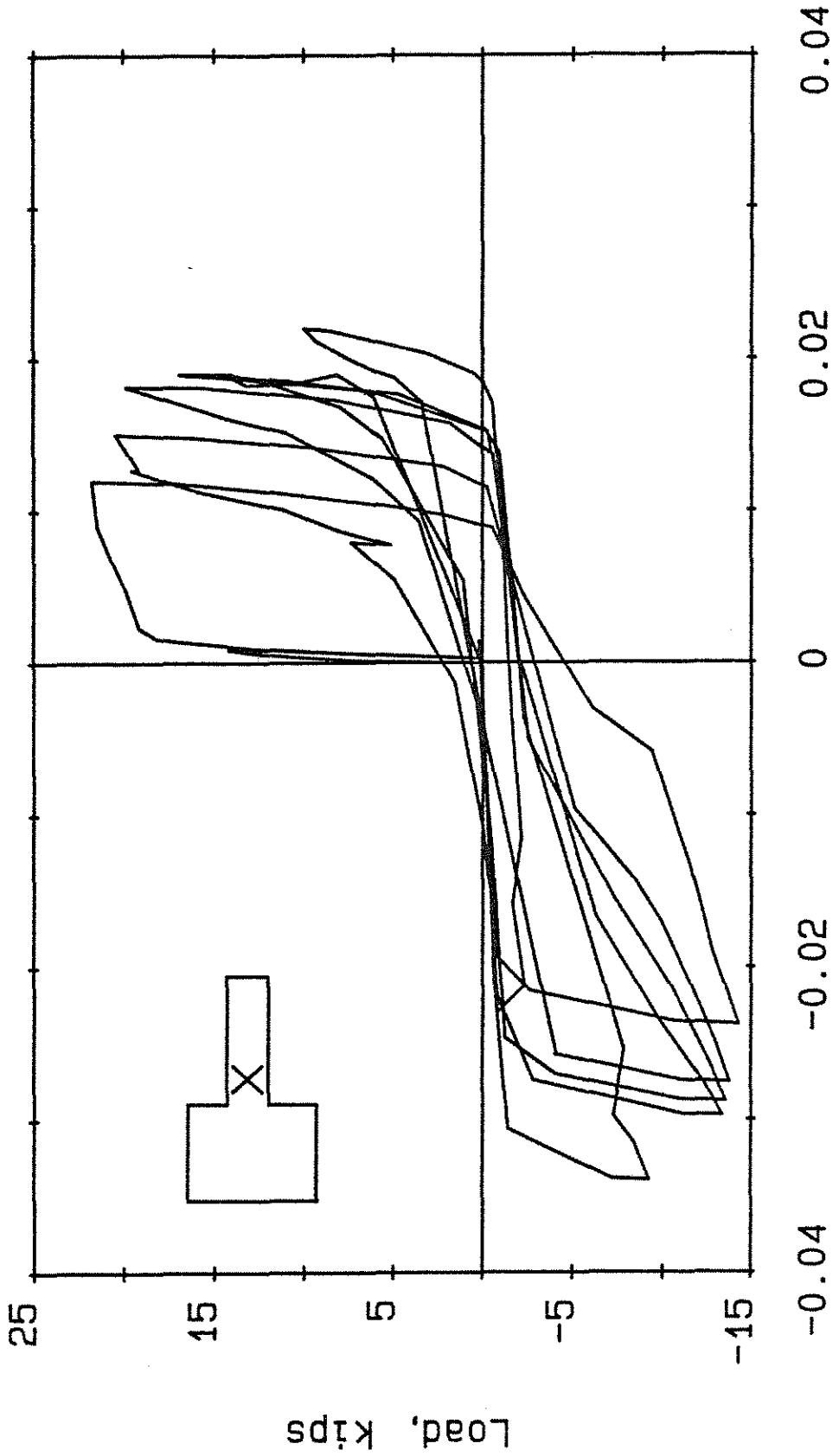

Fig. 2.10(a) Load versus Hinging Zone Shear Deformation, Beam F-1

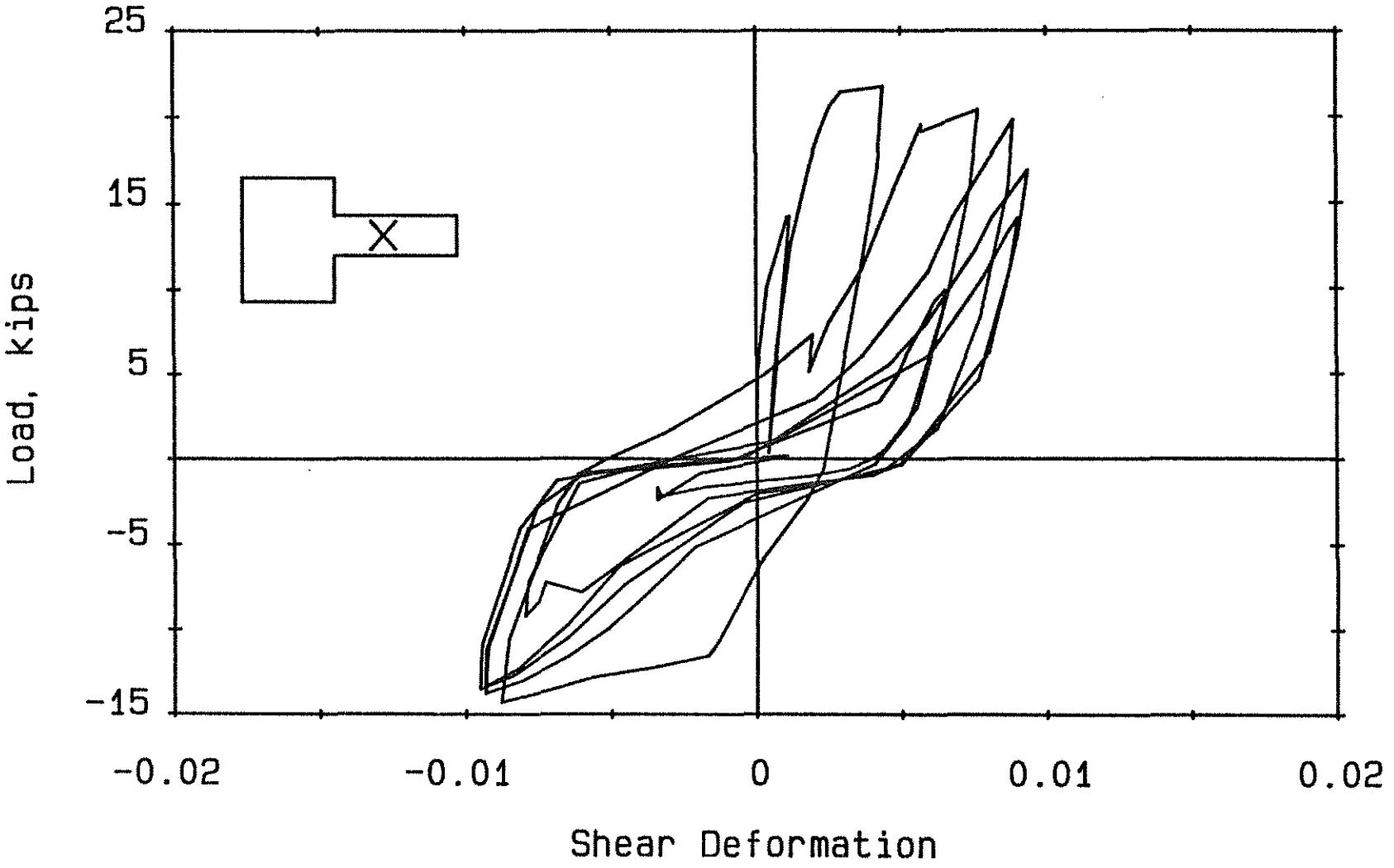

Fig. 2.10(b) Load versus Shear Deformation over Region Extending d to 2d from Column Face, Beam F-1

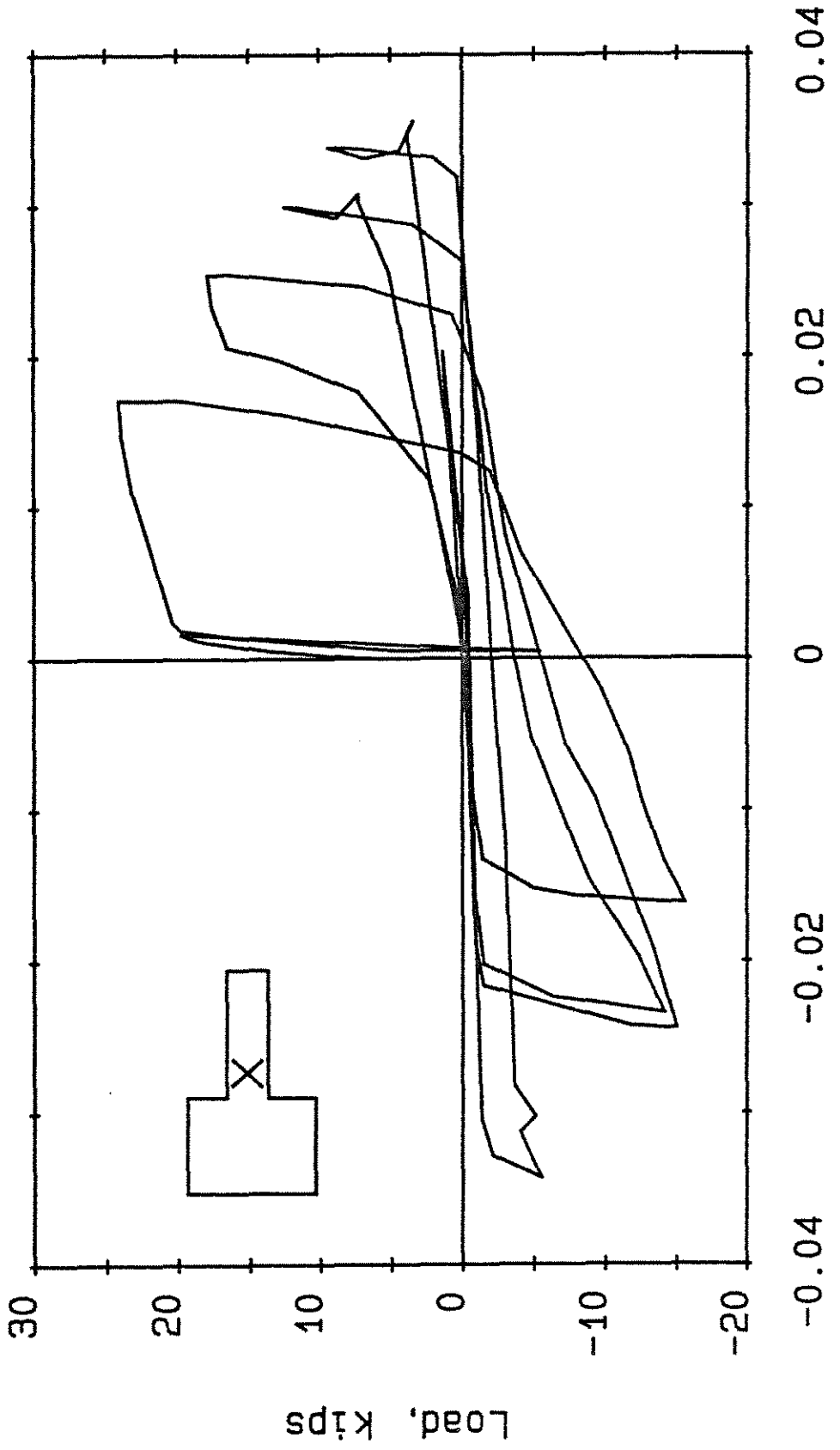

Fig. 2.10(c) Load versus Hinging Zone Shear Deformation, Beam F-2

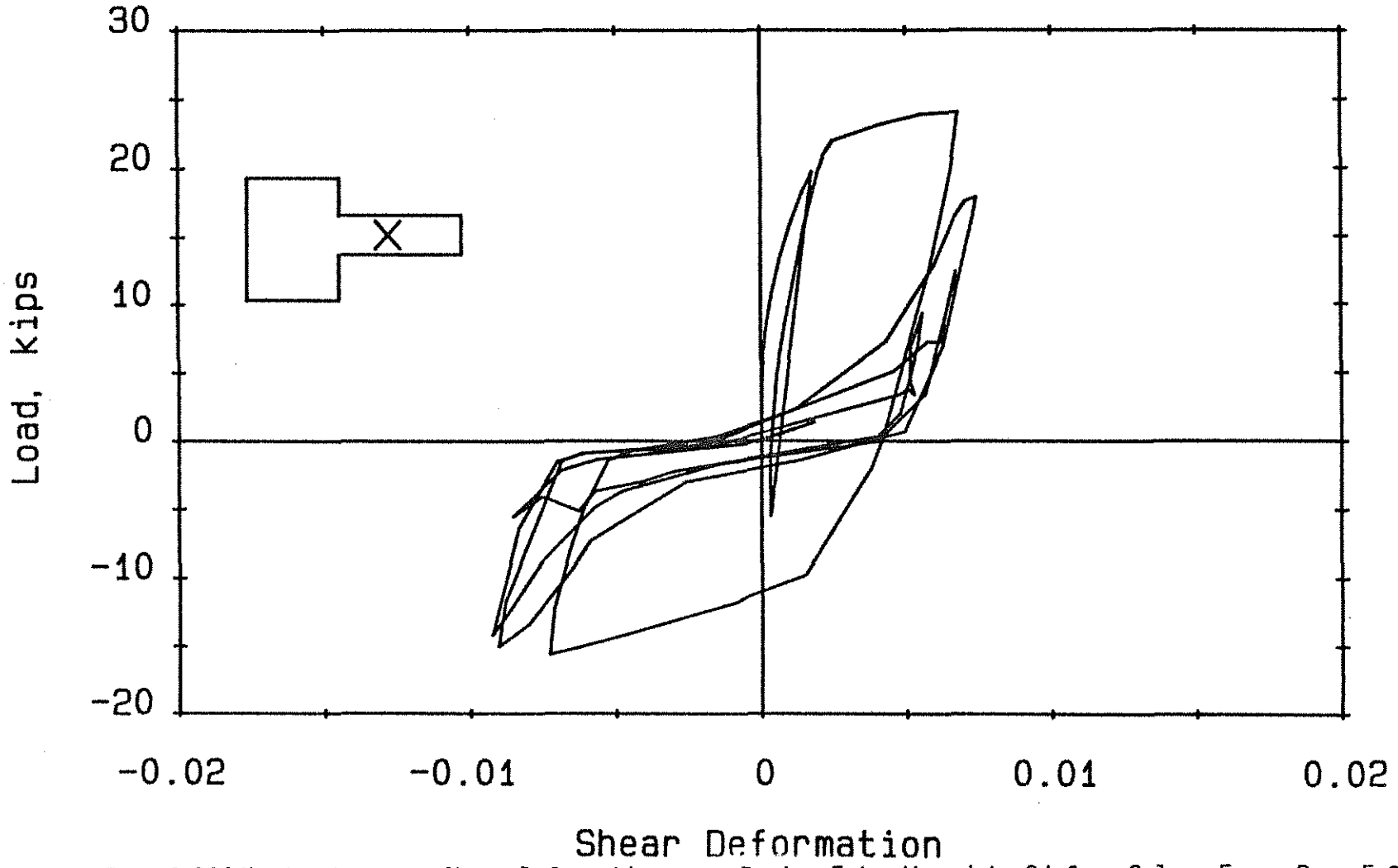

Fig. 2.10(d) Load versus Shear Deformation over Region Extending d to 2d from Column Face, Beam F-2

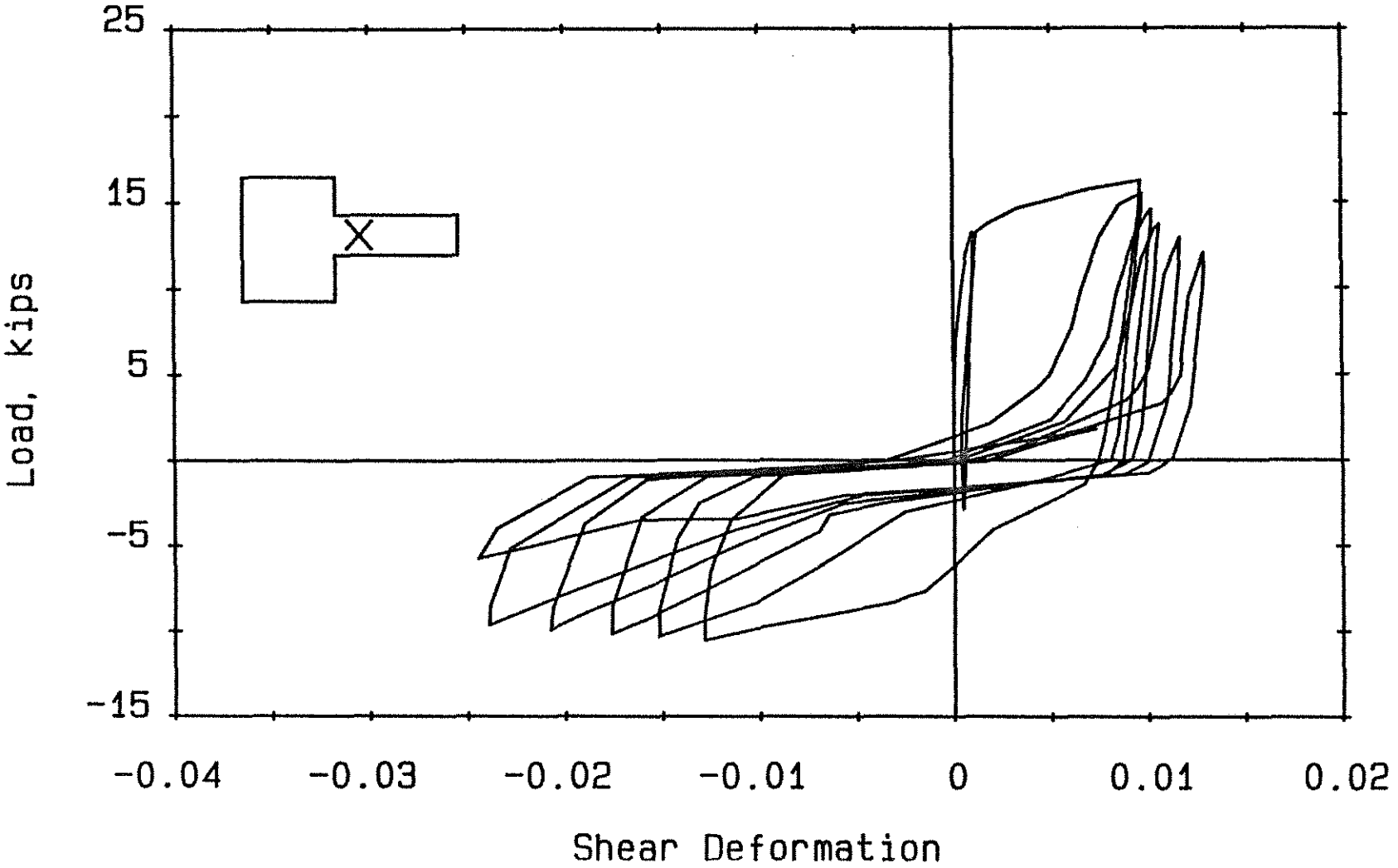

Fig. 2.10(e) Load versus Hinging Zone Shear Deformation, Beam F-3

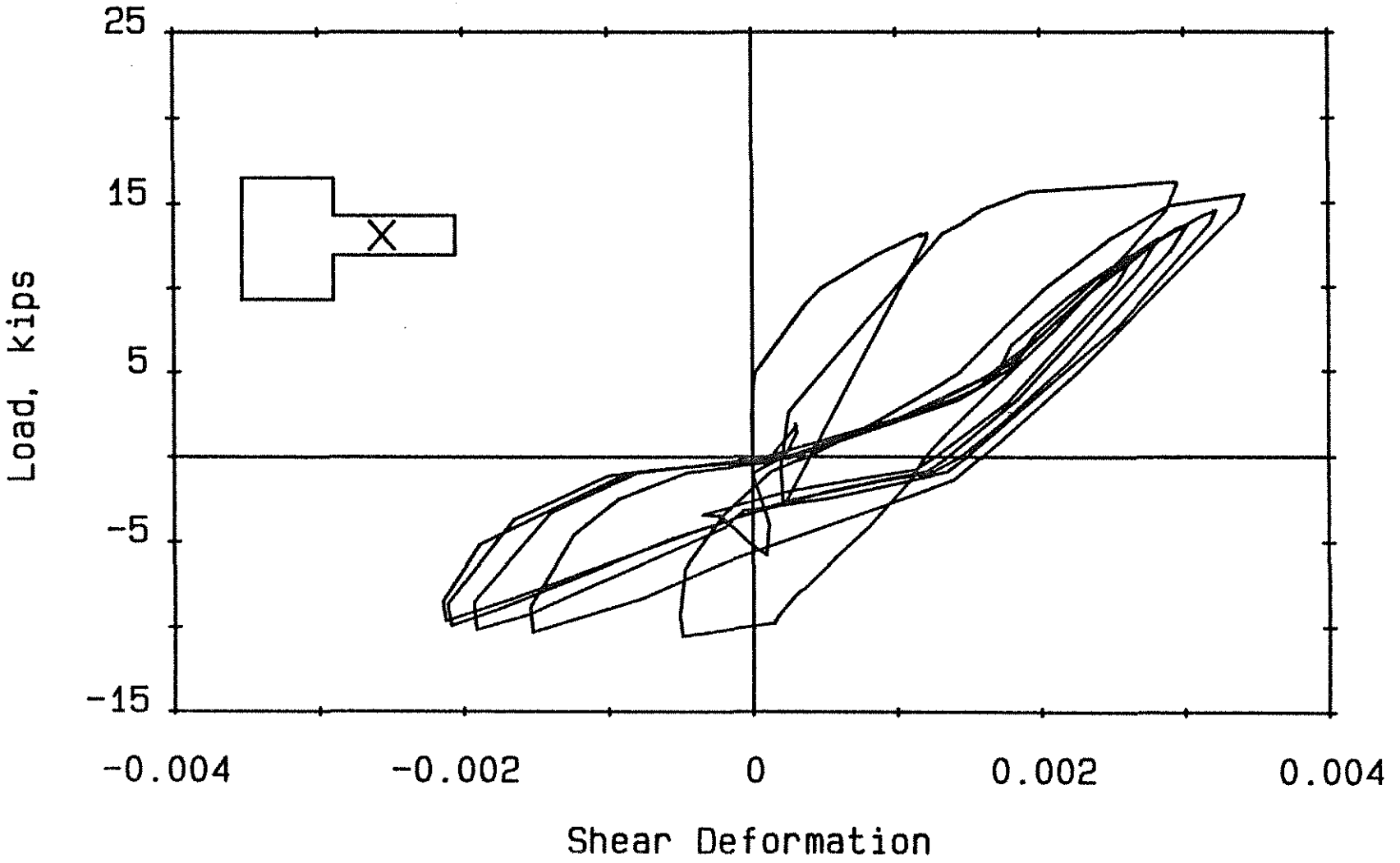

Fig. 2.10(f) Load versus Shear Deformation over Region Extending d to 2d from Column Face, Beam F-3

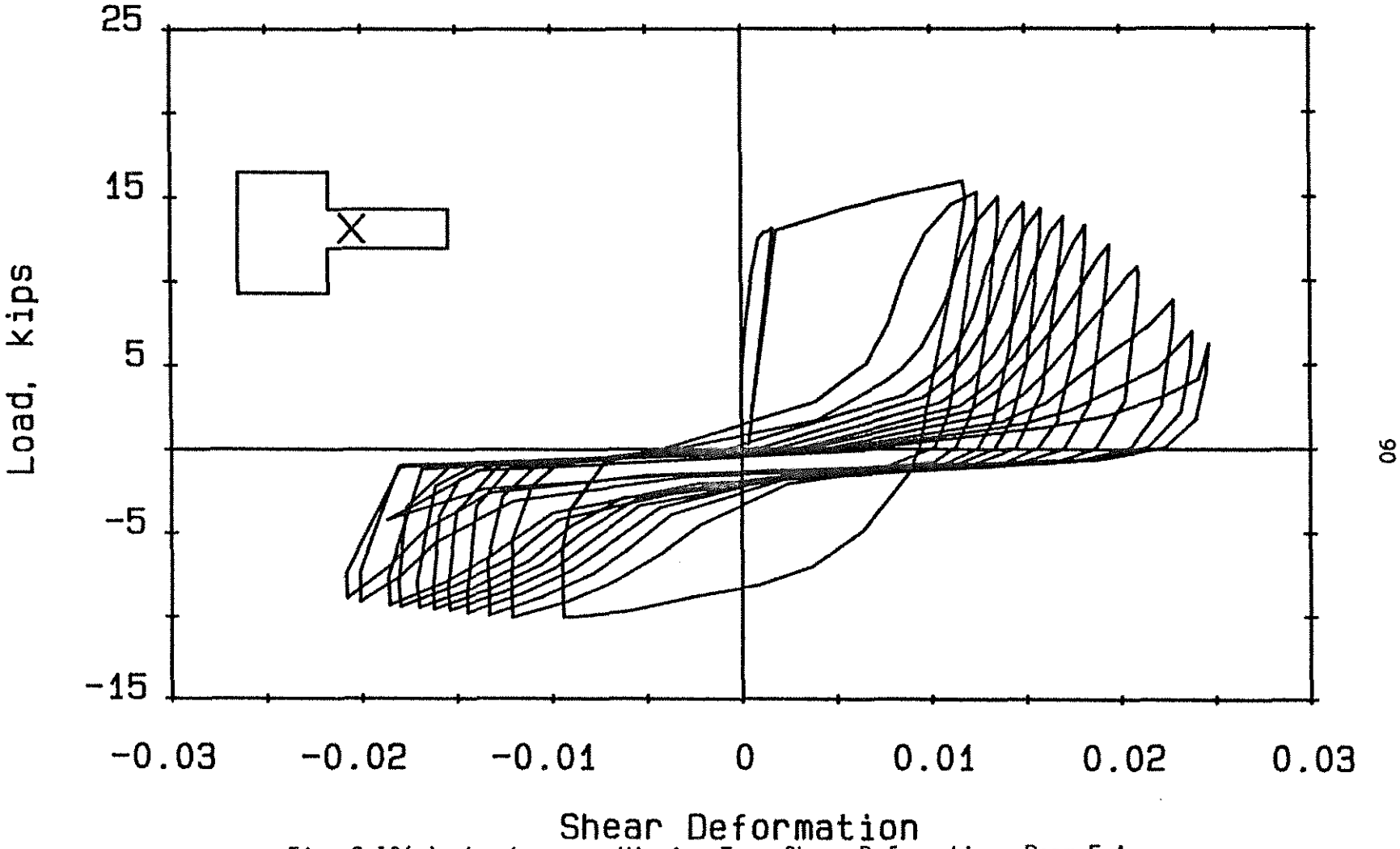

Fig. 2.10(g) Load versus Hinging Zone Shear Deformation, Beam F-4

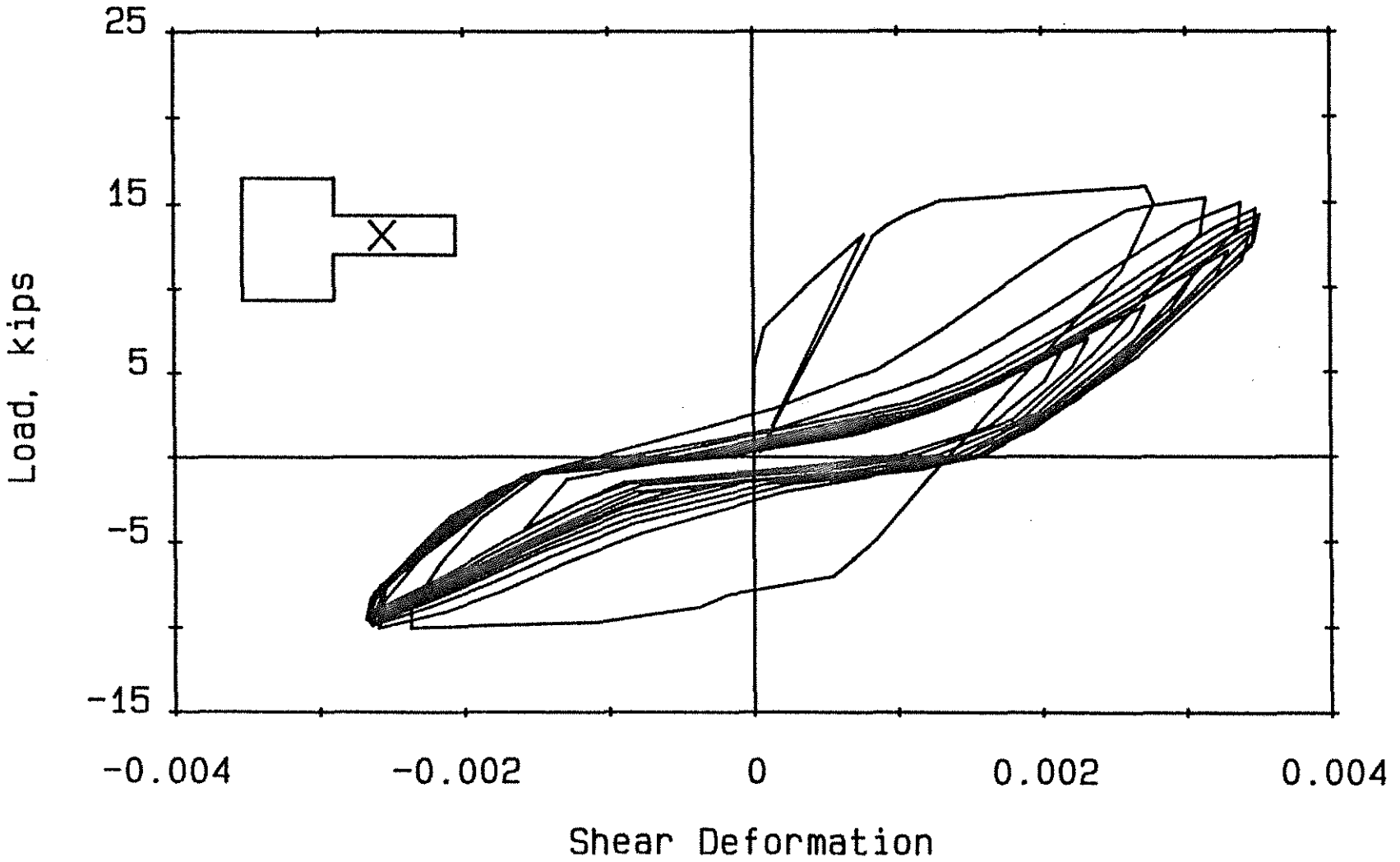

Fig. 2.10(h) Load versus Shear Deformation over Region Extending d to 2d from Column Face, Beam F-4

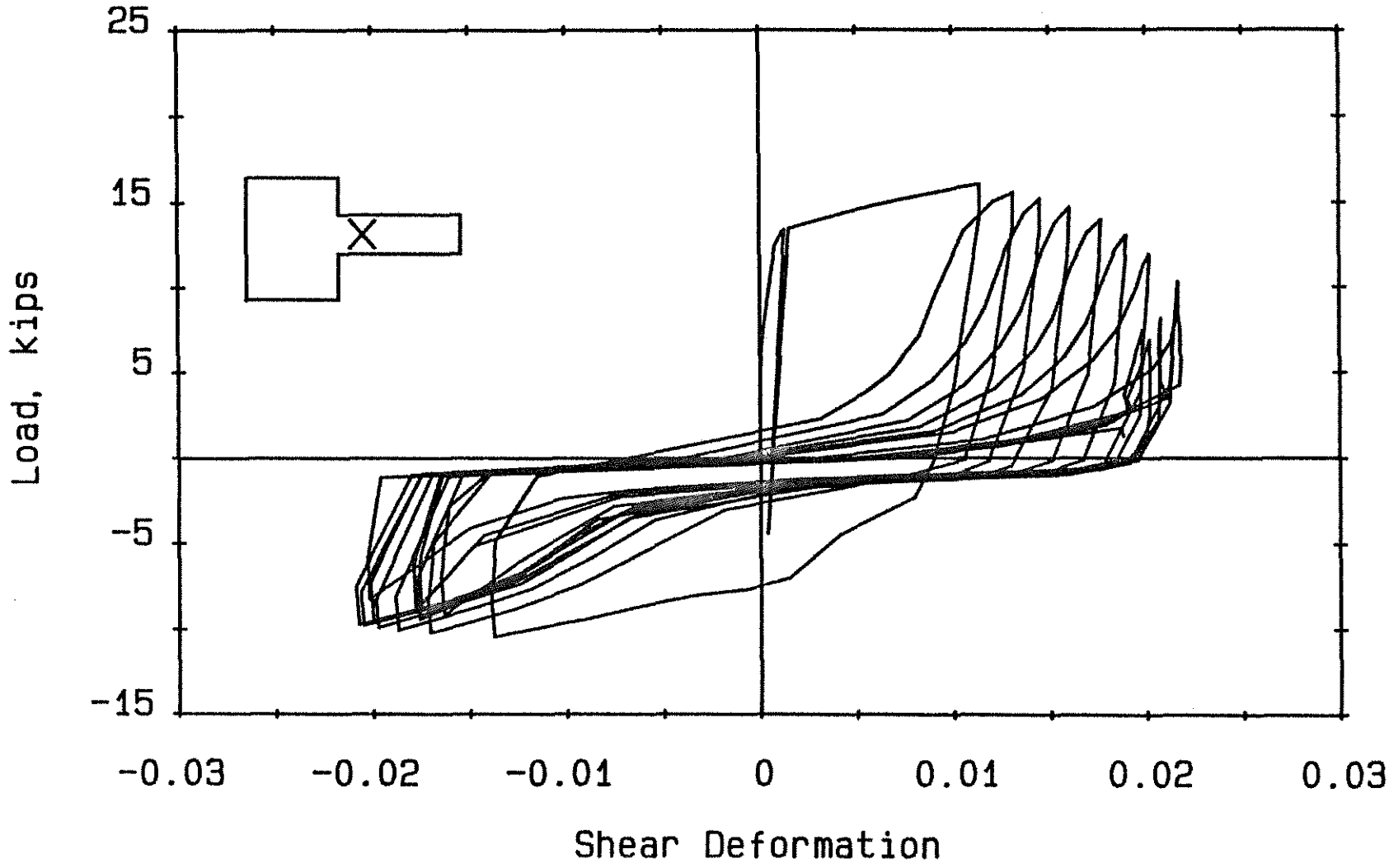

Fig. 2.10(1) Load versus Hinging Zone Shear Deformation, Beam F-5

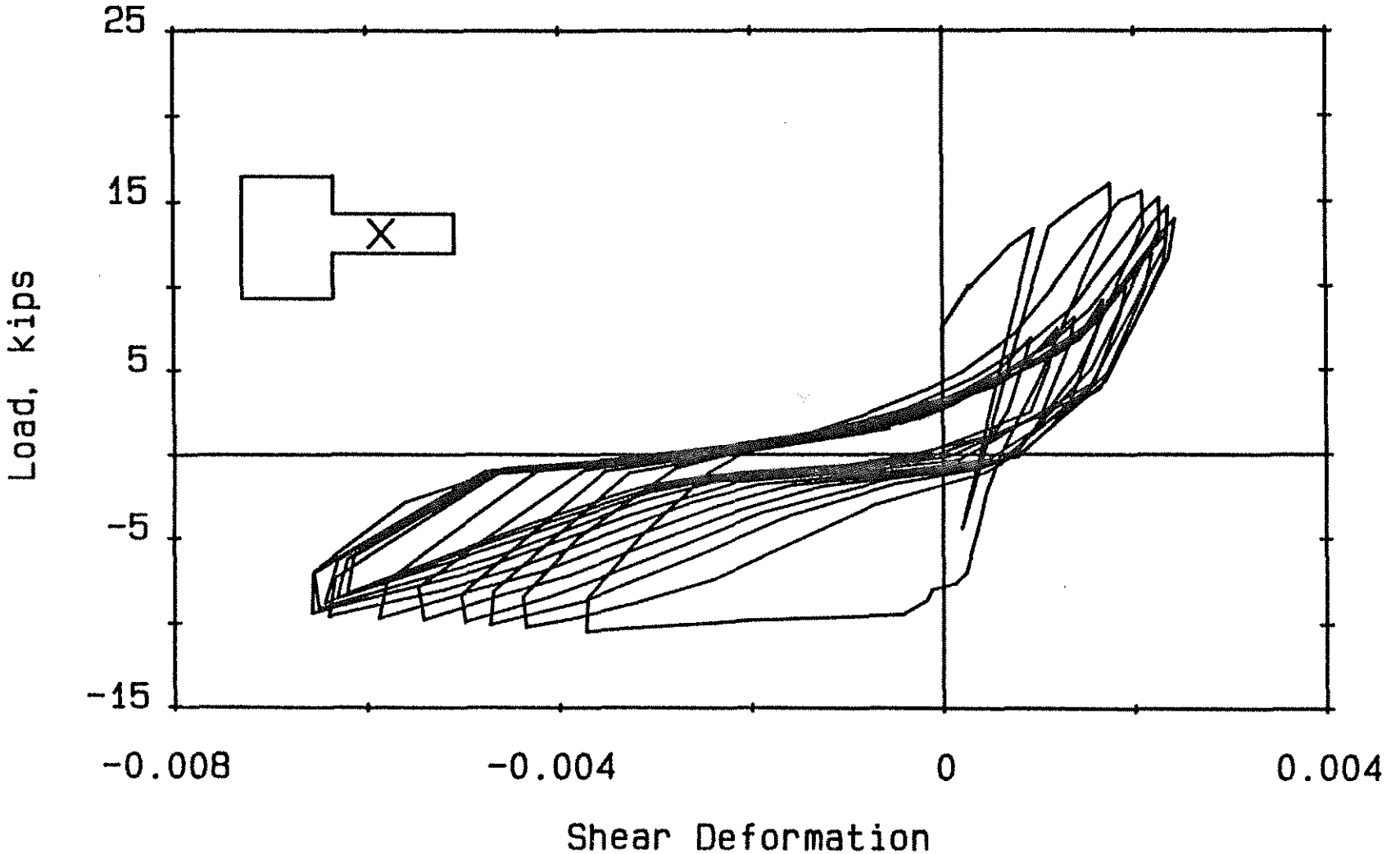

Fig. 2.10(j) Load versus Shear Deformation over Region Extending d to 2d from Column Face, Beam F-5

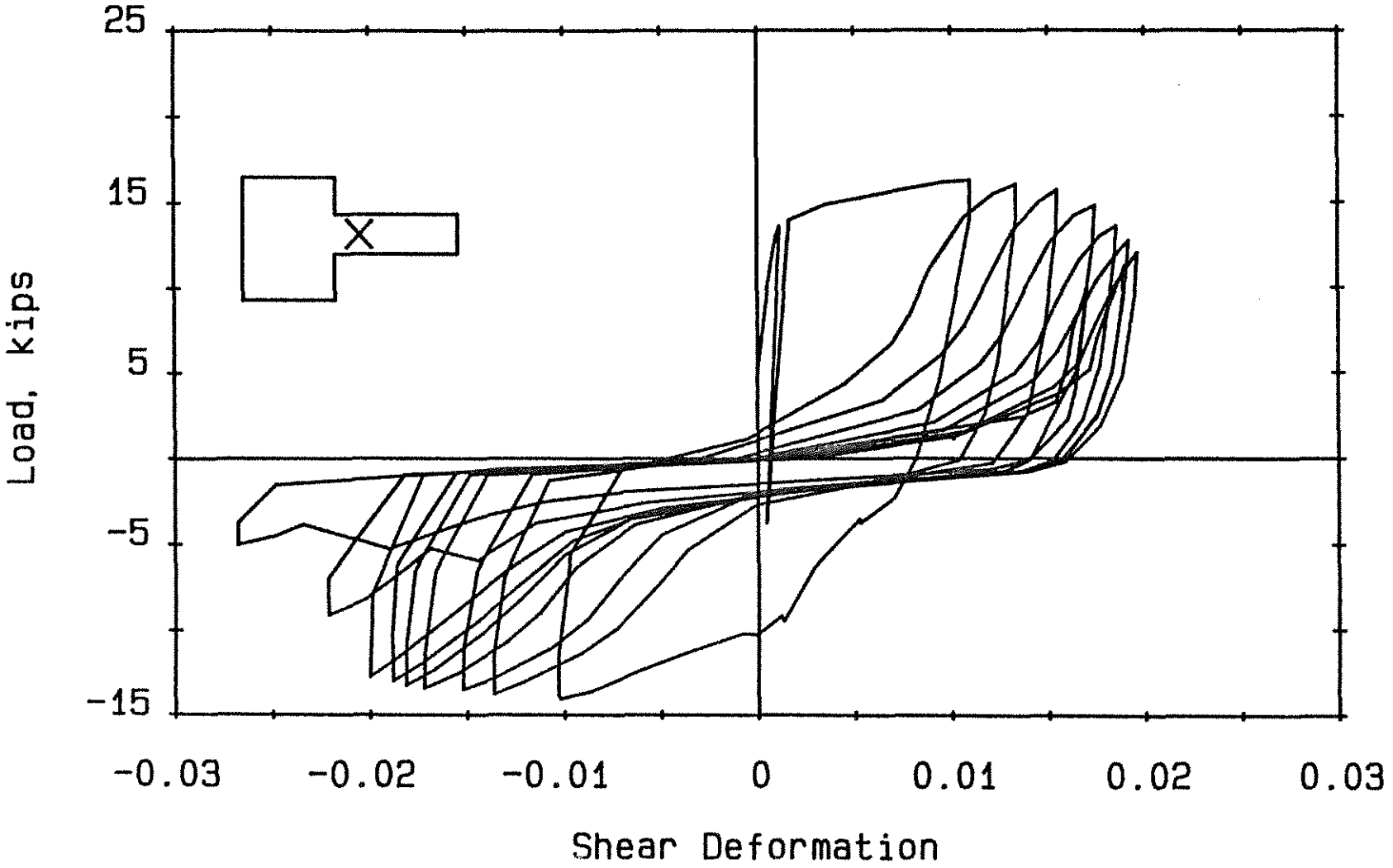

Fig. 2.10(k) Load versus Hinging Zone Shear Deformation, Beam F-6

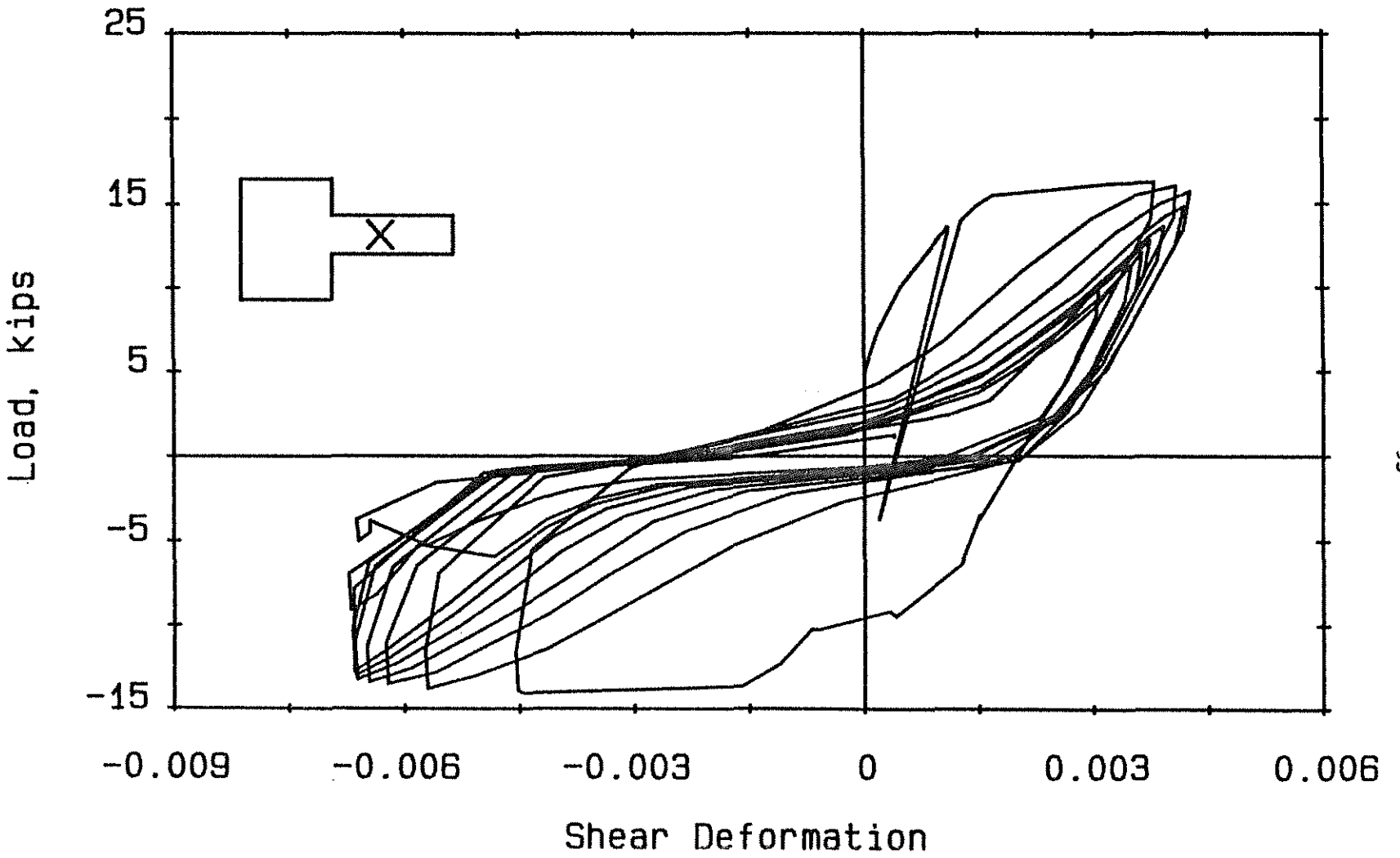

Fig. 2.10(1) Load versus Shear Deformation over Region Extending d to 2d from Column Face, Beam F-6

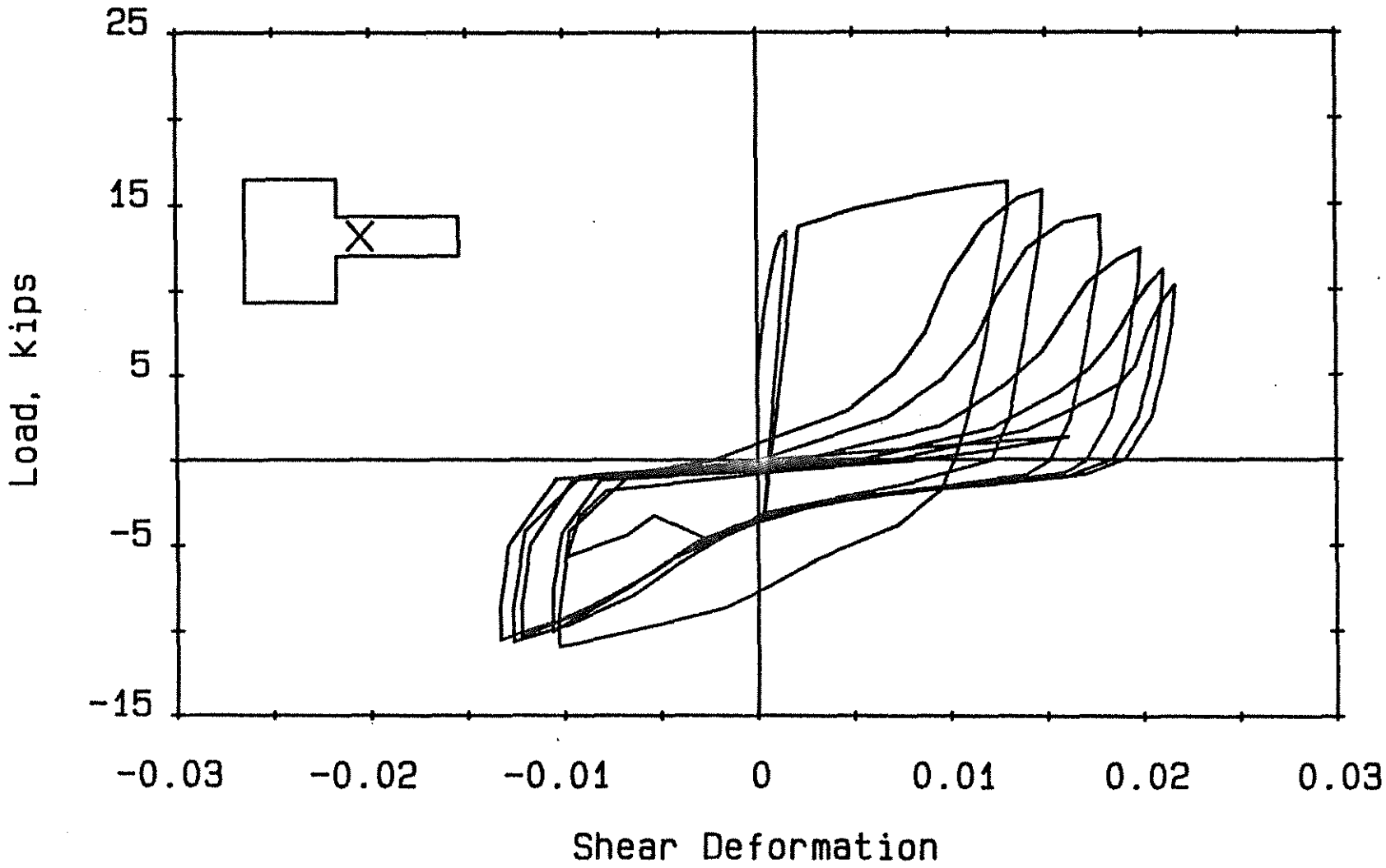

Fig. 2.10(m) Load versus Hinging Zone Shear Deformation, Beam F-7

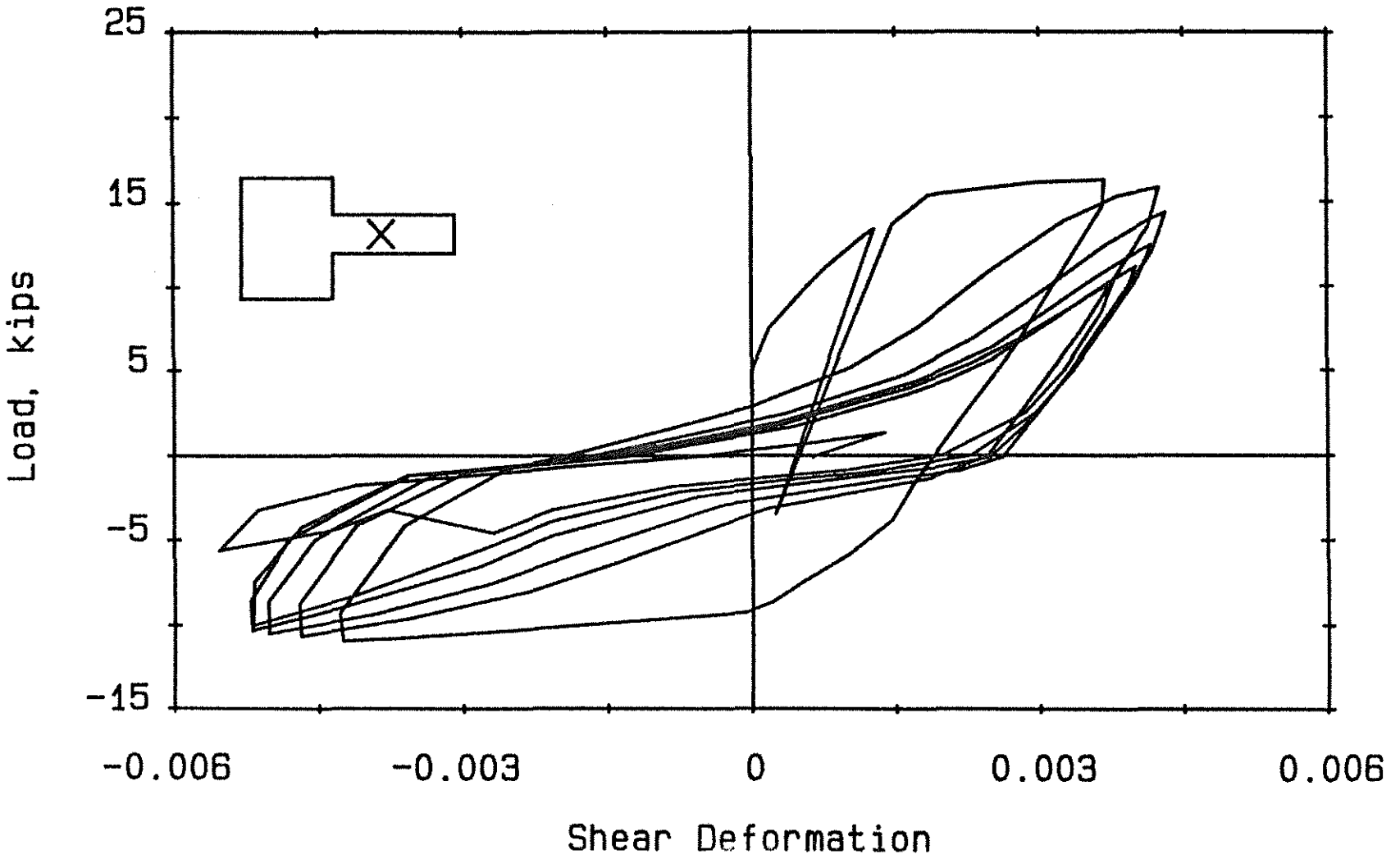

Fig. 2.10(n) Load versus Shear Deformation over Region Extending d to 2d from Column Face, Beam F-7

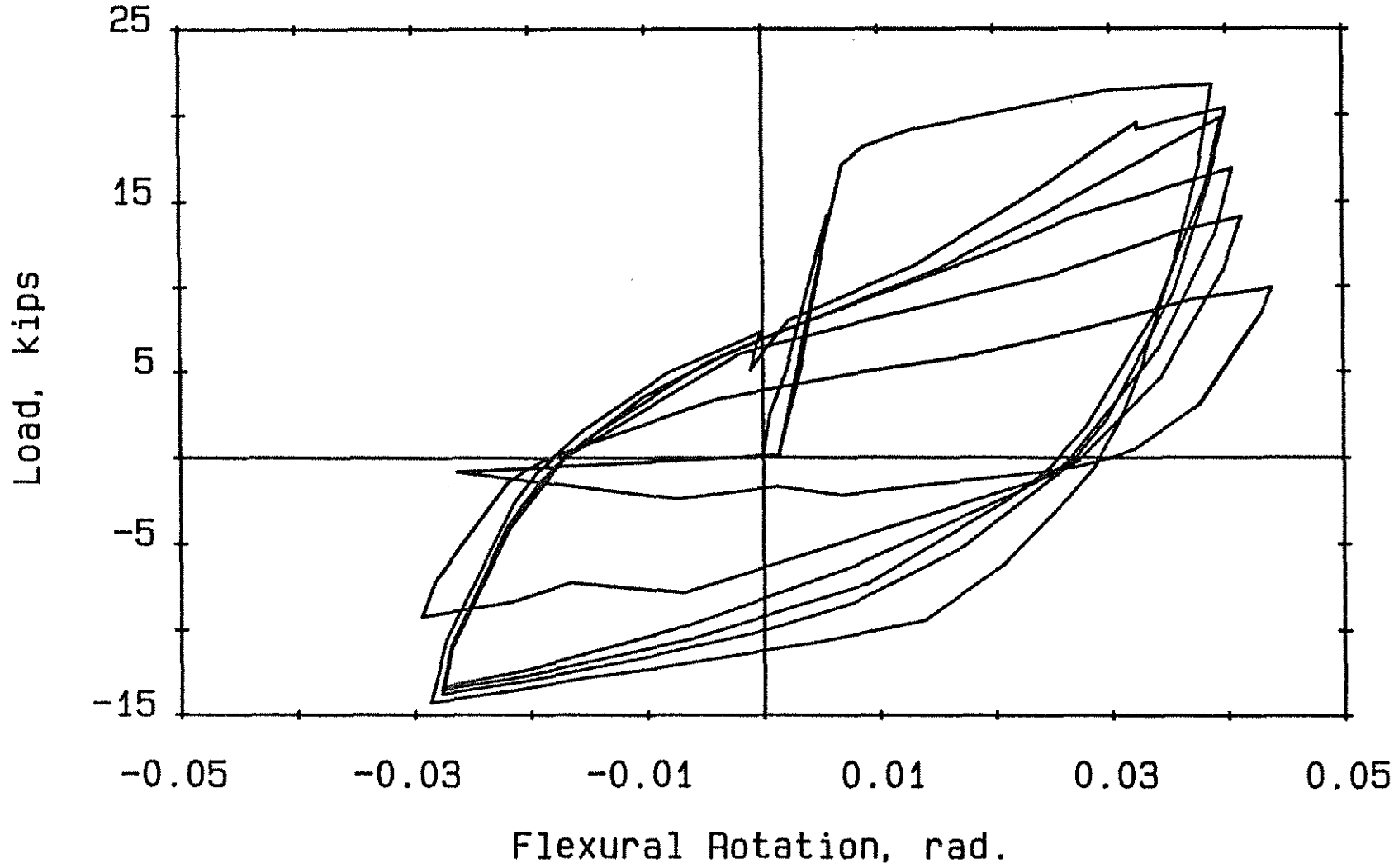

Fig. 2.11(a) Load versus Hinging Zone Flexural Rotation, Beam F-1

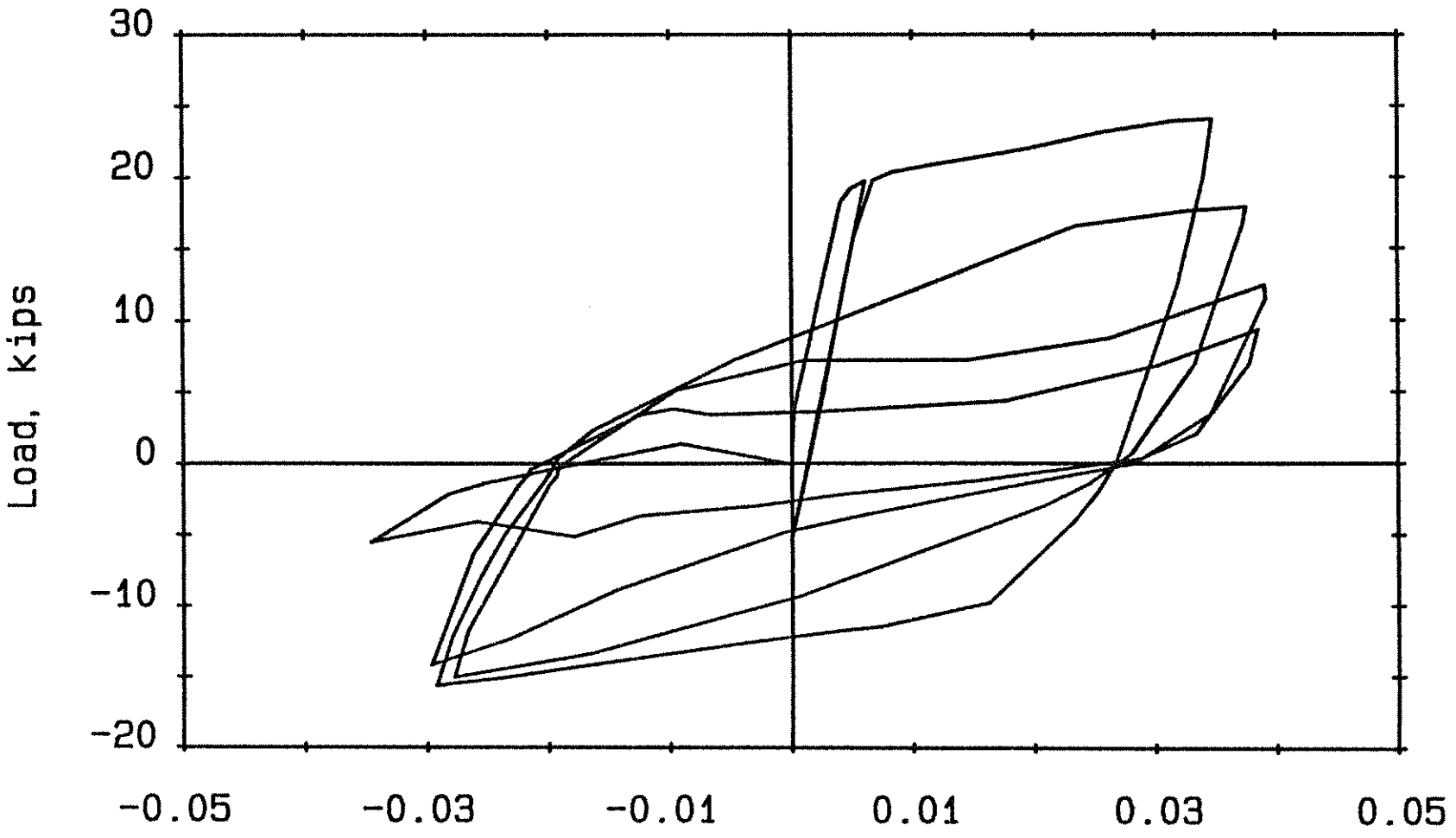

Fig. 2.11(b) Load versus Hinging Zone Flexural Rotation, Beam F-2

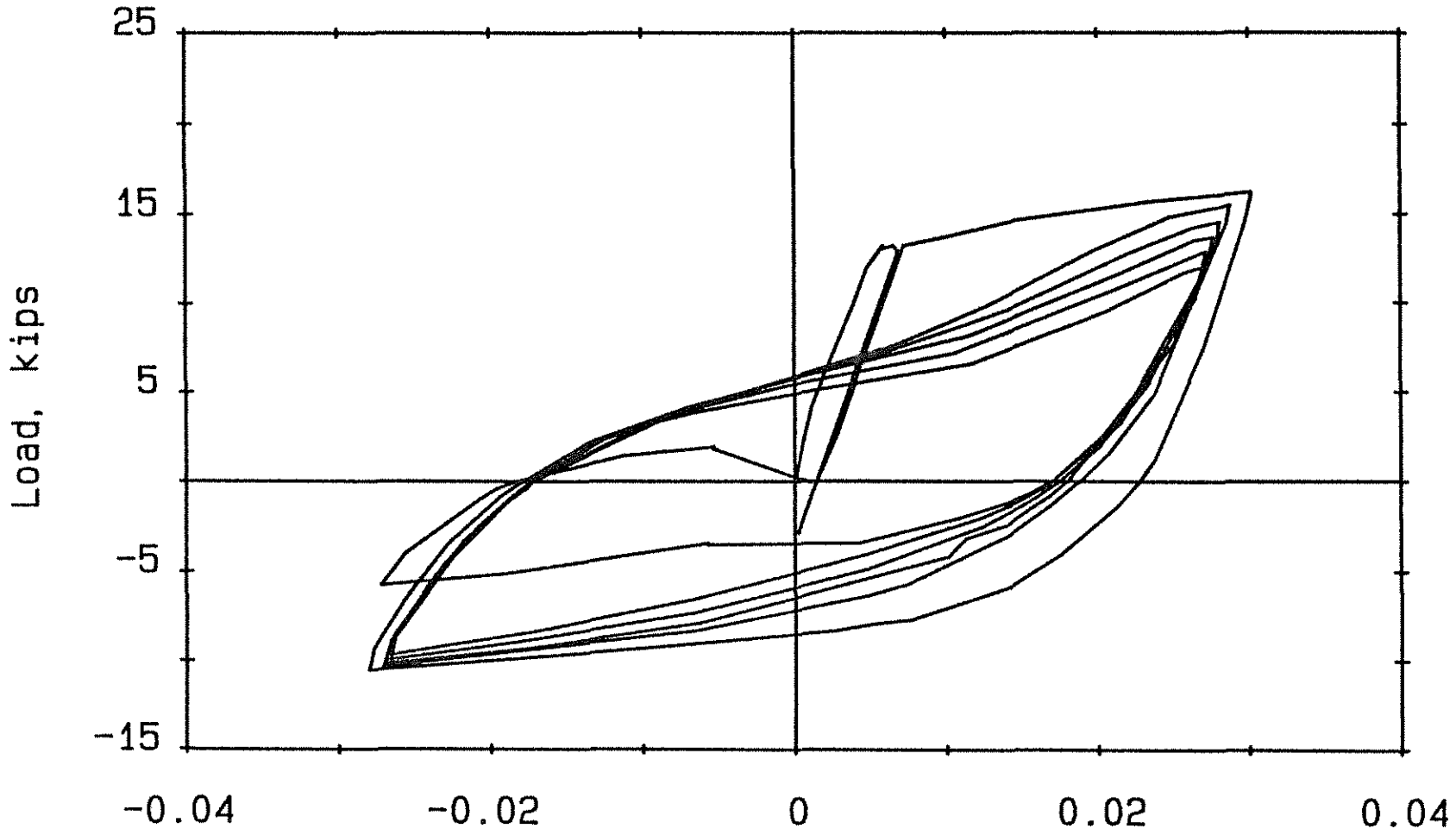

Fig. 2.11(c) Load versus Hinging Zone Flexural Rotation, Beam F-3

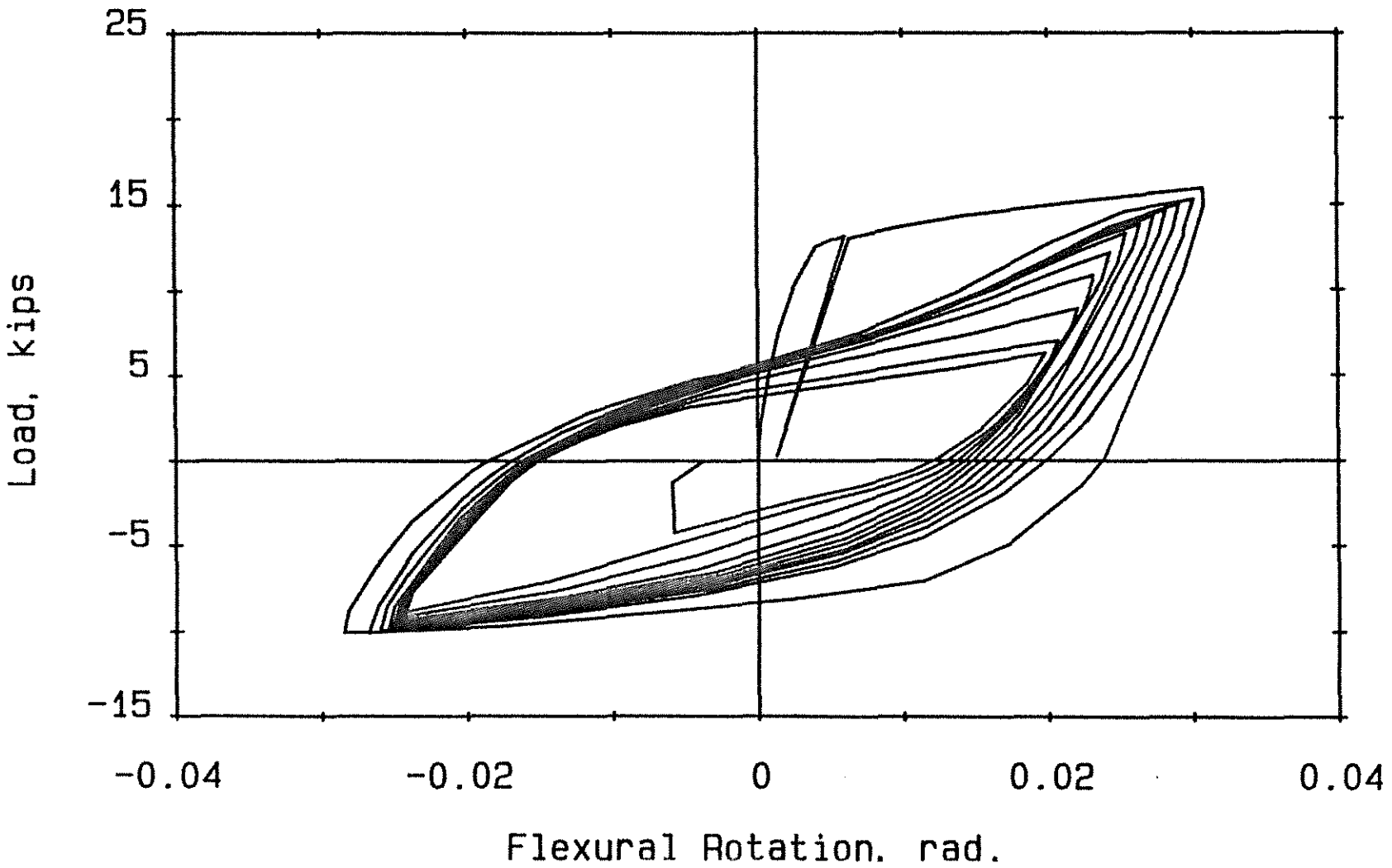

Fig. 2.11(d) Load versus Hinging Zone Flexural Rotation, Beam F-4

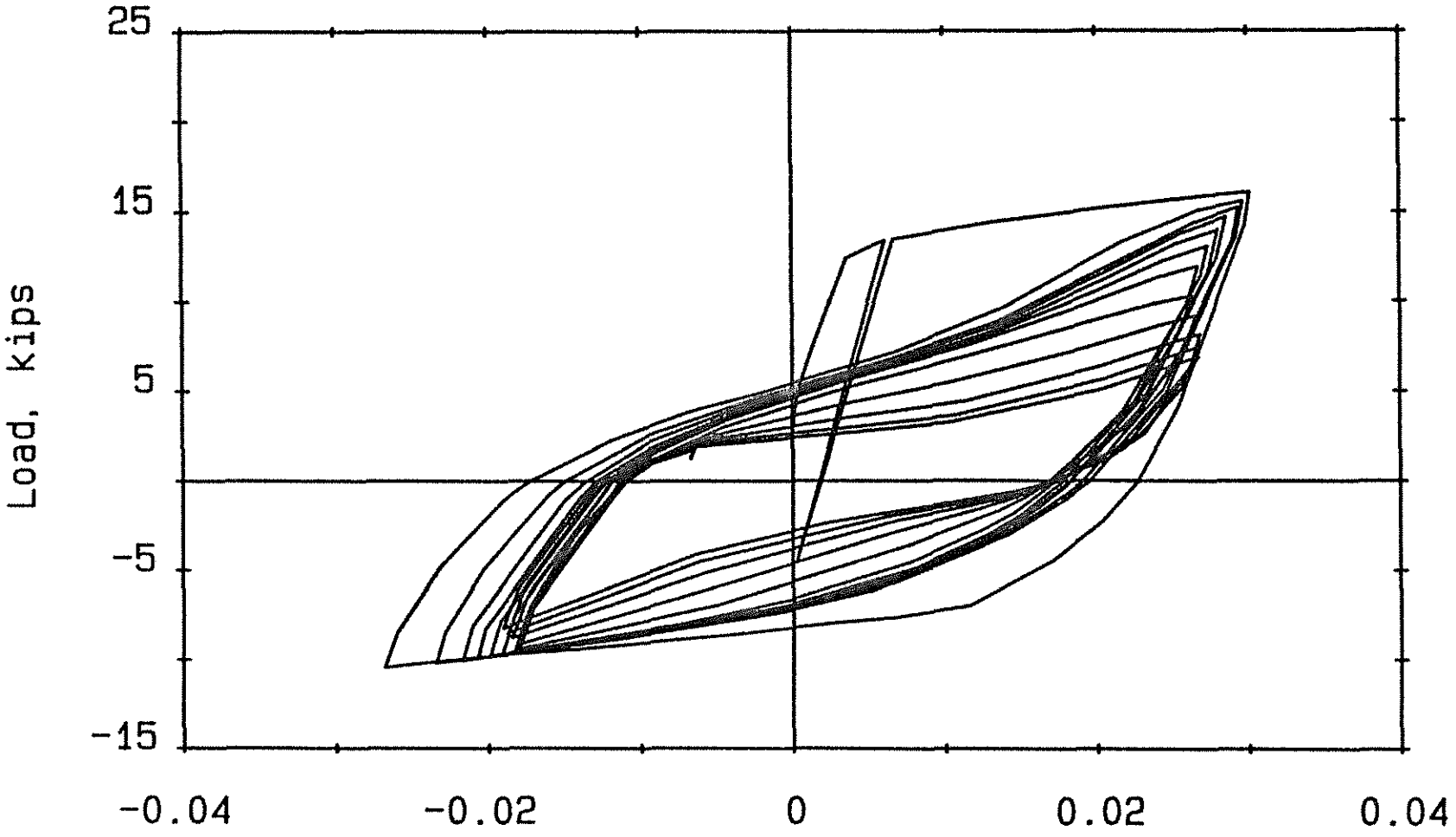

Fig. 2.11(e) Load versus Hinging Zone Flexural Rotation, Beam F-5

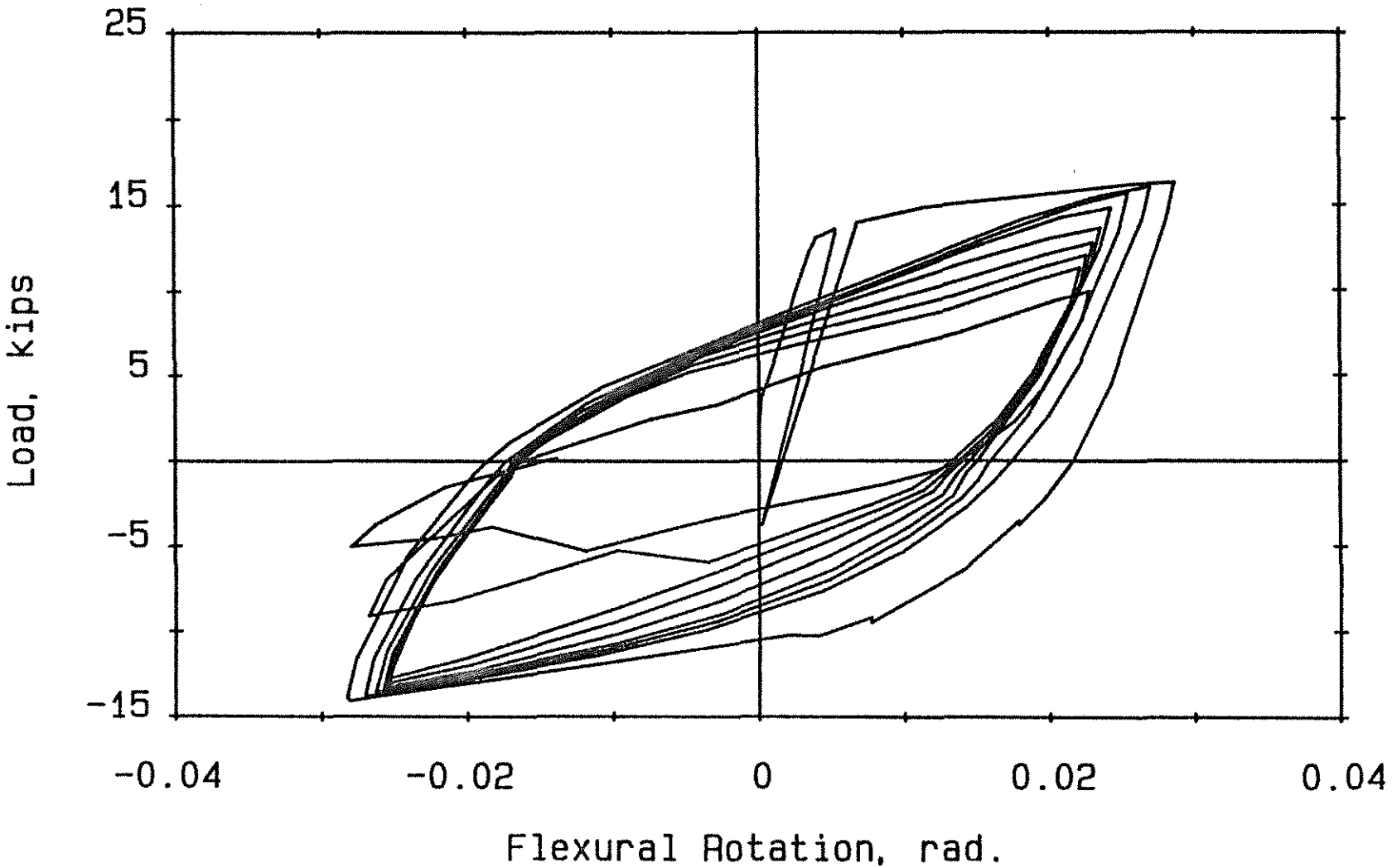

Fig. 2.11(f) Load versus Hinging Zone Flexural Rotation, Beam F-6

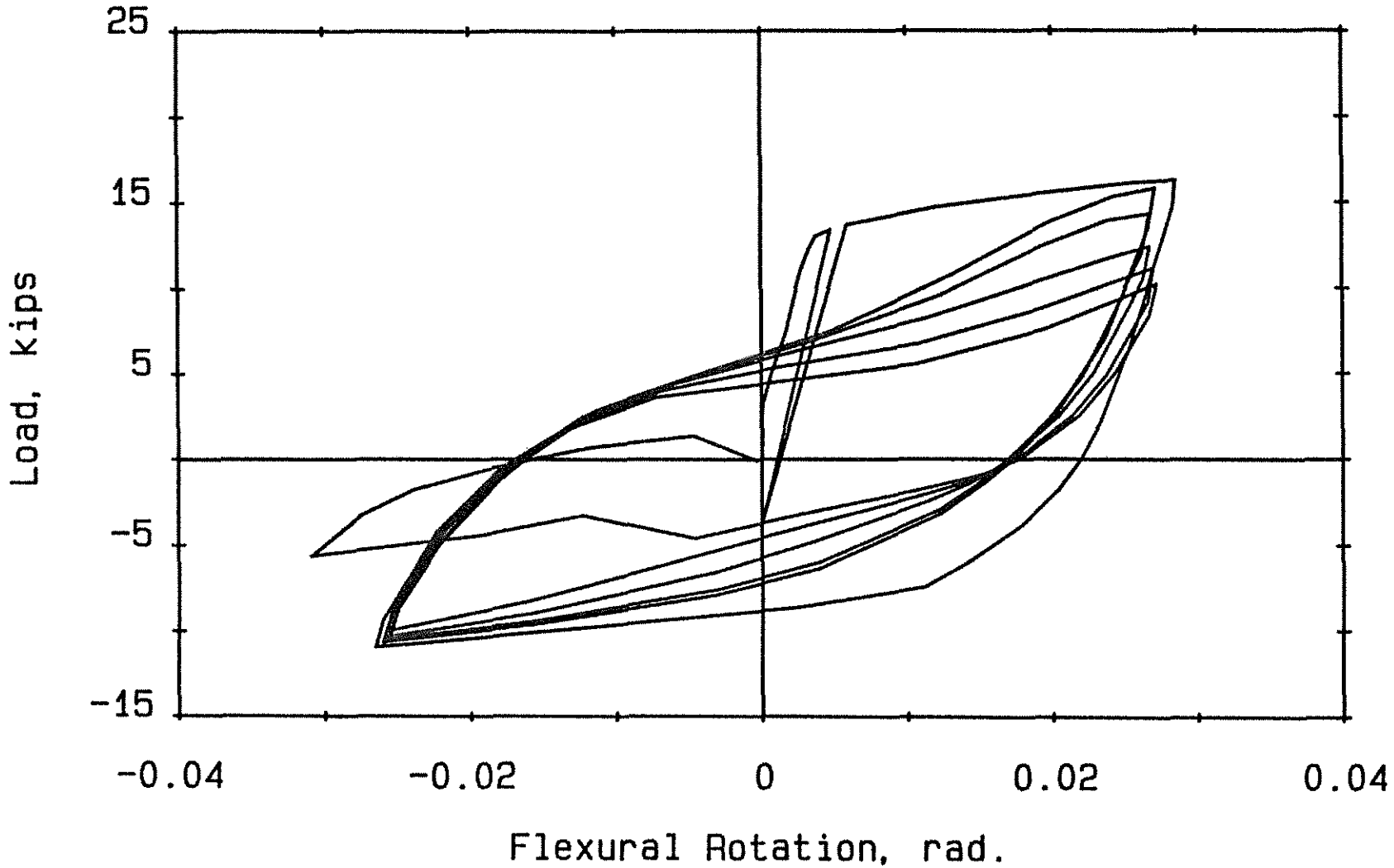

Fig. 2.11(g) Load versus Hinging Zone Flexural Rotation, Beam F-7

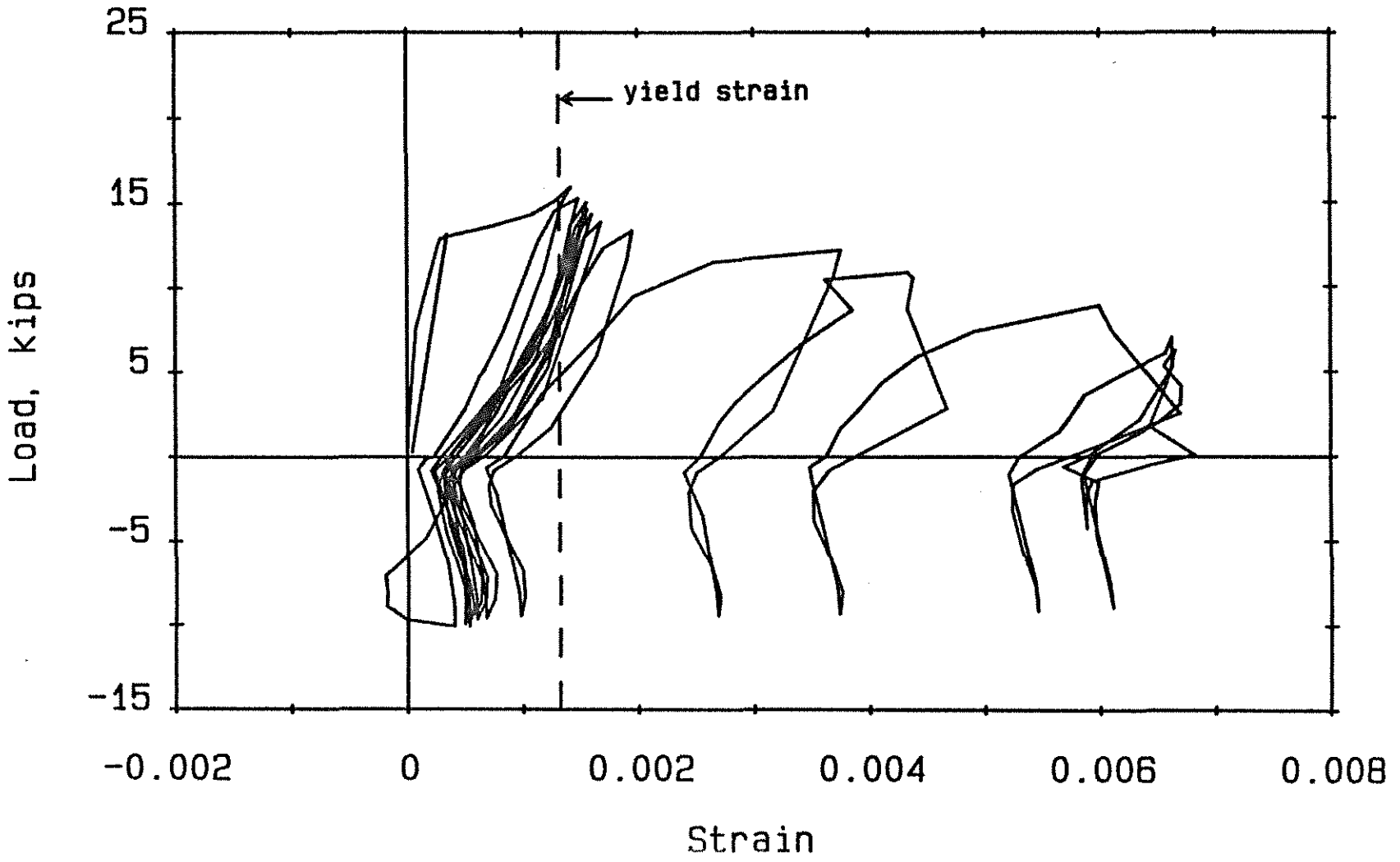

Fig. 2.12 Typical Load versus Stirrup Strain Plot

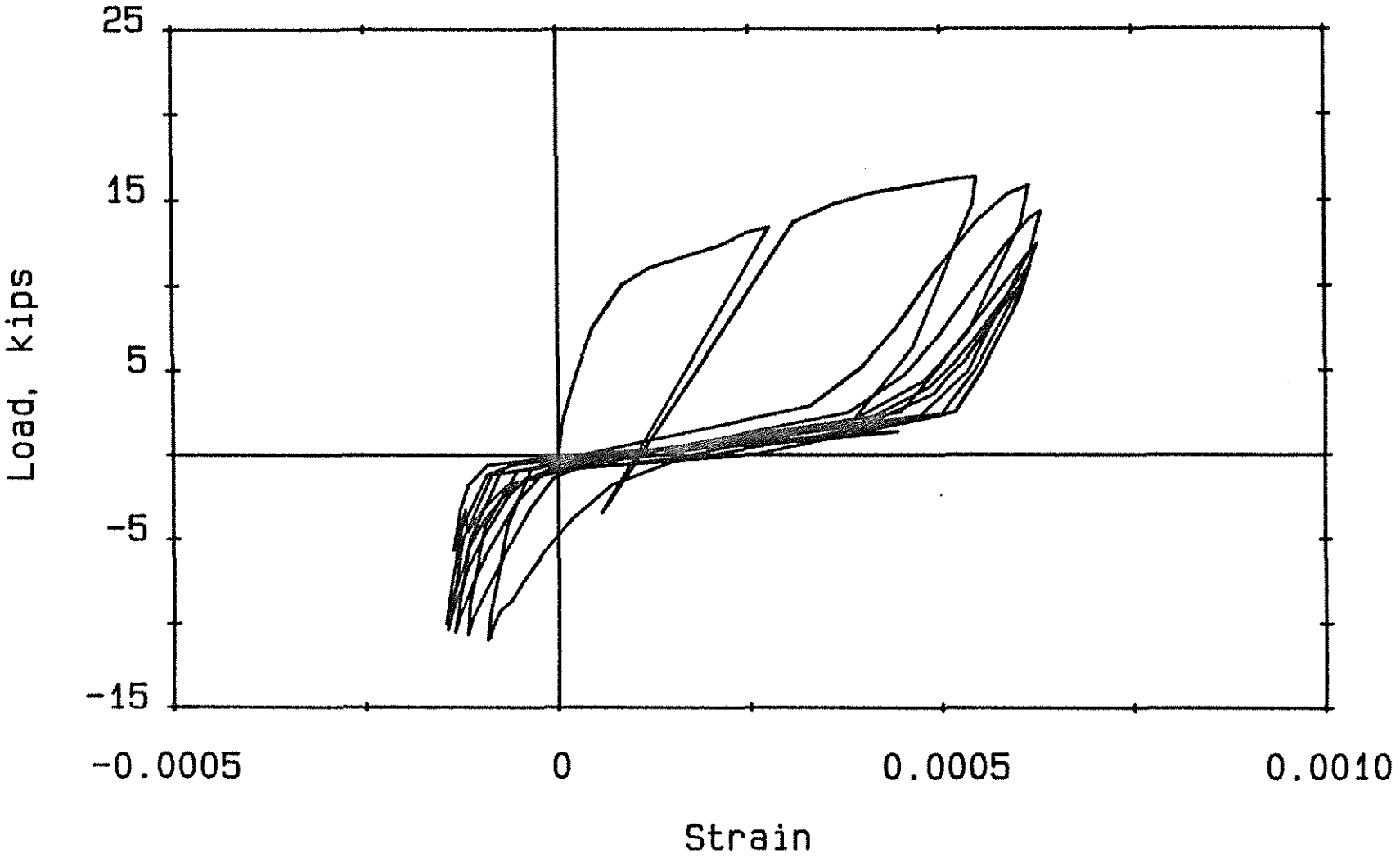

Fig. 2.13(a) Typical Load versus Anchorage Zone Strain, Top Longitudinal Reinforcement

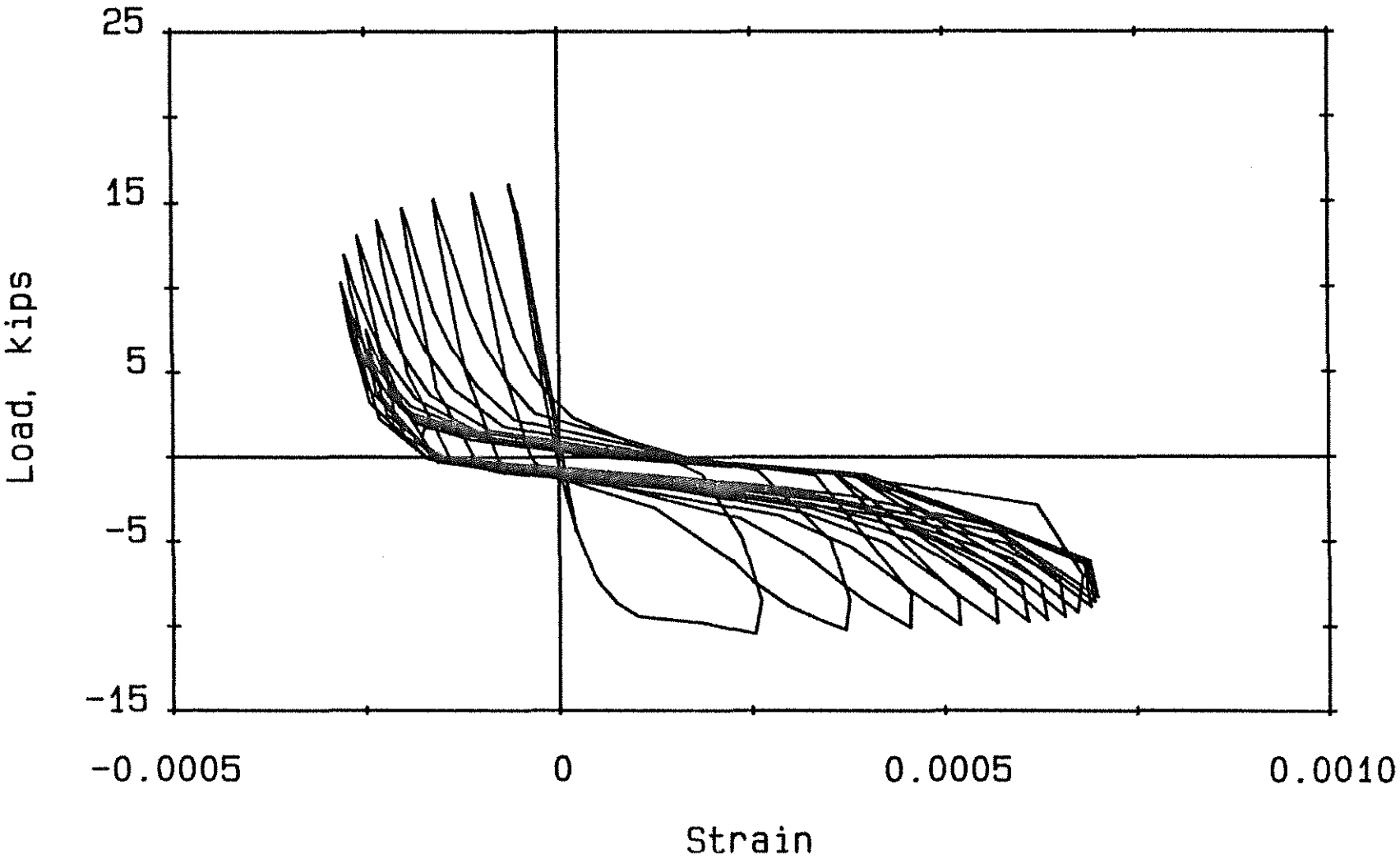

Fig. 2.13(b) Typical Load versus Anchorage Zone Strain, Bottom Longitudinal Reinforcement

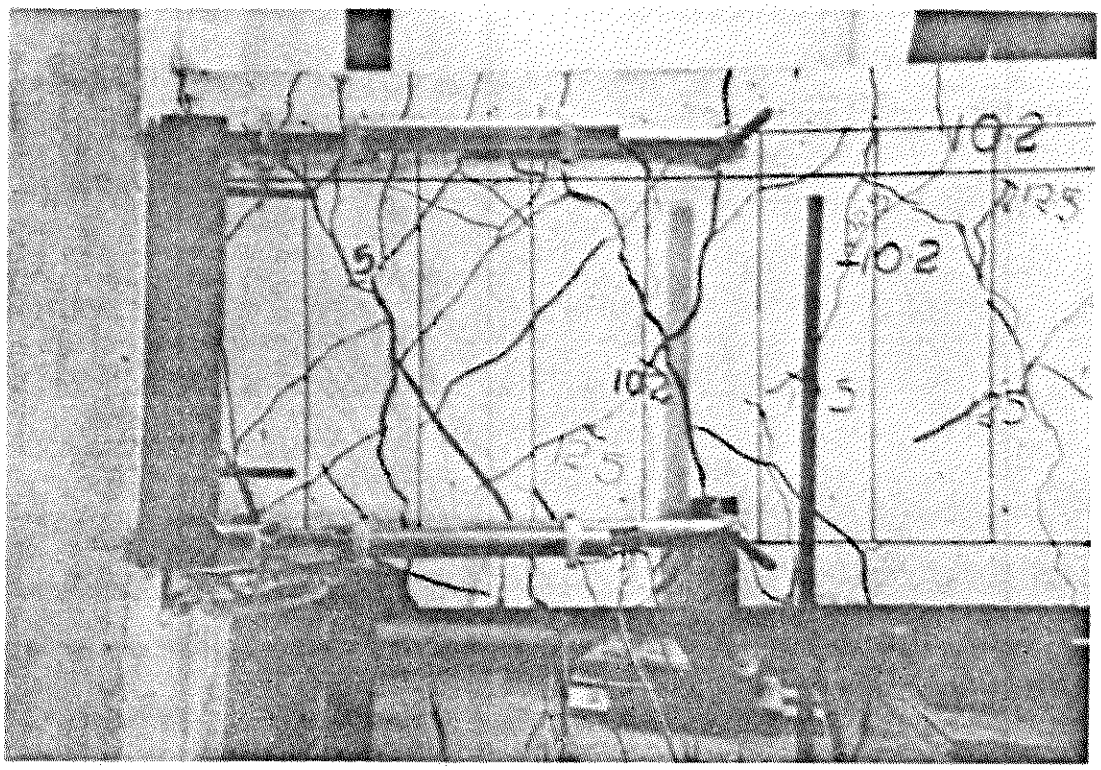

Fig. 2.14(a) Crack Pattern, Beam F-1

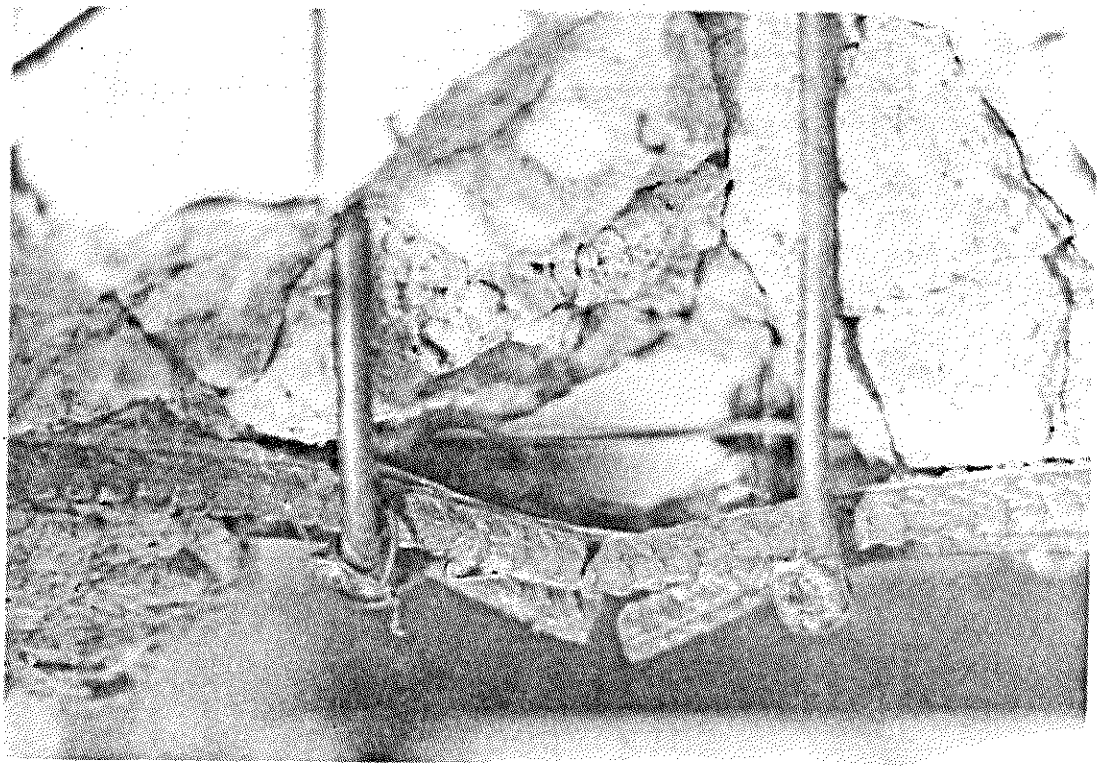

Fig. 2.14(b) Fractured Bottom Reinforcement, Beam F-1

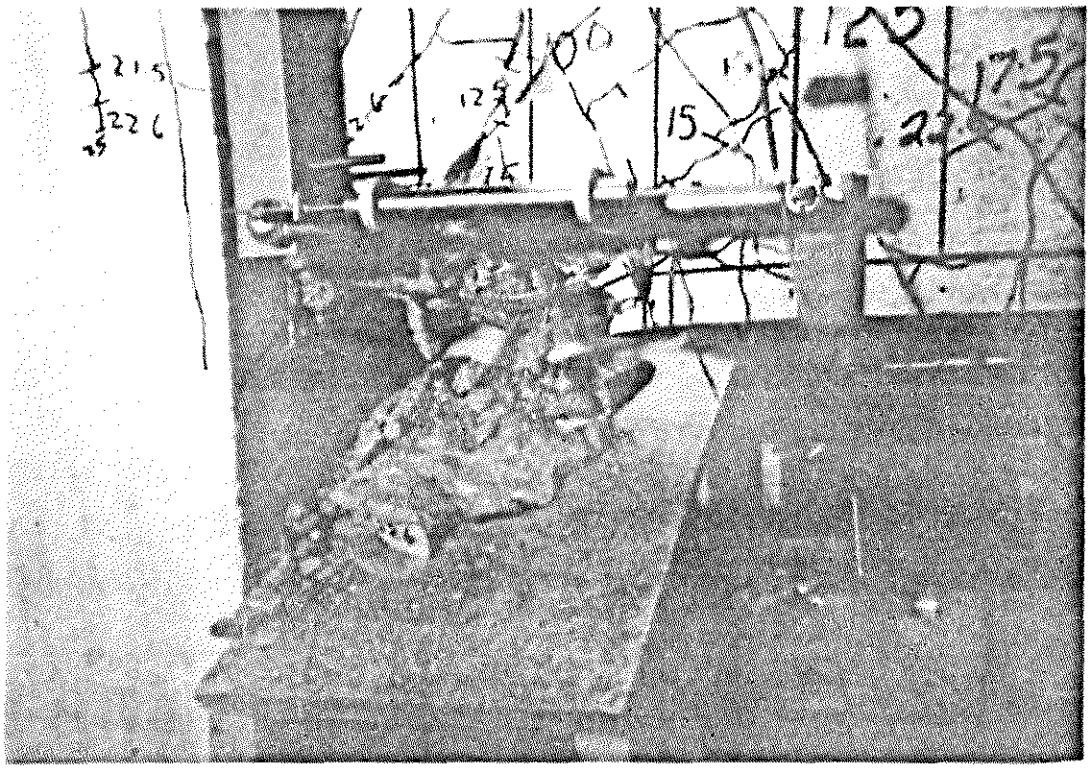

Fig. 2.15(a) Buckled Bottom Reinforcement, Beam F-2

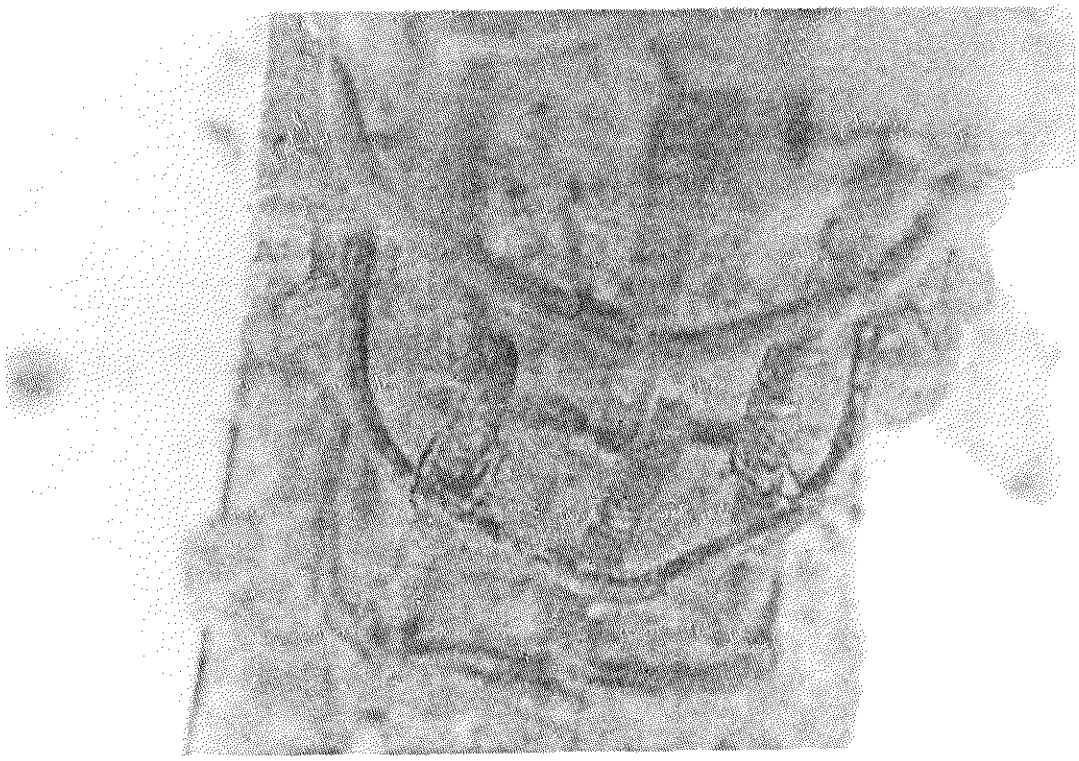

Fig. 2.15(b) Distorted Stirrups due to Severe Buckling, Beam F-2

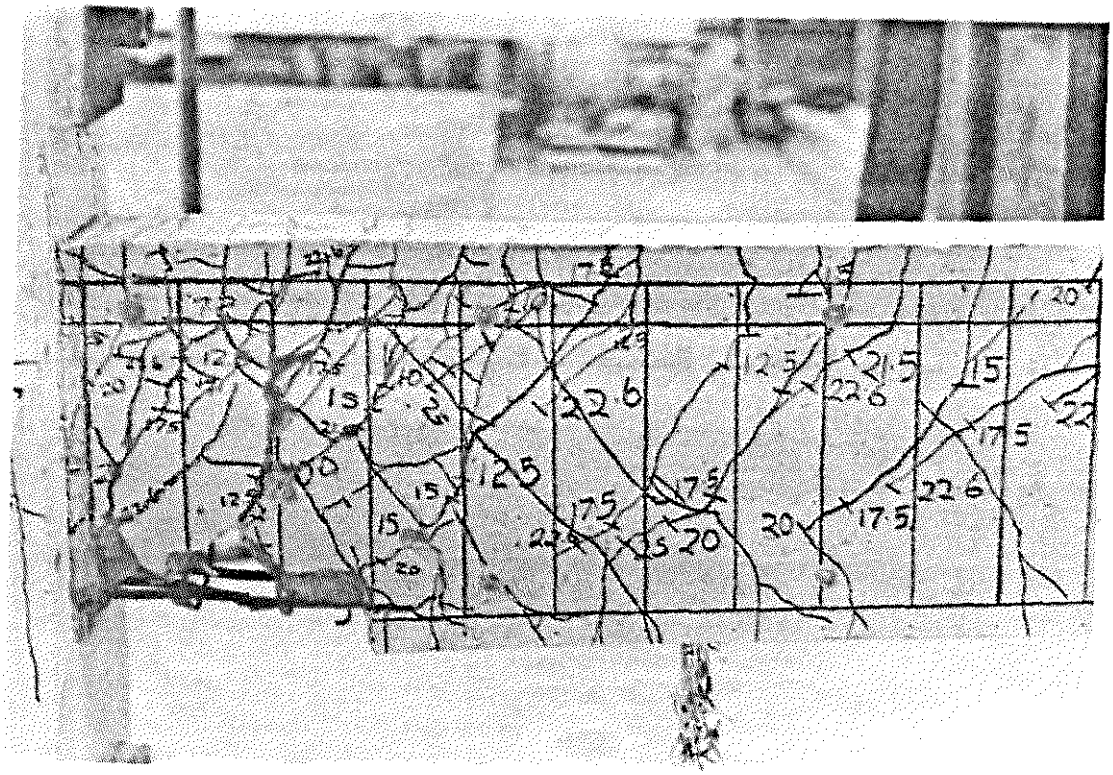

Fig. 2.15(c) Beam F-2 at Conclusion of Test

Fig. 2.16(a) Extent of Crushing within Hinging Zone in Beam F-3, Side 1

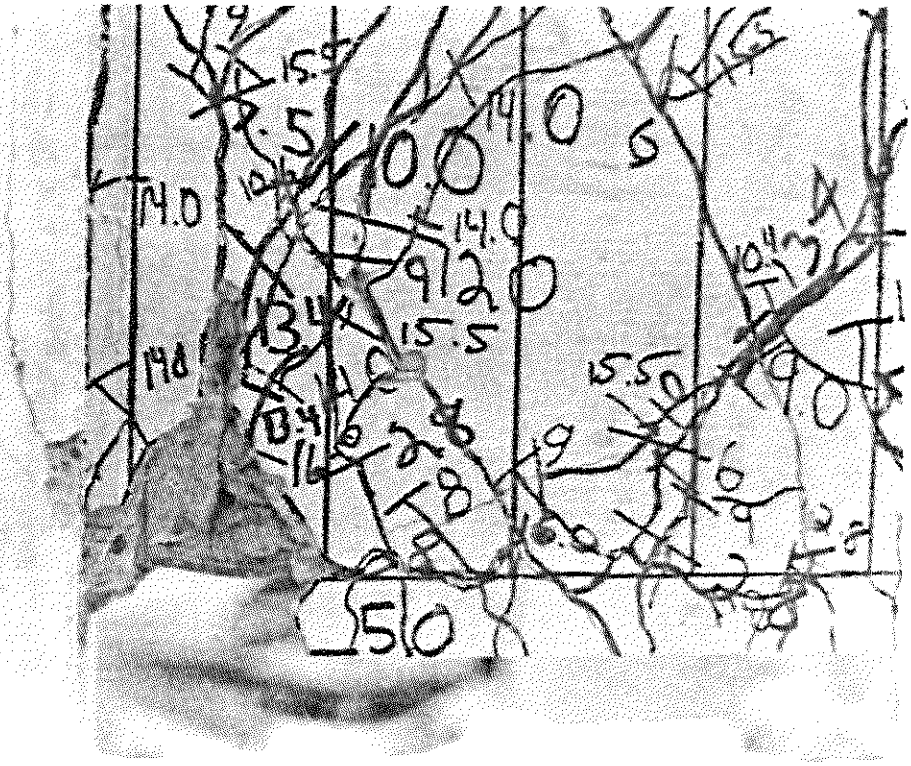

Fig. 2.16(b) Extent of Crushing within Hinging Zone in Beam F-3, Side 2

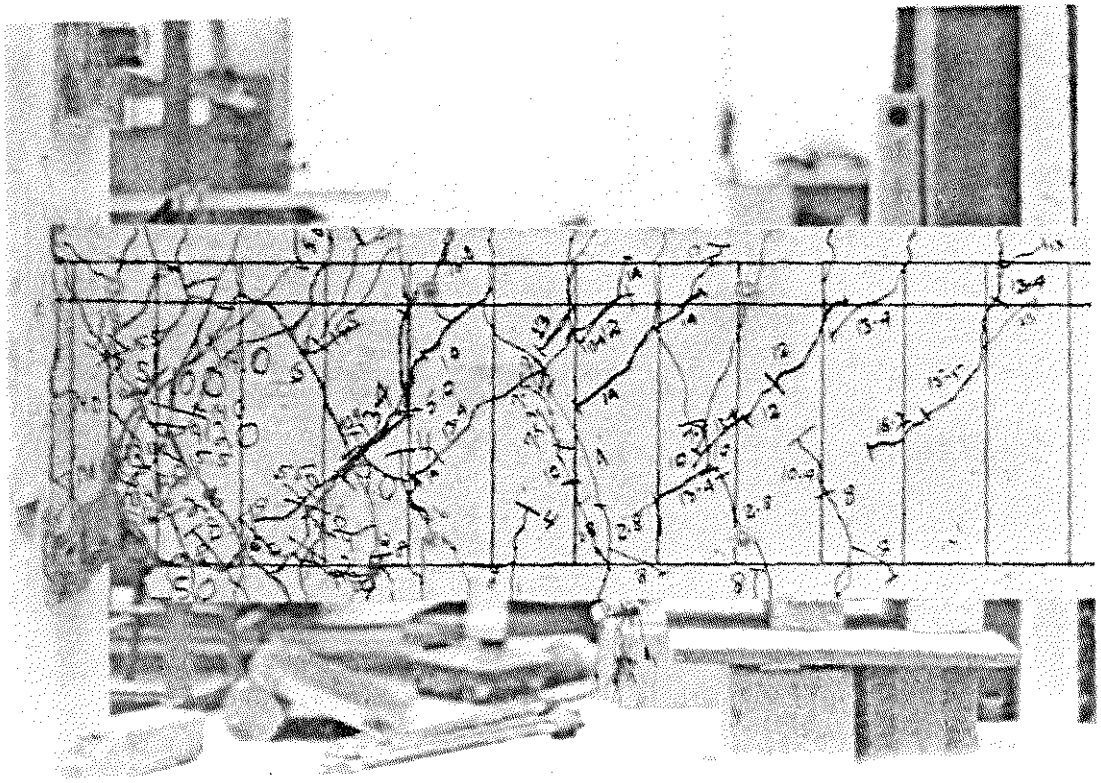

Fig. 2.16(c) Beam F-3 at Conclusion of Test

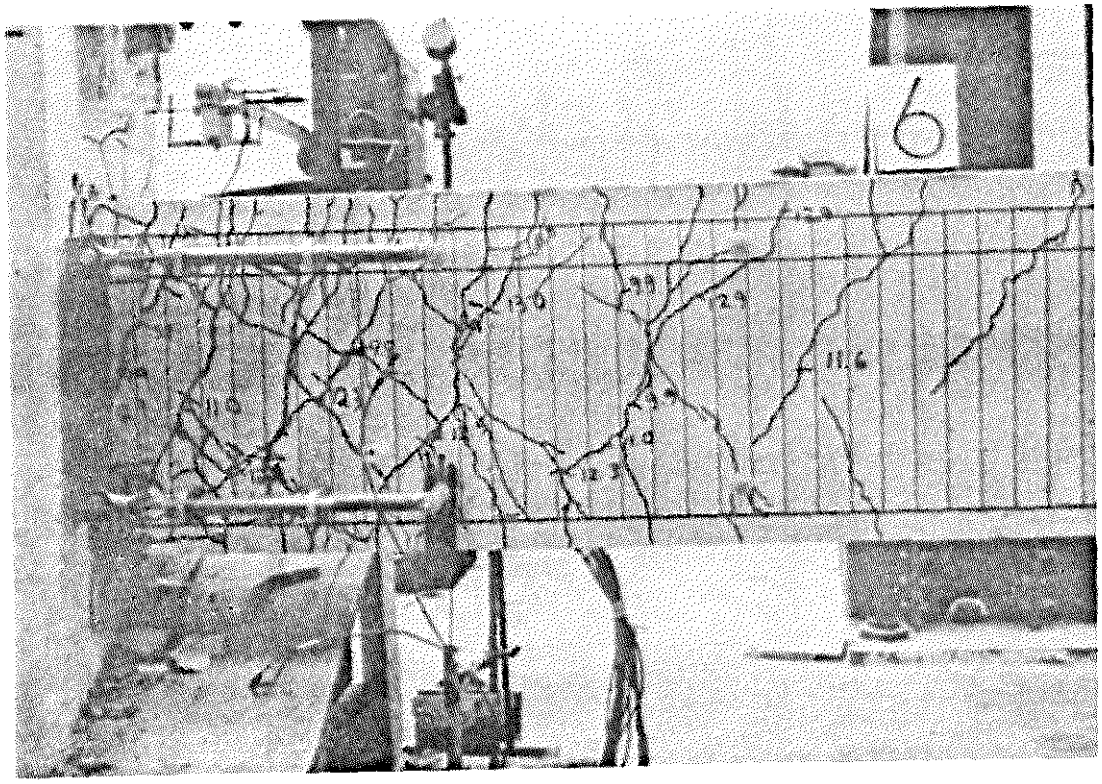

Fig. 2.17 Crack Pattern, Beam F-4

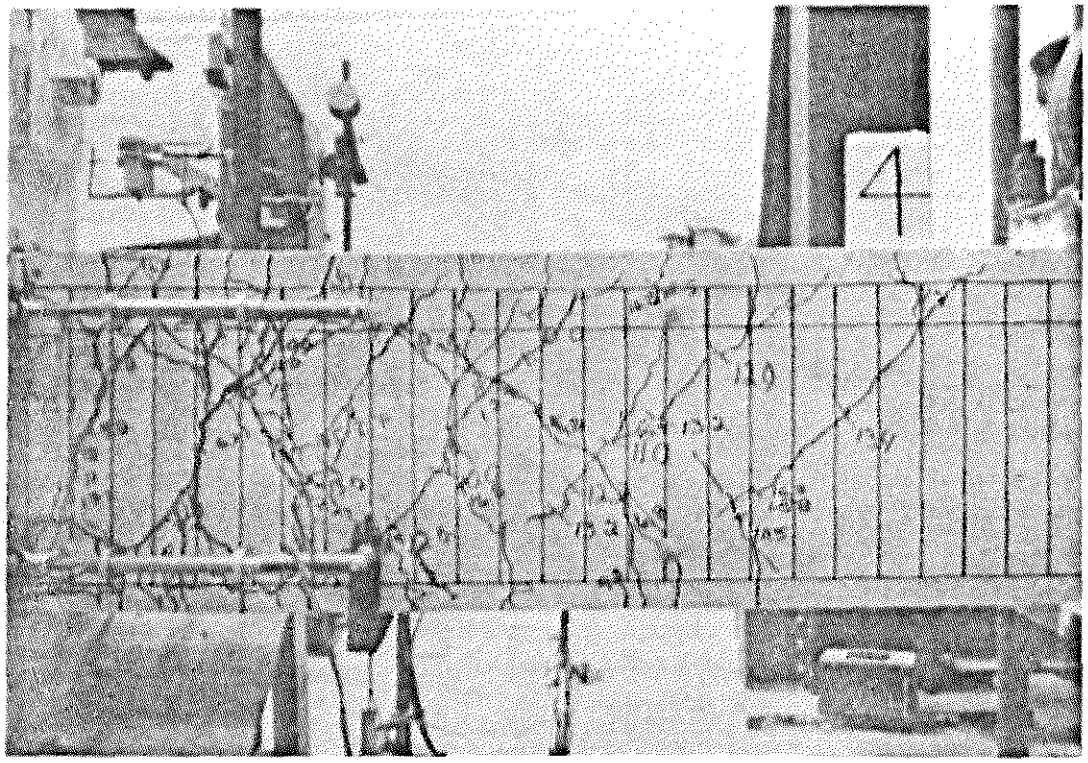

Fig. 2.18(a) Crack Pattern, Beam F-5

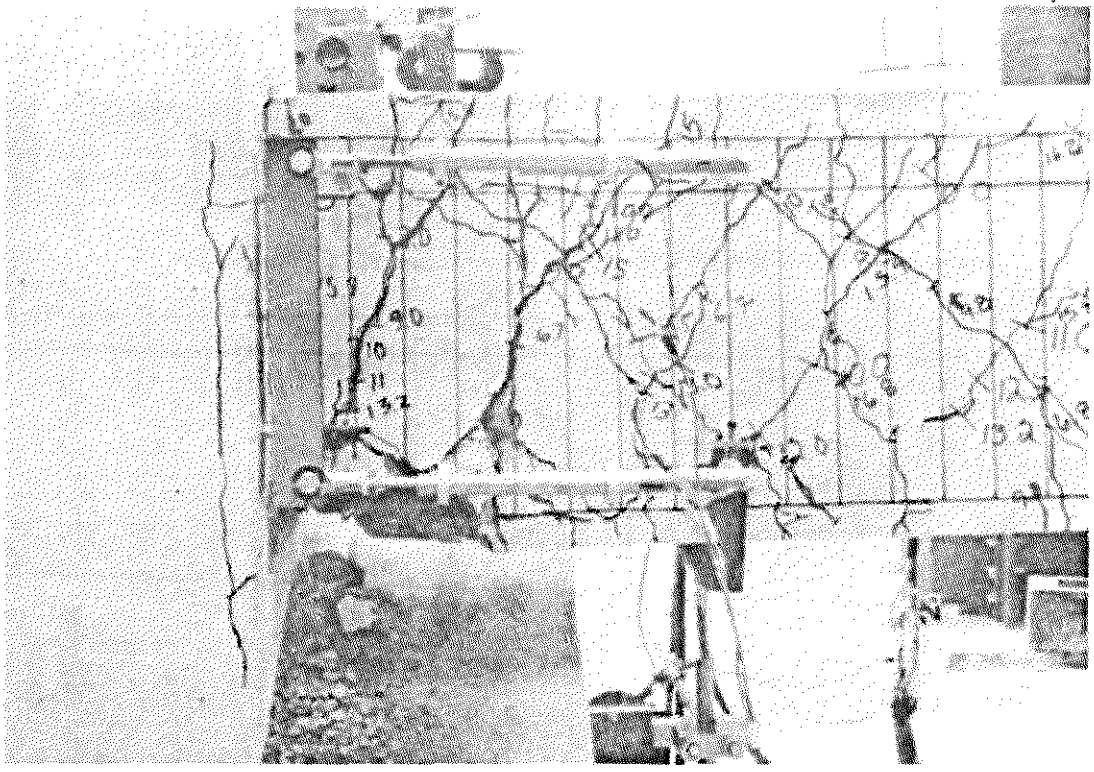

Fig. 2.18(b) Hinging Zone of Beam F-5 at End of Eleventh Cycle

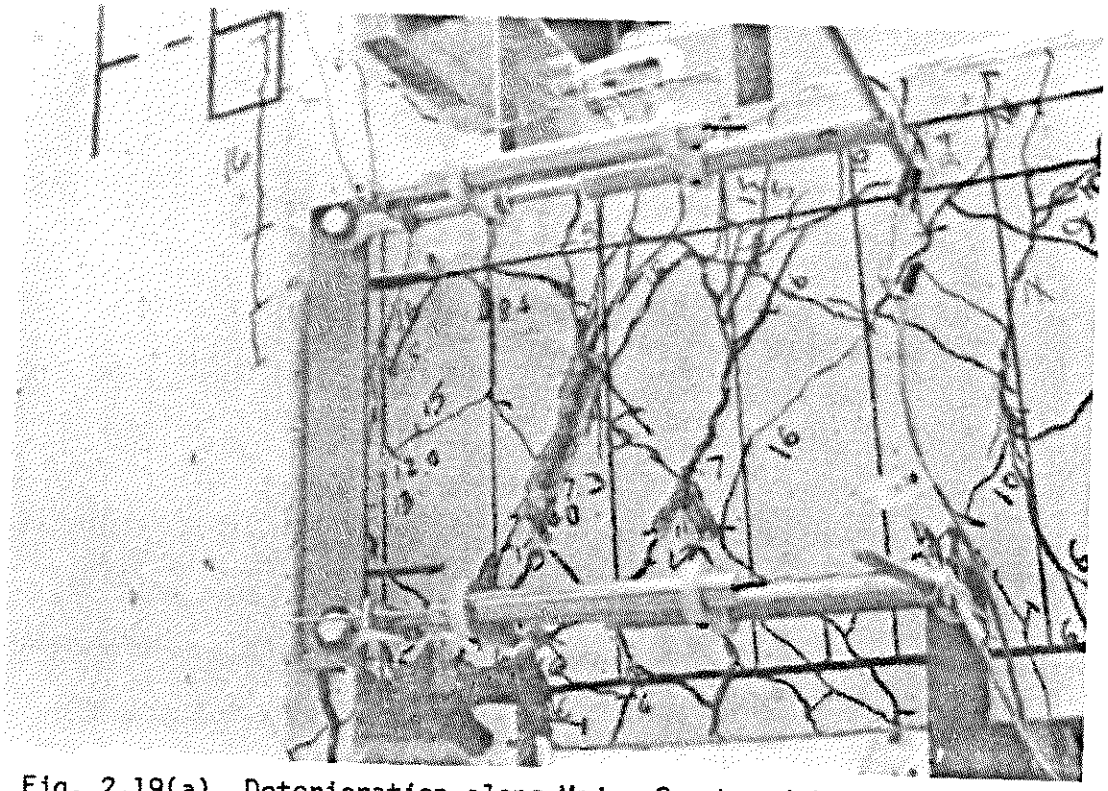

Fig. 2.19(a) Deterioration along Major Cracks within Hinging Zone, Beam F-6

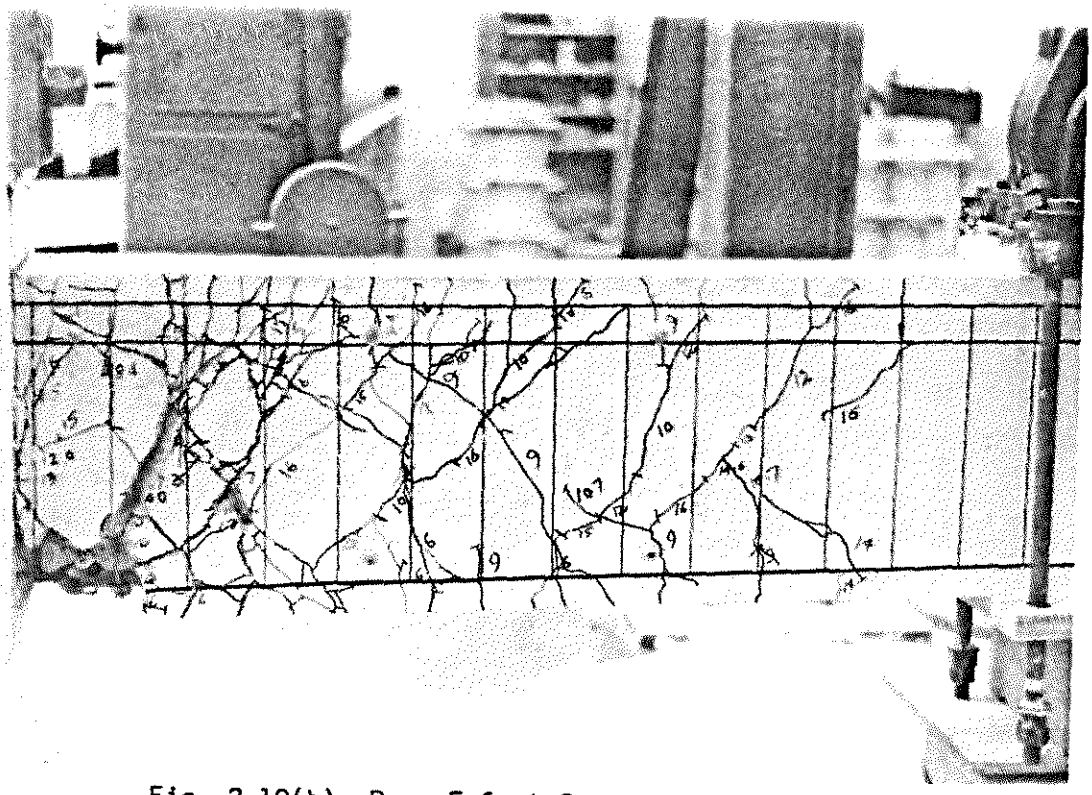

Fig. 2.19(b) Beam F-6 at Conclusion of Test

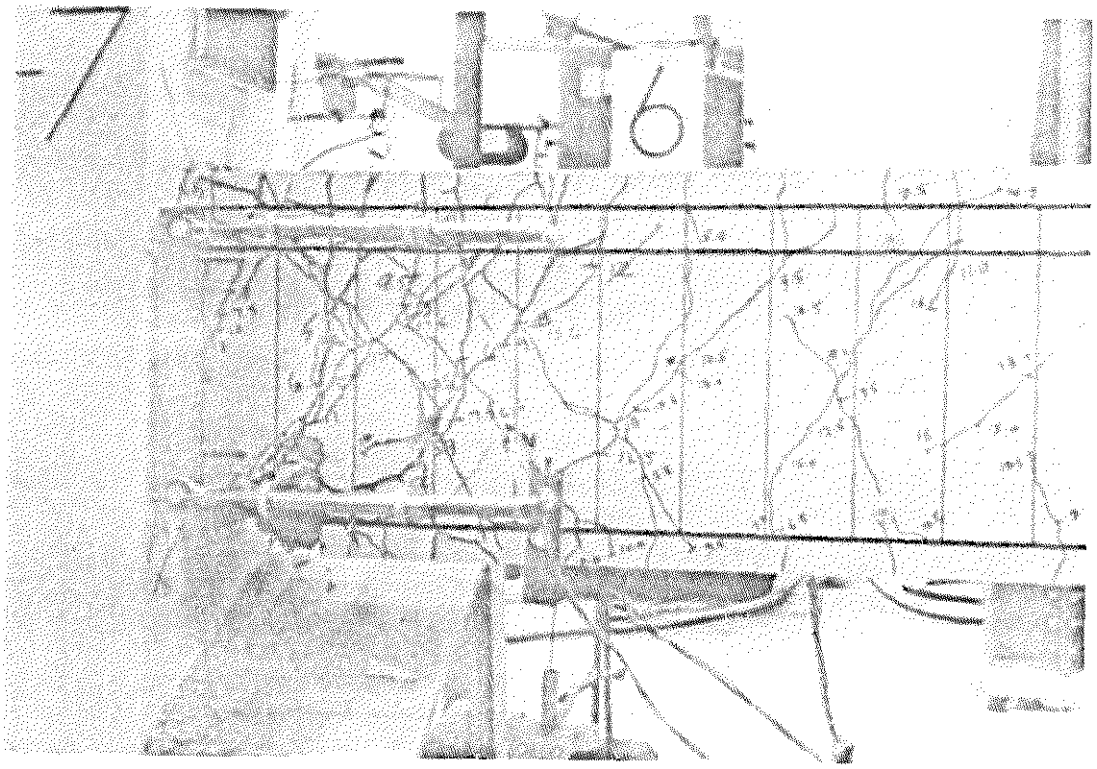

Fig. 2.20 Beam F-7 at Conclusion of Test

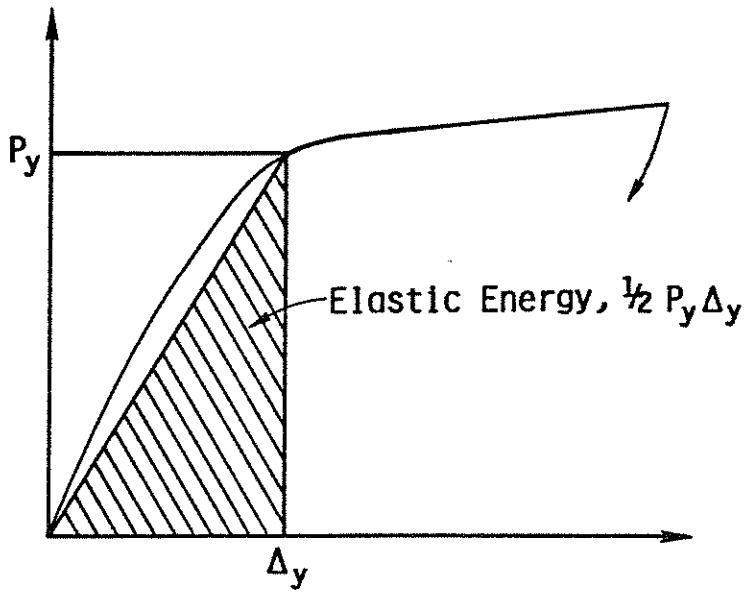

Fig. 3.1 Elastic Energy

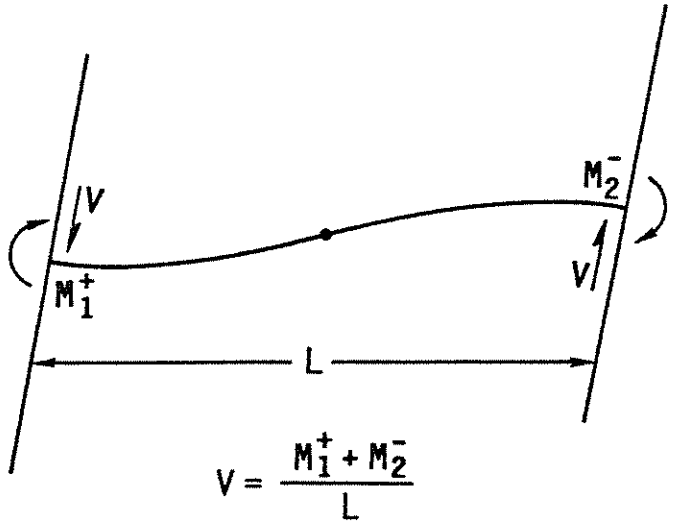

Fig. 3.2 Beam Shear due to Lateral Deformation

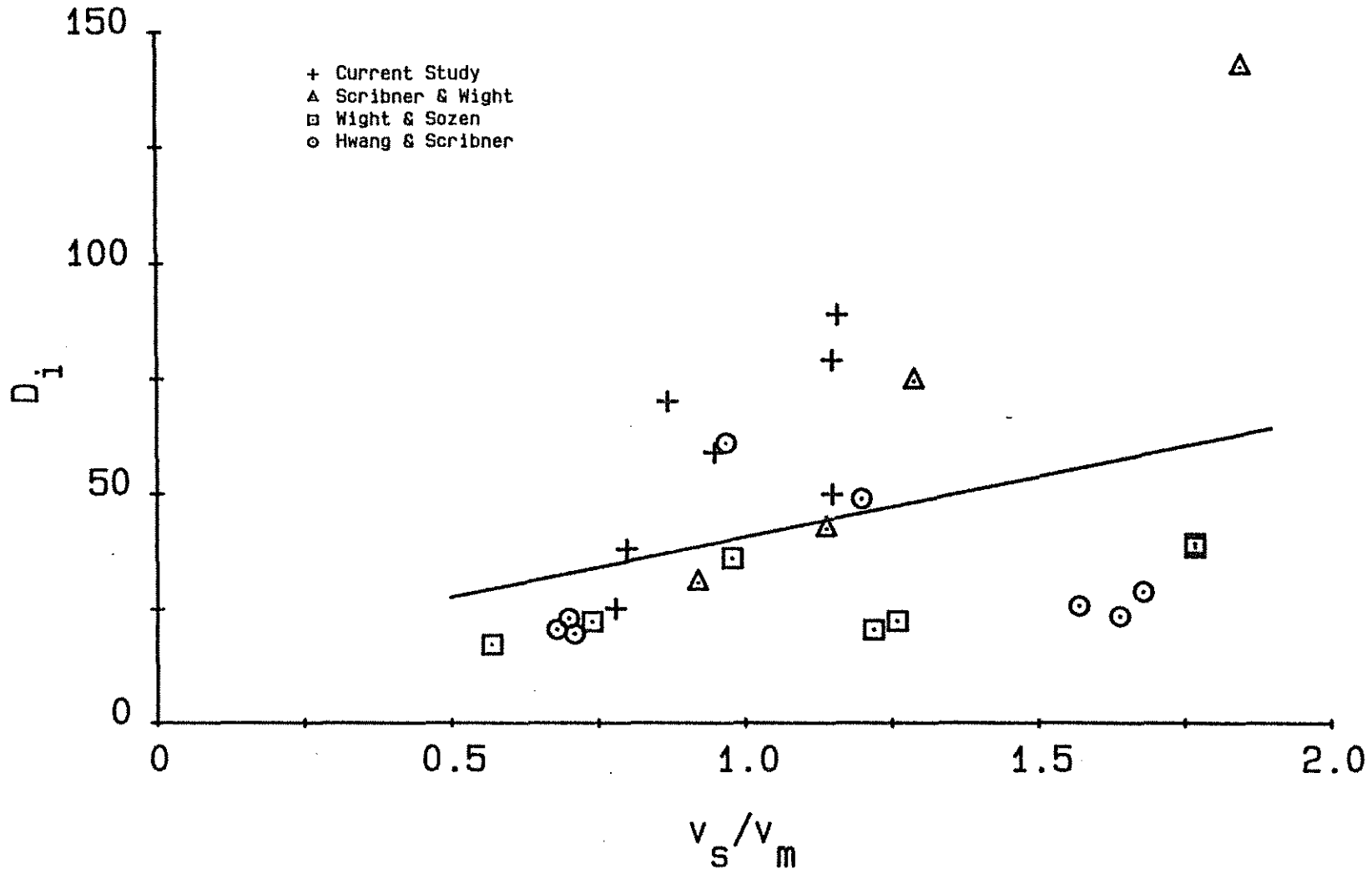

Fig. 3.3(a) D_1 versus v_s/v_m, Beams used in D_1 Analyses

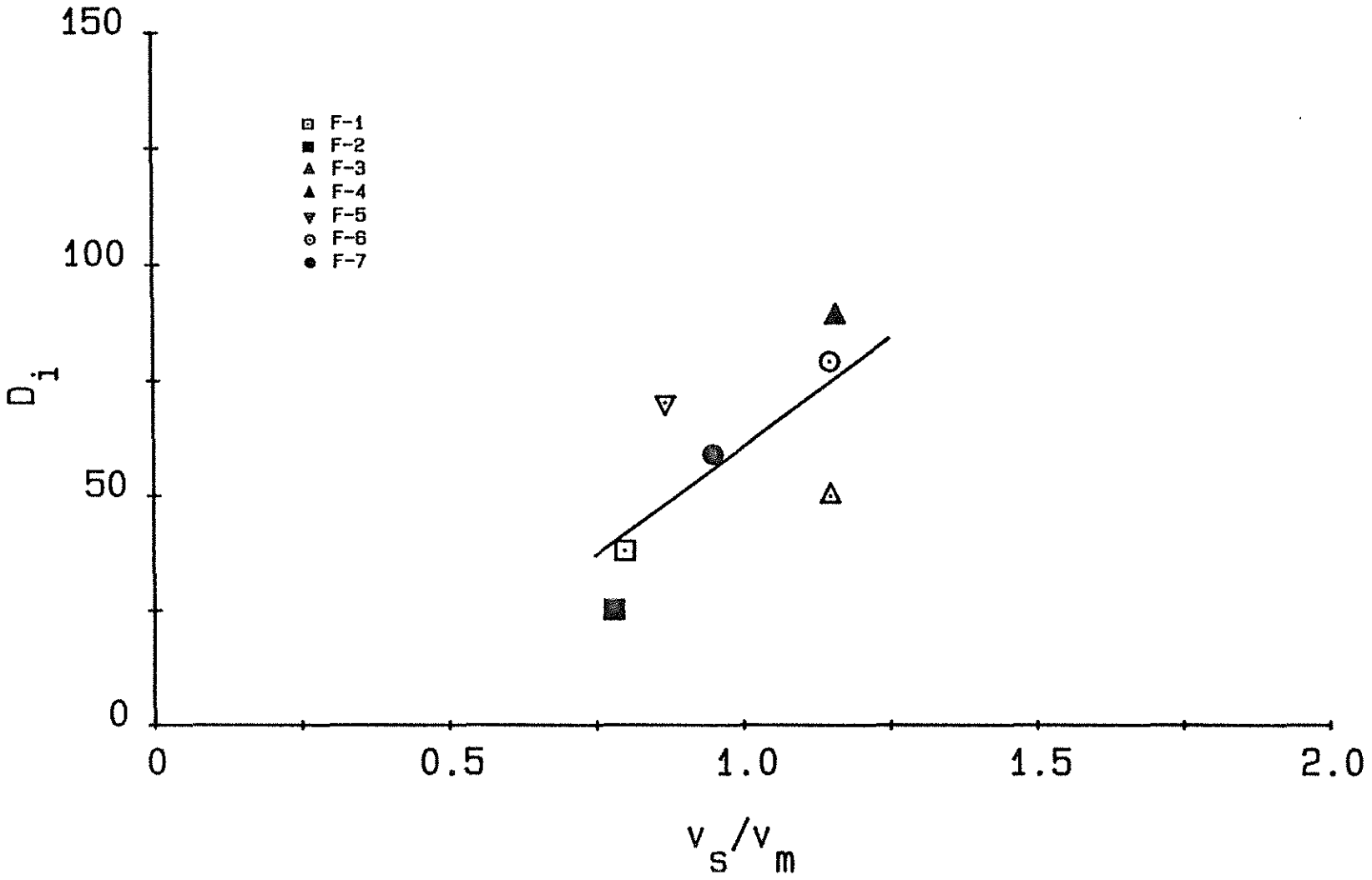

Fig. 3.3(b) D_i versus v_s/v_m, Current Study

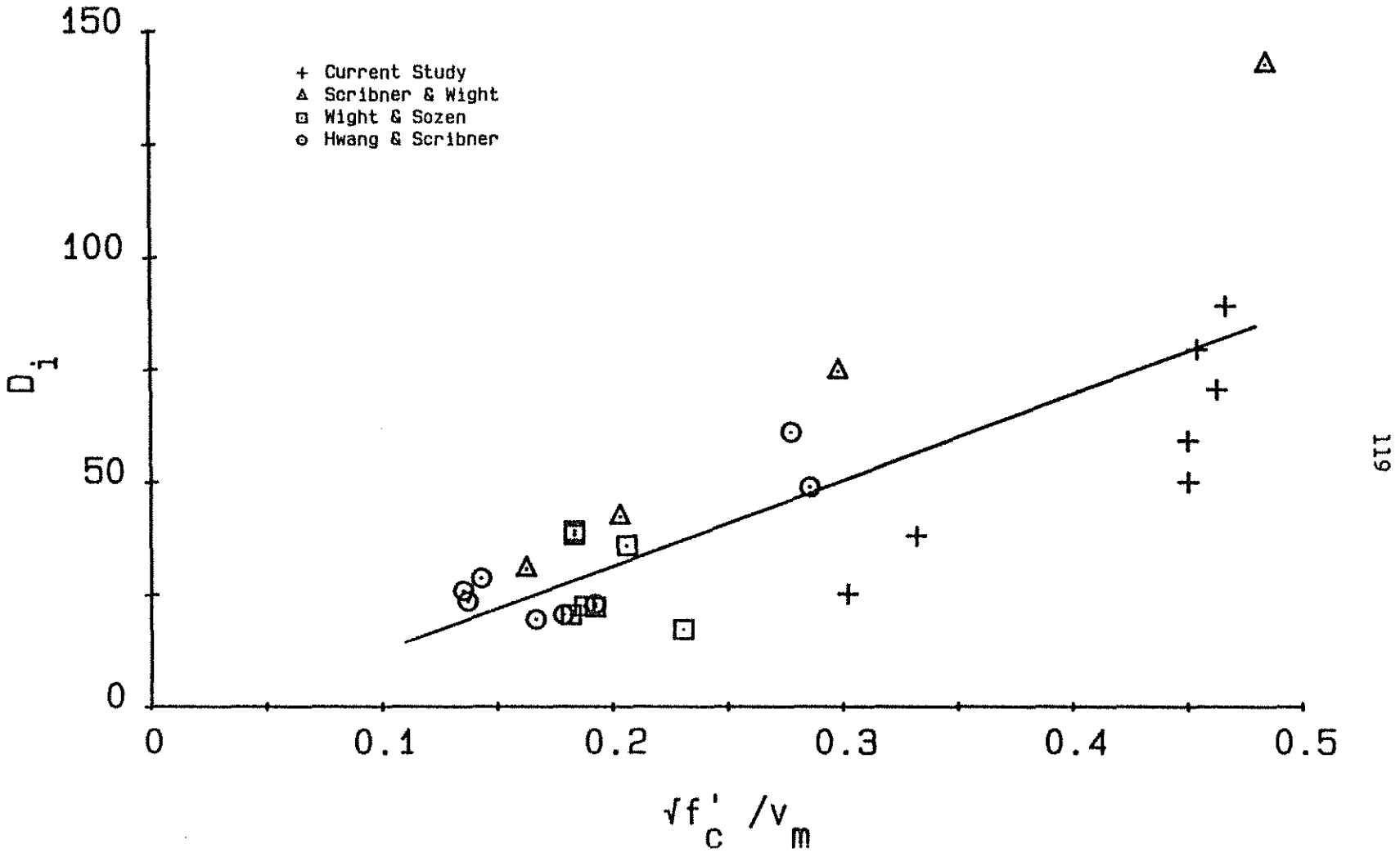

Fig. 3.4(a) D_i versus $\sqrt{f'_c}/v_m$, Beams used in D_i Analyses

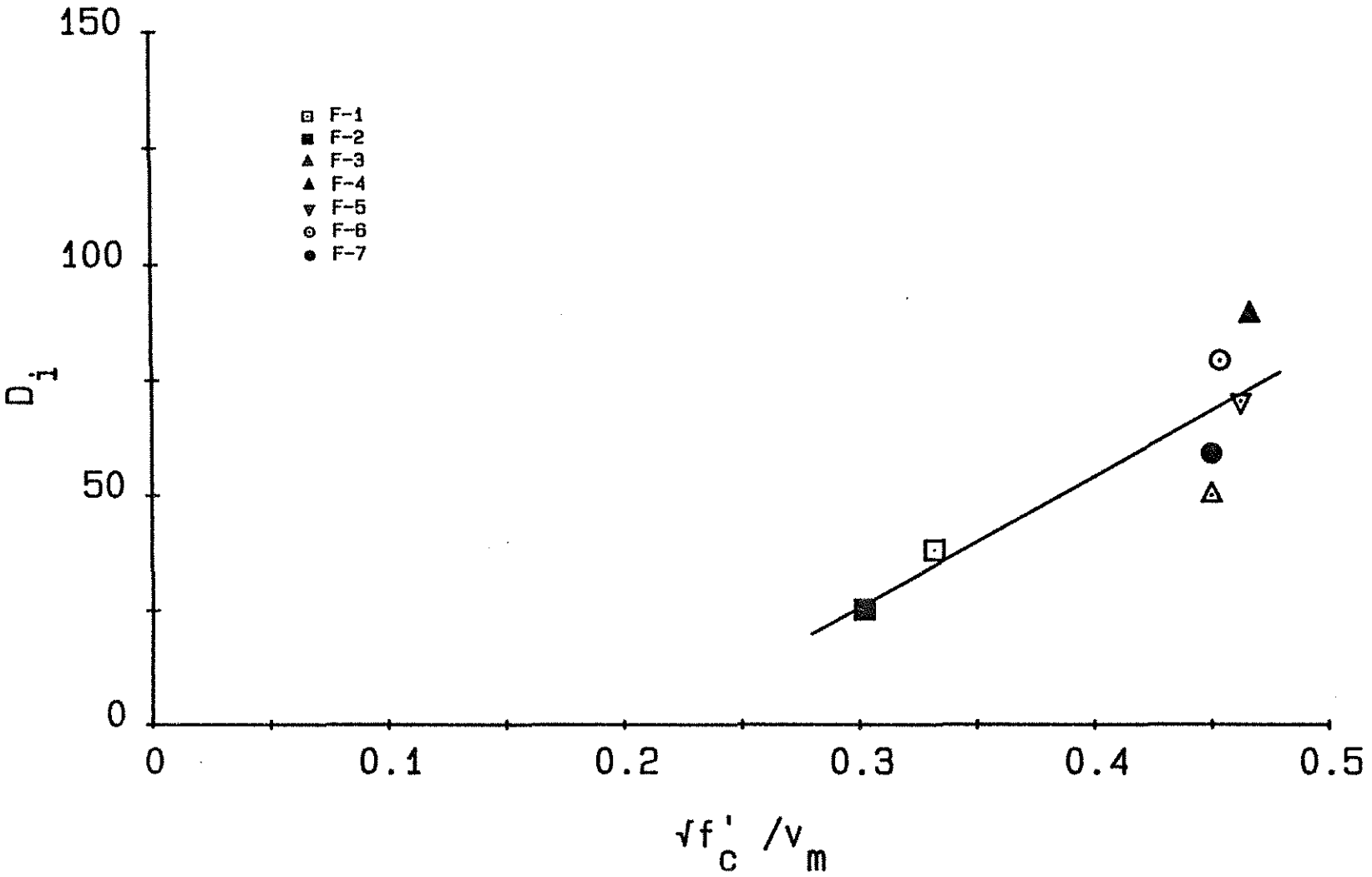

Fig. 3.4(b) D_1 versus $\sqrt{f'_c}/v_m$, Current Study

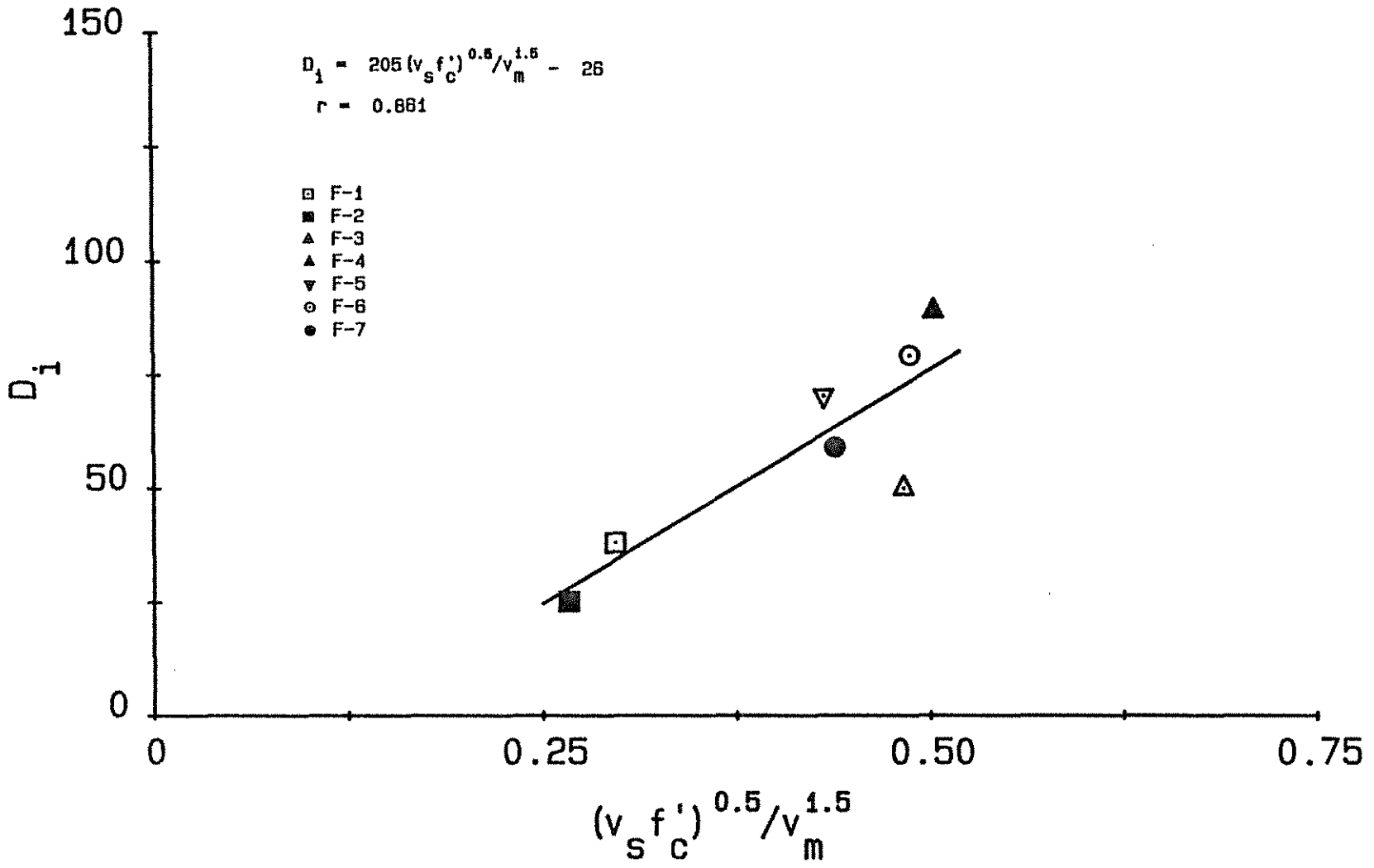

Fig. 3.5(a) Di versus $(v_s f'_c)^{0.5}/v_m^{1.5}$, Current Study

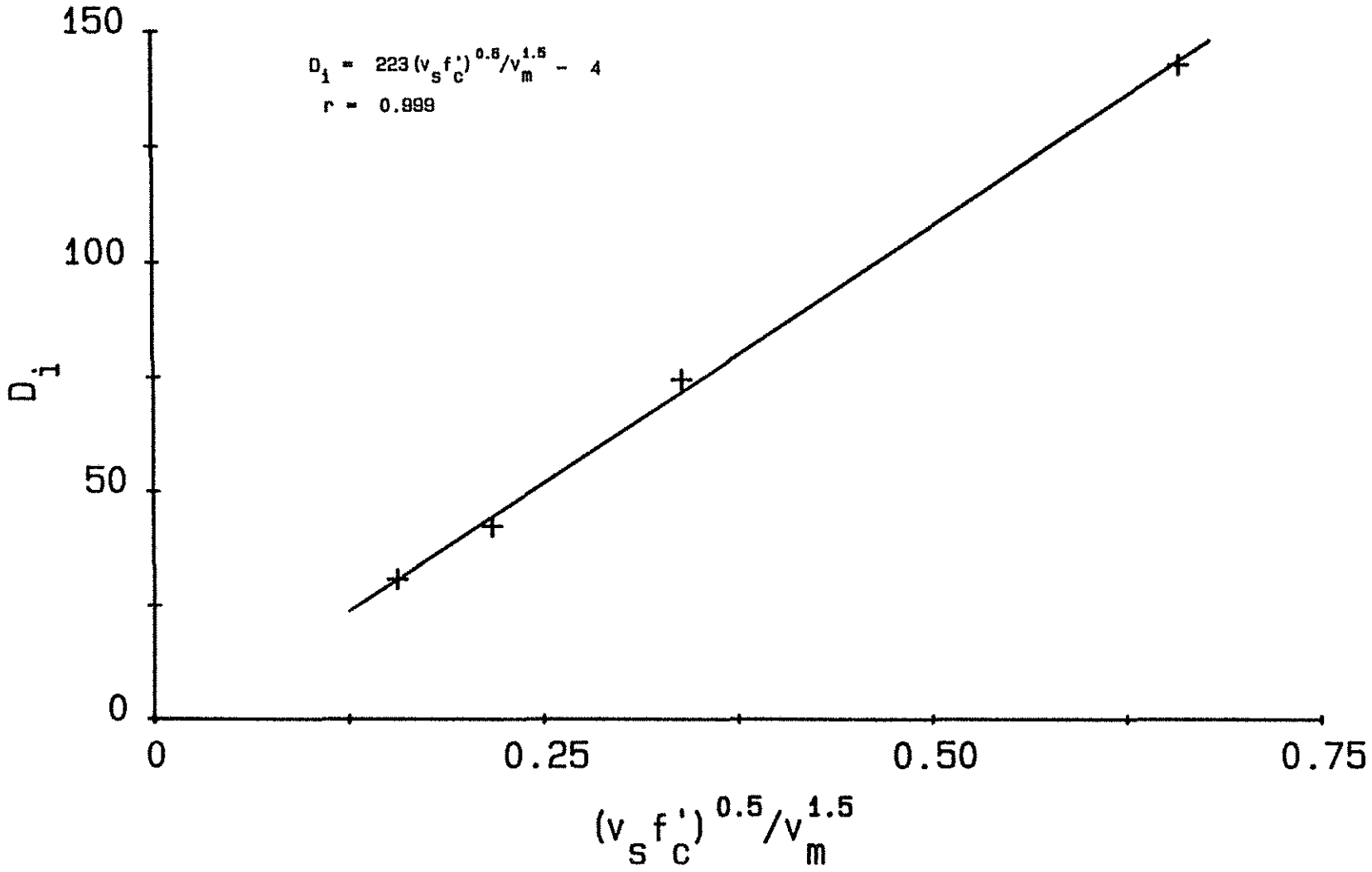

Fig. 3.5(b) D_i versus $(v_s f_c')^{0.5}/v_m^{1.5}$, Scribner & Wight (23,24)

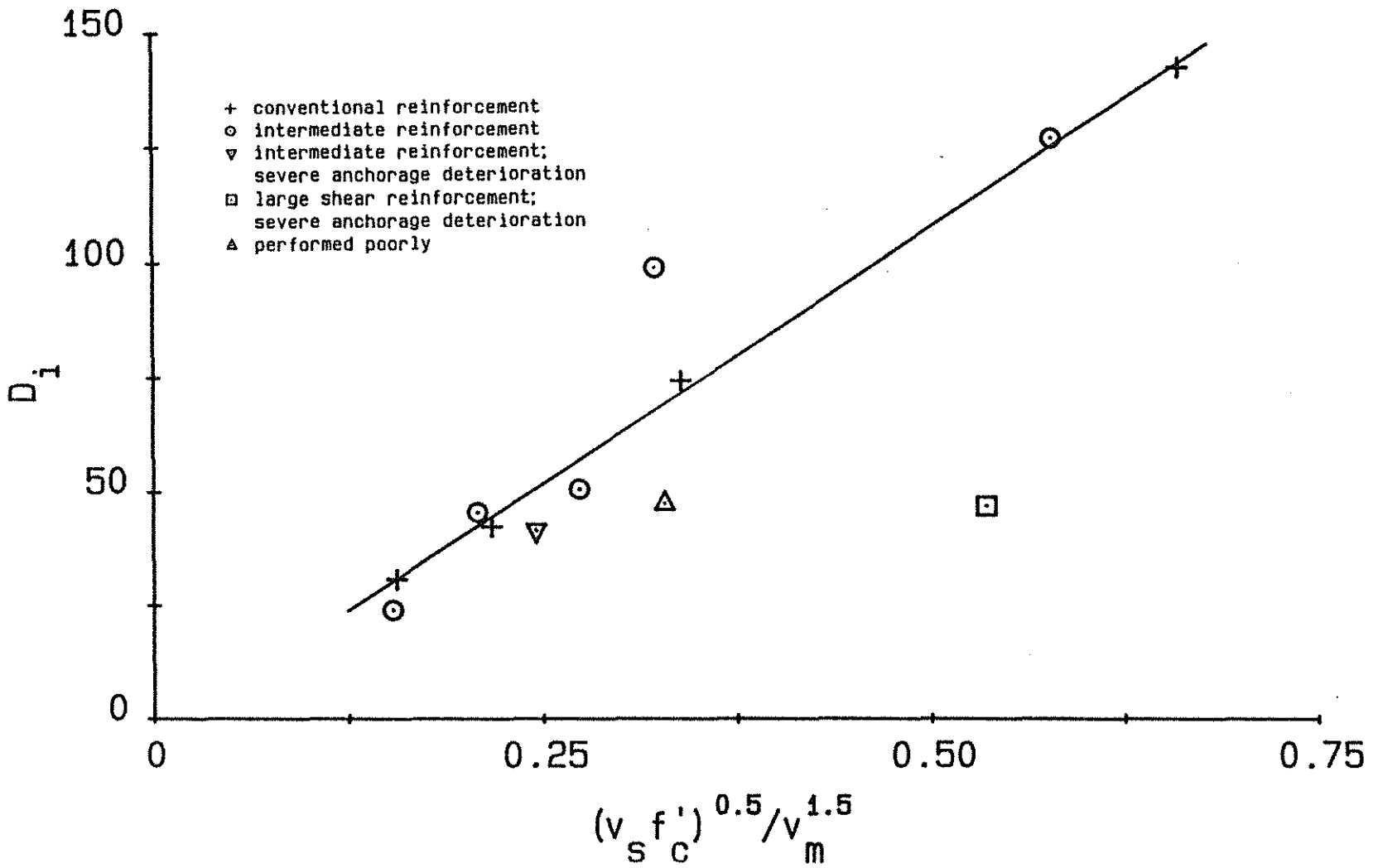

Fig. 3.5(c) Effect of Intermediate Reinforcement and Anchorage Slip, D_i versus $(v_s f'_c)^{0.5}/v_m^{1.5}$, Scribner & Wight (23,24)

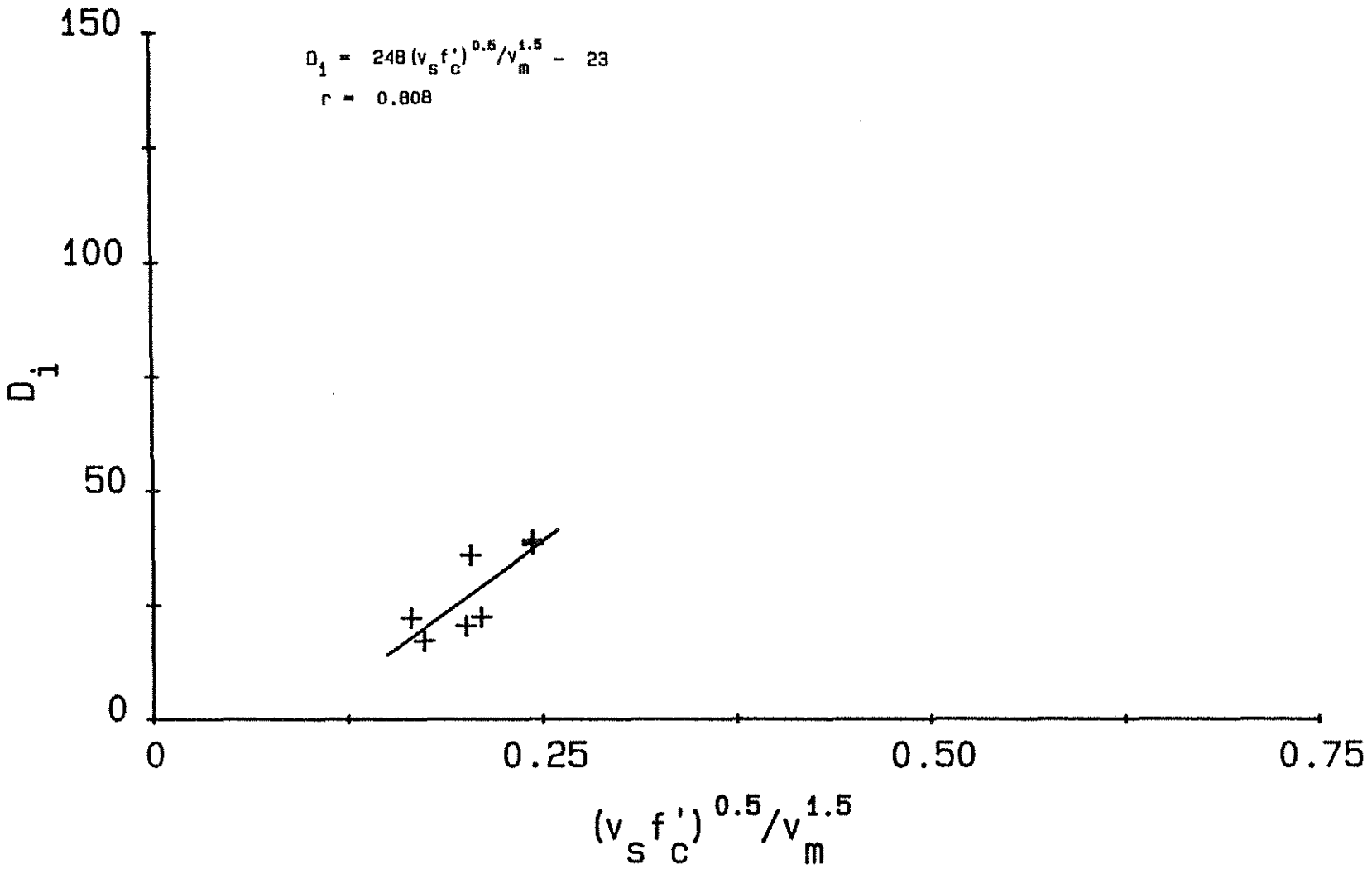

Fig. 3.5(d) D_i versus $(v_s f'_c)^{0.5}/v_m^{1.5}$, Wight & Sozen (31,32)

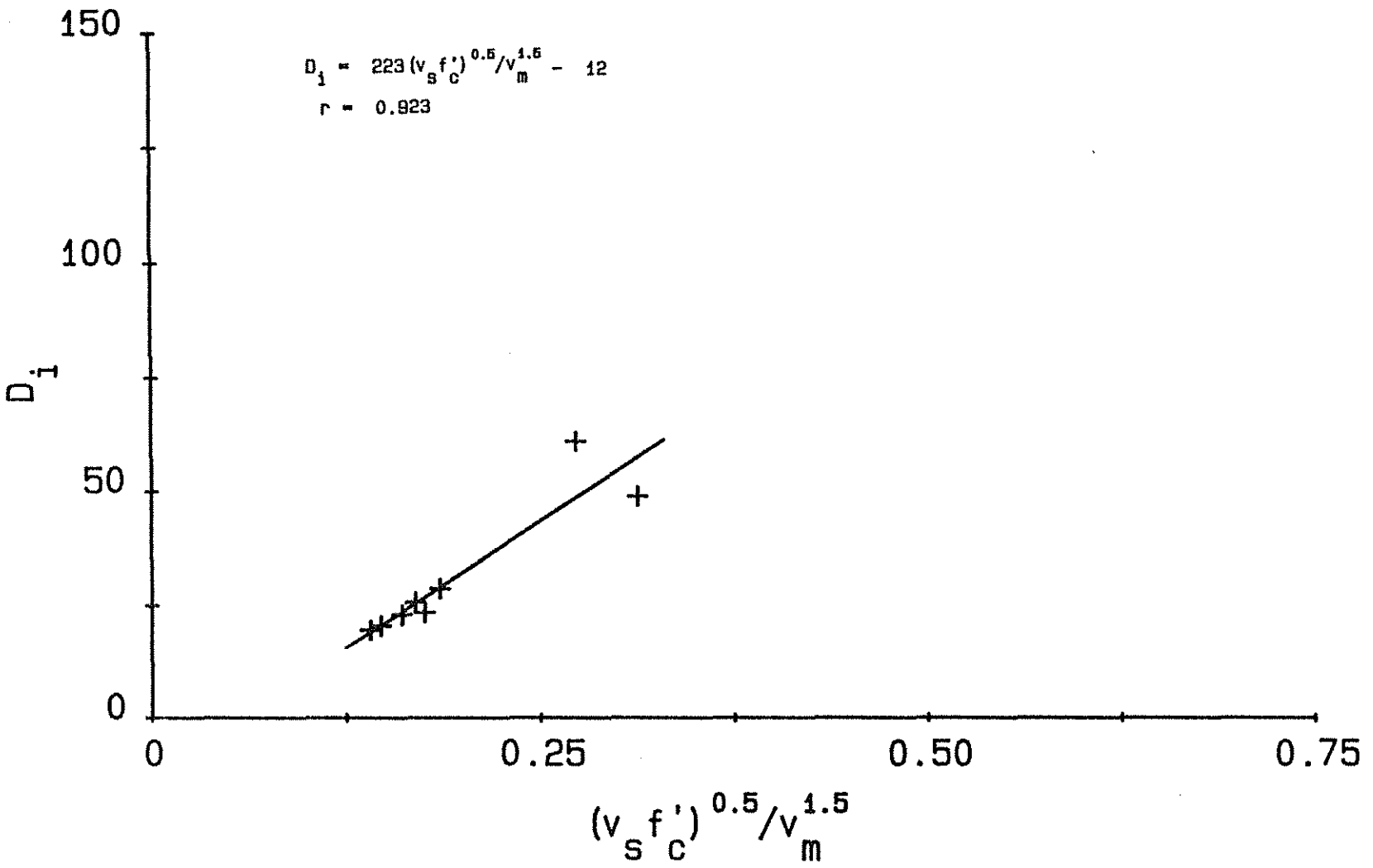

Fig. 3.5(e) D_1 versus $(v_s f'_c)^{0.5}/v_m^{1.5}$, Hwang & Scribner (13,14)

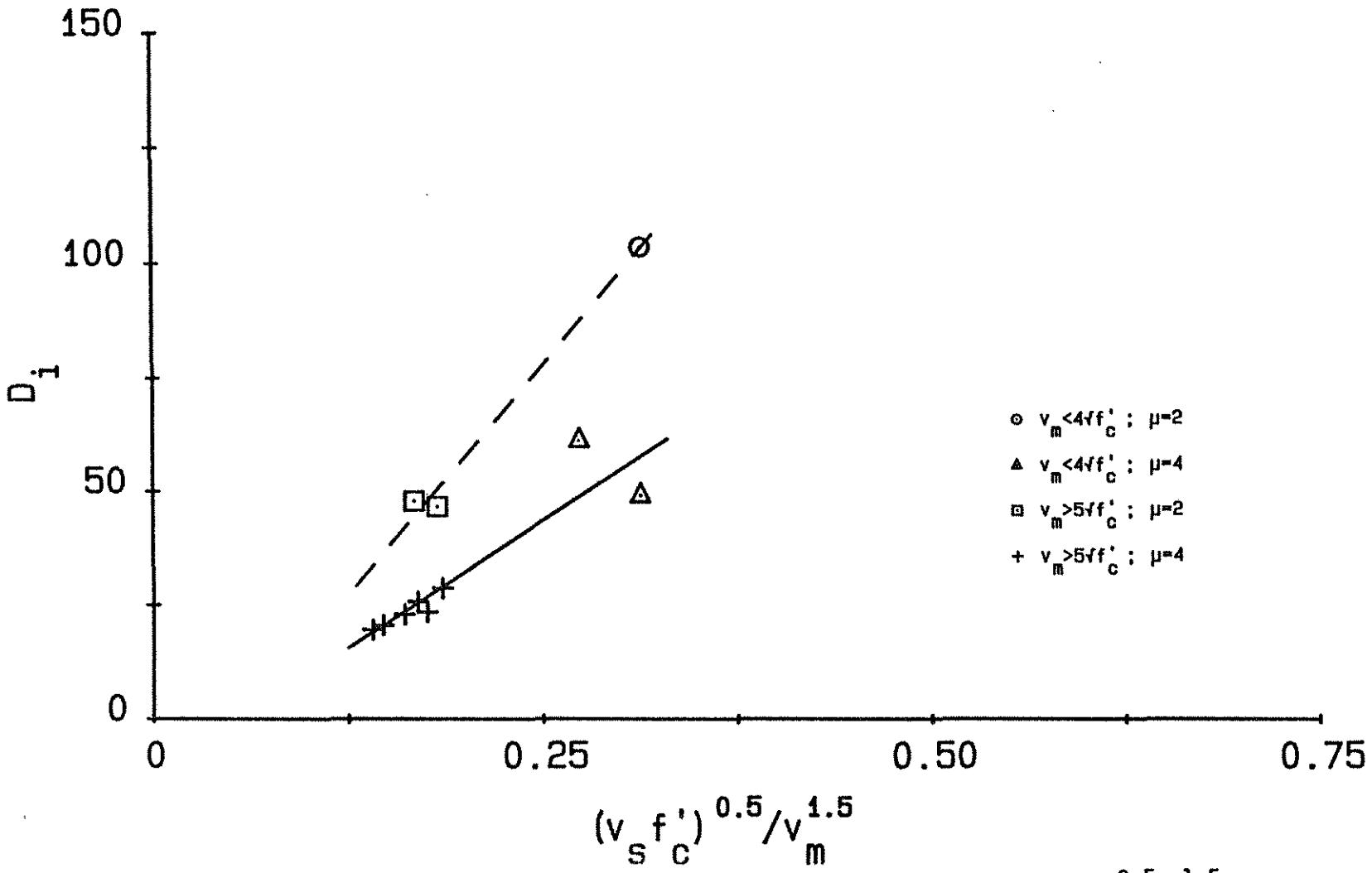

Fig. 3.5(f) Effect of Displacement Ductility Factor, D_i versus $(v_s f_c')^{0.5}/v_m^{1.5}$, Hwang & Scribner (13,14)

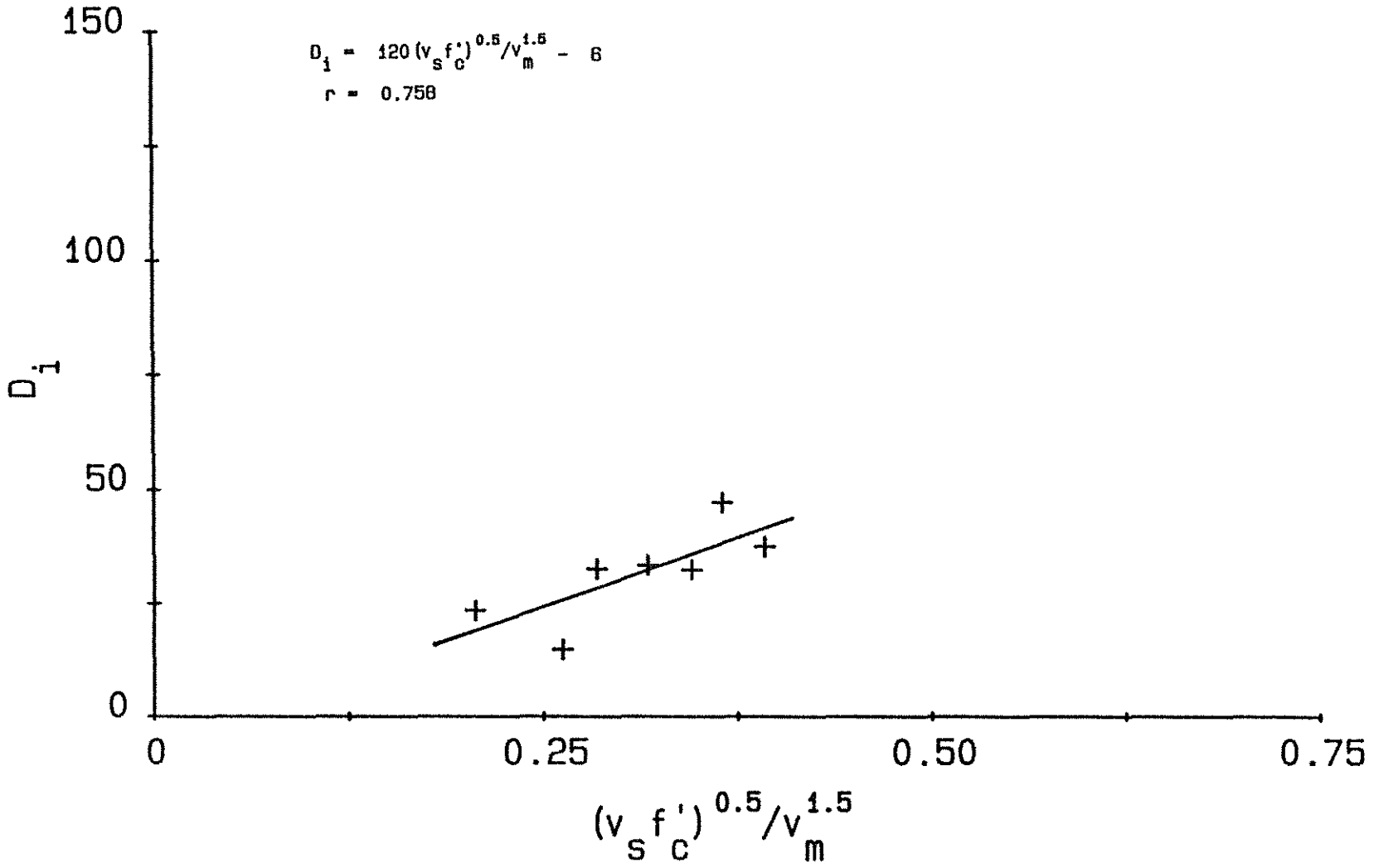

Fig. 3.5(g) D_i versus $(v_s f'_c)^{0.5}/v_m^{1.5}$, Ma, Bertero & Popov (18)

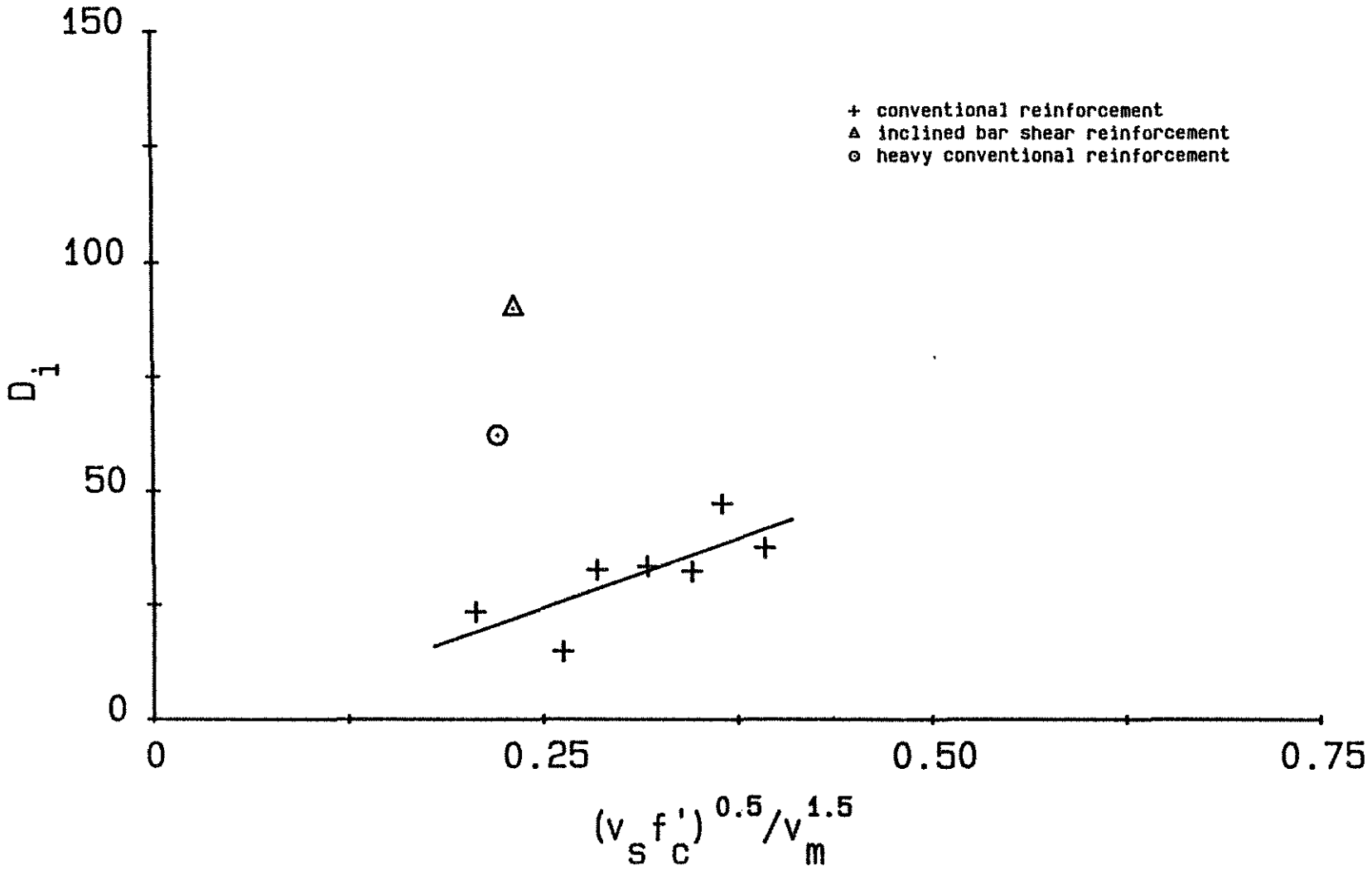

Fig. 3.5(h) Effect of special Web Reinforcement, D_i versus $(v_s f'_c)^{0.5}/v_m^{1.5}$, Bertero, Popov et. al (4,18)

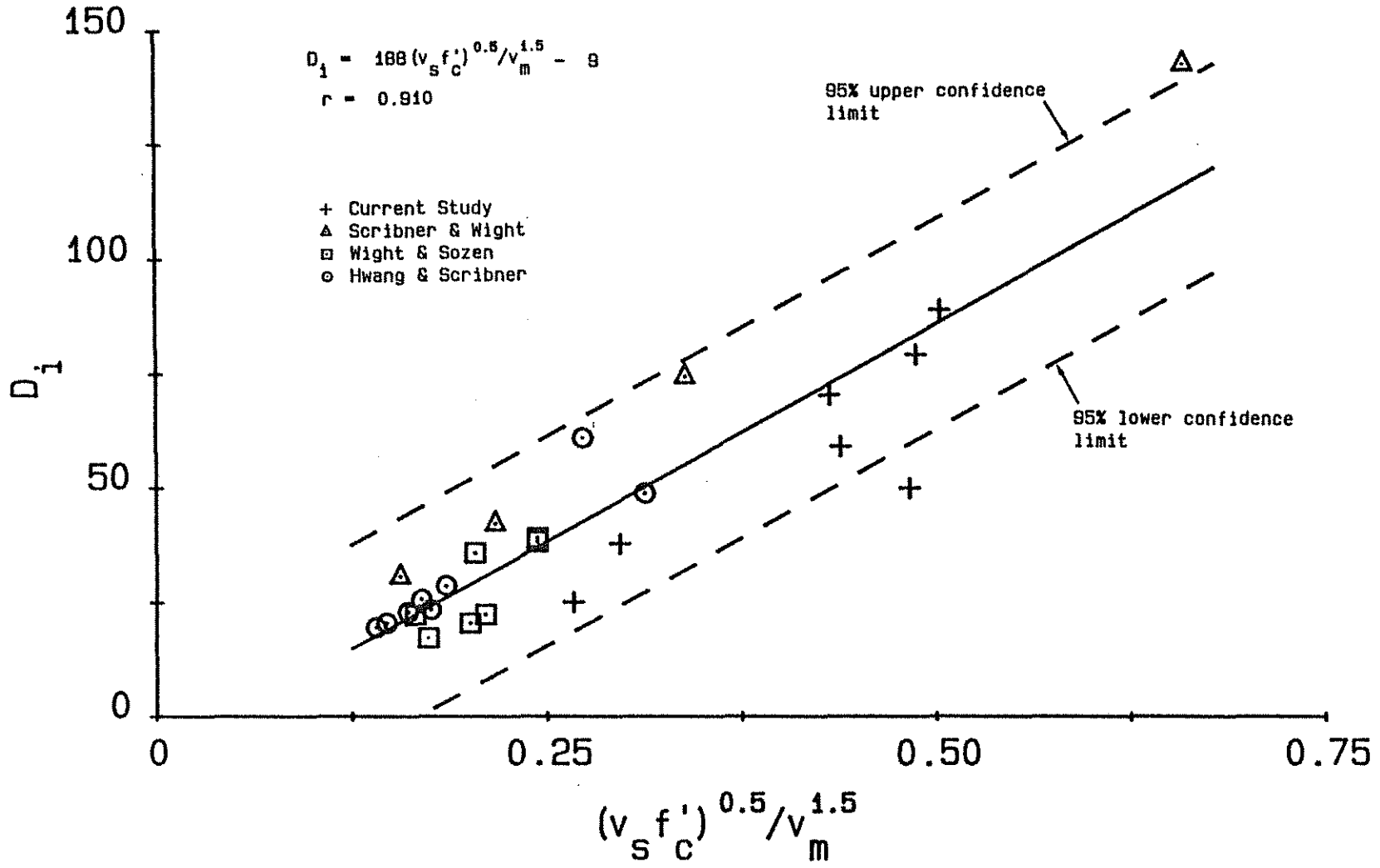

Fig. 3.6(a) D_1 versus $(v_s f'_c)^{0.5}/v_m^{1.5}$, Beams used in D_1 Study

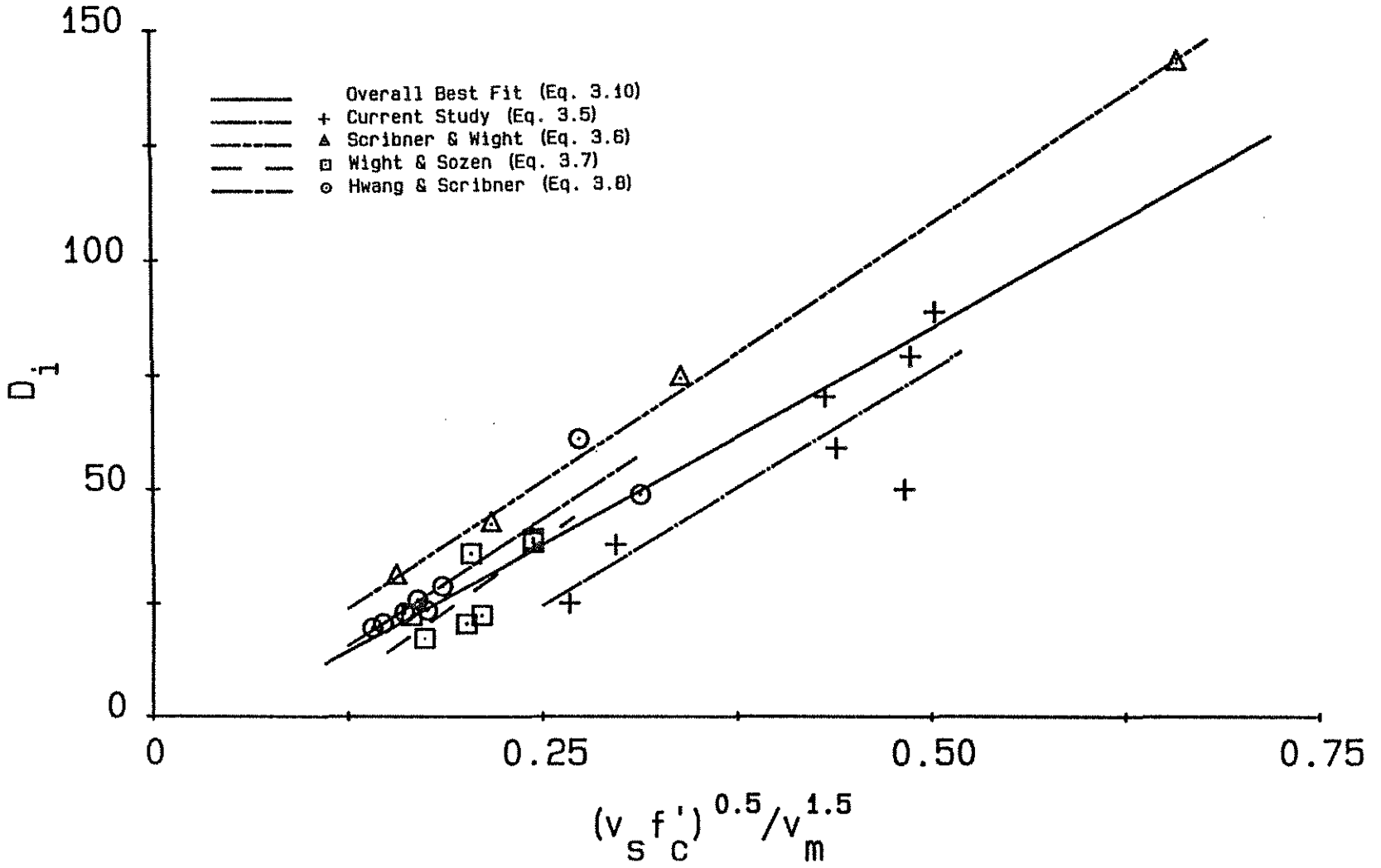

Fig. 3.6(b) D_i versus $(v_s f'_c)^{0.5}/v_m^{1.5}$, Comparison of Eq. (3.10) with Eq. (3.5), (3.6), (3.7), and (3.8)

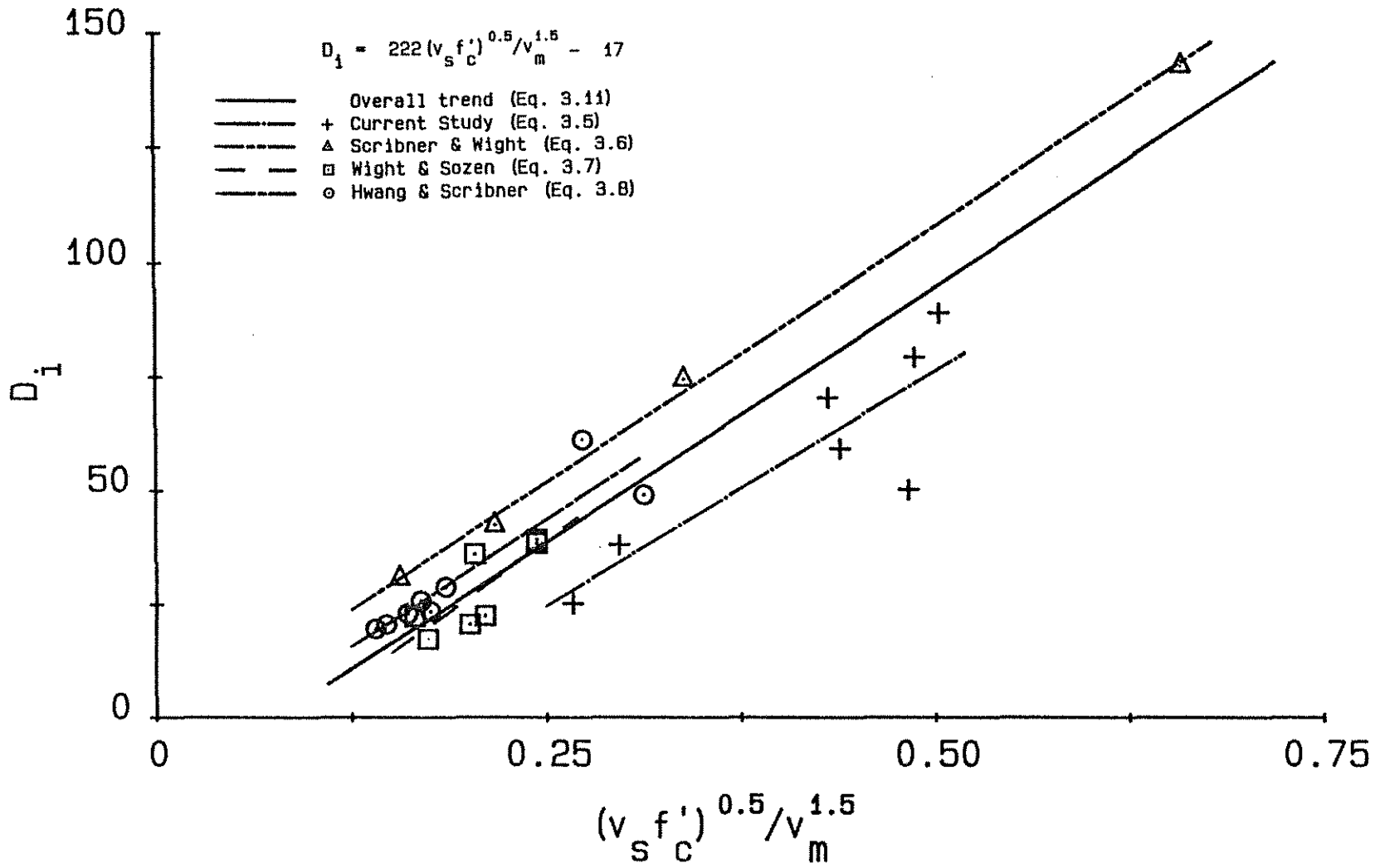

Fig. 3.7 D_i versus $(v_s f'_c)^{0.5}/v_m^{1.5}$, Comparison of Eq. (3.11) with Eq. (3.5), (3.6), (3.7), and (3.8)

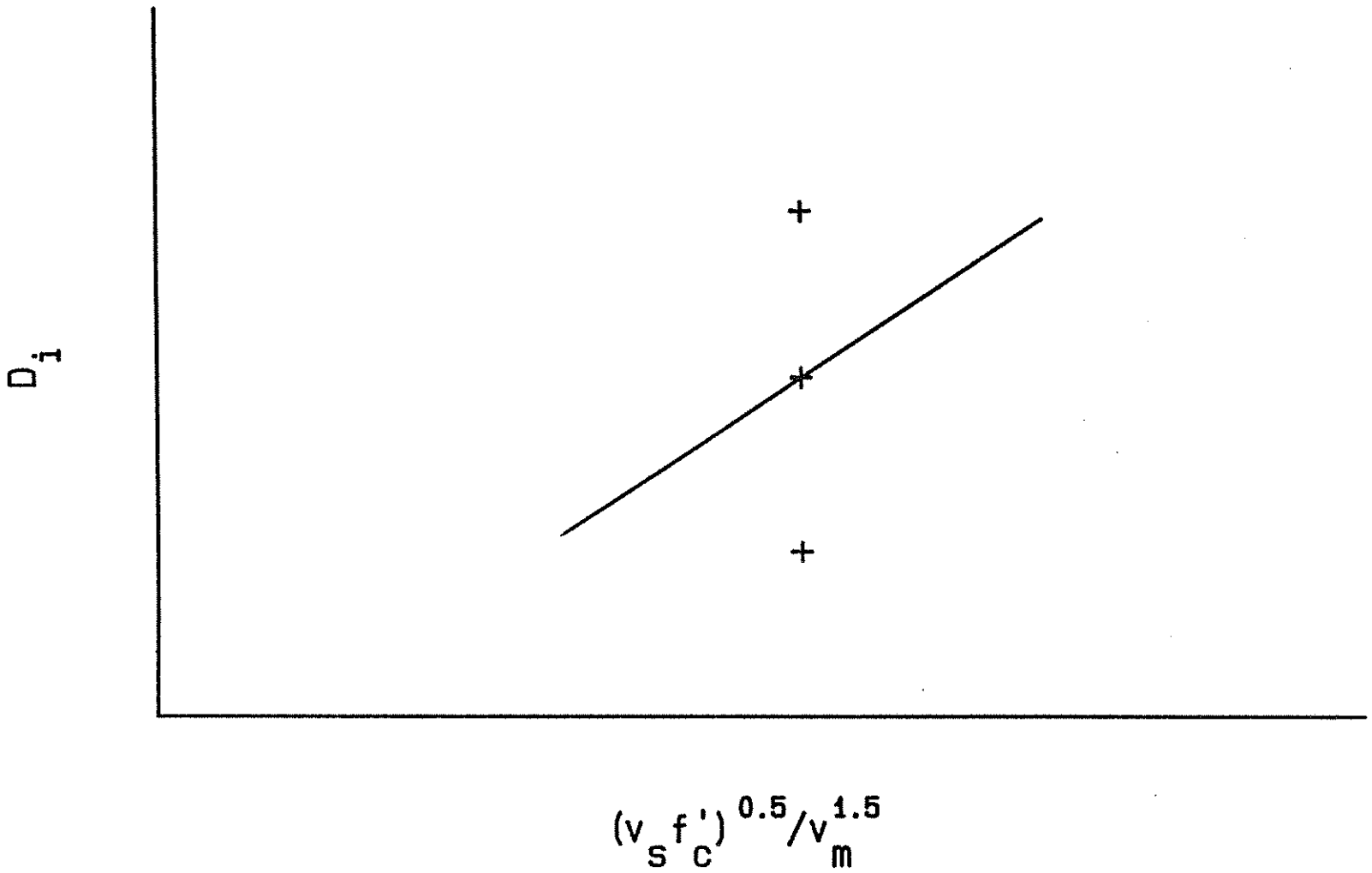

Fig. 3.8 D_i versus $(v_s f'_c)^{0.5}/v_m^{1.5}$, Beam Efficiency with Respect to Statistical Mean

APPENDIX A

NOTATION

a = shear span

A_{core} = area of core

A_g = gross area of section

A_s = area of top reinforcing steel

A'_s = area of bottom reinforcing steel

A_v = area of shear reinfocement

b = width of beam section = b_w

b_c = width of concrete core measured to outside of stirrups

b_w = width of rectangular beam or web width of T-beam

d = effective depth (distance from bottom of beam to centroid of top reinforcement)

d_1 = effective depth (distance from top of beam to centroid of bottom reinforcement)

d_c = depth of concrete core measured to outside of stirrups

D = diagonal dimension of region spanned by each set of diagonal LVDTs

D_i = energy dissipation index = $E/0.5P_y\Delta_y[1 + (A'_s/A_s)^2]$

E = total energy dissipated for cycles in which $P_{n-} \geq 0.75P_y$

f'_c = compressive strength of concrete measured on 6 x 12 inch cylinders

f_r = modulus of rupture from 6 x 6 x 22 inch flexural specimens

NOTATION (continued)

f_{vy} = yield strength of shear reinforcement

f_y = yield strength of flexural reinforcement

h = height of beam cross section

h_h = horizontal dimension of region spanned by diagonal LVDTs

h_v = vertical dimension of region spanned by diagonal LVDTs

H = height of column-stub

I_w = work index = $\sum P_n \Delta_n / P_y \Delta_y$

I'_w = modified work index = $I_w(1 - d_c/a)(1 + 0.0005N/A_{core})$

l = span of beam

L = center to center length between two columns

L_l = length of column-stub

M^+ = positive moment capacity at a column face

M^- = negative moment capacity at a column face

N = axial compression

P_n = maximum beam load in nth cycle of loading

P_y = beam load at yielding of top flexural reinforcement

P'_y = beam load at yielding of bottom flexural reinforcement

r = correlation coefficient

s = stirrup spacing

v_n = nominal shear stress = $V_n/b_w d$

v_m = maximum shear stress = $V_m/b_w d$

v_s = stirrup stress = $V_s/b_w d$

NOTATION (continued)

v_u = factored shear stress = $V_u/b_w d$

V = shear force due to lateral deformation = $(M_1^+ + M_2^-)/L$

V_c = nominal shear force carried by concrete

V_n = nominal shear force

V_m = maximum shear force

V_s = nominal stirrup shear capacity = $A_v f_{vy}/bs$

V_u = factored shear force

V_y = shear force at yielding of main flexural reinforcement = P_y

W = width of column-stub

α = coefficient of v_s used in regression analysis

β = coefficient of f'_c used in regression analysis

γ = shear deformation = $(\gamma_1 + \gamma_2)/2$

γ_1 = first component of total shear deformation

= $[\sqrt{(D + \Delta_1)^2 - h_h^2} - h_v]/h_h$

γ_2 = second component of total shear deformation

= $[h_v - \sqrt{(D + \Delta_2)^2 - h_h^2}]/h_h$

Δ_b = change in length measured with LVDT #8

Δ_n = maximum load-point deflection in nth cycle of loading

Δ_t = change in length measured with LVDT #7

Δ_y = load-point deflection at yielding of top flexural reinforcement

Δ'_y = load-point deflection at yielding of bottom flexural reinforcement

NOTATION (continued)

Δ_1 = change in length of diagonal measured with LVDT #3 or #5

Δ_2 = change in length of diagonal measured with LVDT #4 or #6

θ = beam flexural rotation relative to column-stub = $(\Delta_b + \Delta_t)/2$

μ = displacement ductility factor

ρ = flexural reinforcement ratio

ϕ = strength reduction factor = 0.85 for shear

APPENDIX B

COMPUTATION OF SHEAR DEFORMATION AND BEAM FLEXURAL ROTATION RELATIVE TO COLUMN-STUB

B.1 Computation of Shear Deformation

The shear deformation, γ, was computed using a model developed by Ehsani and Wight (11). The total shear deformation consists of two components, γ_1 and γ_2 (Fig. B.1), given by

$$\gamma_1 = [\sqrt{(D + \Delta_1)^2 - h_h^2} - h_v]/h_h \qquad (B.1)$$

and

$$\gamma_2 = [h_v - \sqrt{(D + \Delta_2)^2 - h_h^2}]/h_h \qquad (B.2)$$

in which γ_1 = first component of total shear deformation

γ_2 = second component of total shear deformation

D = diagonal dimension of region spanned by each set of diagonal LVDTs

h_h = horizontal dimension of region spanned by diagonal LVDTs = 15 in.

h_v = vertical dimension of region spanned by diagonal LVDTs = 12 in.

Δ_1 = change in length of diagonal measured with LVDT #3 or #5

Δ_2 = change in length of diagonal measured with LVDT #4 or #6

The shear deformation, γ, was then computed as follows:

$$\gamma = (\gamma_1 + \gamma_2)/2 \qquad (B.3)$$

B.2 Computation of Beam Flexural Rotation Relative to Column-Stub

The flexural rotation of the beam relative to the column-stub, θ, was computed as follows:

$$\theta = (\Delta_b + \Delta_t)/h_v \qquad (B.4)$$

in which Δ_b = change in length measured with LVDT #8

Δ_t = change in length measured with LVDT #7

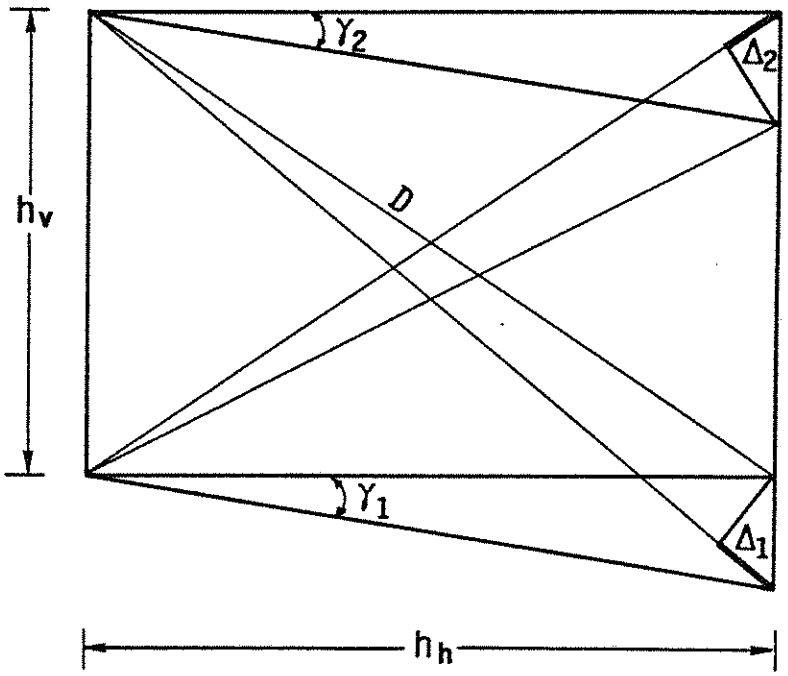

Fig. B.1 Shear Deformation Measurement

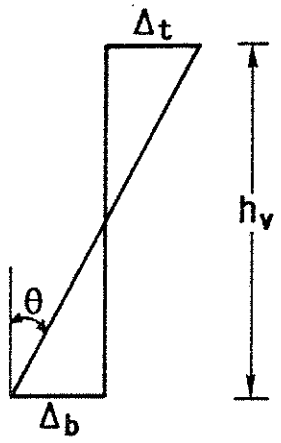

Fig. B.2 Relative Flexural Rotation Measurement